The role of ATAD3A and SLC25 proteins in OPA1 function

By: Jacob Wong

This thesis is submitted as a partial fulfillment of

the M.Sc. program in Neuroscience

Jan. 31st, 2014

Department of Cellular and Molecular Medicine

Faculty of Medicine

The University of Ottawa

STATEMENT OF CONTRIBUTION

Data from a manuscript entitled “OPA1 senses metabolic changes through SLC25 family proteins to regulate mitochondrial structure and function” for which I am 3rd author is included within this thesis and has been submitted for publication. D. Patten performed the experiments in figures 12, 21, and 23C.

ABSTRACT

OPA1 regulates cristae structure and mitochondrial DNA (mtDNA) maintenance. Recently, our lab identified ATAD3A and SLC25 proteins as OPA1 interactors. After validating these interactions by co-immunoprecipitation, the role of these proteins in OPA1 function was examined. Previously, ATAD3A was implicated in mtDNA maintenance. However, no change in mtDNA content or nucleoid number was observed in my studies following long-term and short-term ATAD3A knockdown suggesting that OPA1 maintains mtDNA independently of ATAD3A. Previous data from our lab demonstrates that OPA1 oligomerization and cristae structure is altered by nutrients. SLC25 proteins transport nutrients into mitochondria. Therefore, OPA1 oligomerization and cristae structure was analyzed following SLC25 protein inhibition and knockdown. Decreased OPA1 oligomerization and cristae remodeling was observed following SLC25 protein inhibition and OGC knockdown. In addition these changes correlate with decreased ATP synthase monomers and oligomers suggesting that cristae remodeling may affect metabolism. Overall, these studies enhance our understanding of OPA1 function.

TABLE OF CONTENTS

LIST OF TABLES

LIST OF FIGURES

LIST OF ABBREVIATIONS

AAA	ATPase associated with diverse cellular activities
ADP	Adenosine diphosphate
ADOA	Autosomal dominant optic atrophy
AGC	Aspartate glutamate carrier
ANOVA	Analysis of variance
ATAD3A	ATPase family AAA+ domain-containing protein 3A
ATP5A	ATP synthase, H+ transporting, mitochondrial F_1 complex, alpha 1
ATP	Adenosine triphosphate
BM	Butylmalonate
BN-PAGE	Blue native polyacrylamide gel electrophoresis
c-state	Cytosolic state
CC	Coil-coiled domain
Cdk1	Cyclin-dependent kinase 1
CI	Complex I
CII	Complex II
CIII	Complex III
CIV	Complex IV
CMT2A	Charcot-Marie-Tooth neuropathy type 2A
CO_2	Carbon dioxide
COI	Cytochrome c oxidase subunit I
CoQ	Coenzyme Q

CV	Complex V
Cytc	Cytochrome c
D-loop	Displacement loop
DIC	Dicarboxylate carrier
DMEM	Dulbecco's modified Eagle's medium
DNA	Deoxyribonucleic acid
DRP1	dynamin-related protein 1
EBSS	Earl's balanced salt solution
EDC	1-Ethyl-3-[3-dimethylaminopropyl] carbodiimide hydrochloride
$FADH_2$	Flavin adenine dinucleotide
FBS	Fetal bovine serum
GED	GTPase effector domain
GFP	Green fluorescent protein
GTP	Guanosine triphosphate
HBSS	Hank's balanced salt solution
HSP	Heavy strand promoter
HT-MEF	Highly transfectable mouse embryonic fibroblasts
IBM	Inner boundary membrane
IM	Inner membrane
IMS	Intermembrane space
IP	Immunoprecipitates
KO	Knockout

L-OPA1	Long OPA1 isoforms
LSP	Light strand promoter
m-AAA	Matrix-facing ATPase associated with diverse cellular activities
m-state	Matrix state
MARCH5	Membrane-associated RING-CH 5
MEF	Mouse embryonic fibroblast
Mff	Mitochondrial fission factor
Mfn	Mitofusin
MiD49	Mitochondrial dynamics factor 49
Mief1	Mitochondrial elongation factor 1
Mito-YFP	Mitochondrially targeted yellow fluorescent protein
mRNA	Messenger ribonucleic acid
mtDNA	Mitochondrial deoxyribonucleic acid
MTS	Mitochondrial targeting sequence
NAD+	Nicotinamide adenine dinucleotide
NADH	Reduced nicotinamide adenine dinucleoitide
NDUFA9	NADH dehydrogenase (ubiquinone) alpha subcomplex 9
NS	No substrate
O_2	Oxygen
OGC	Oxoglutarate carrier
OH	Origin of heavy strand replication

OL	Origin of light strand replication
OM	Outer membrane
OMA1	Overlapping with the m-AAA protease 1
OPA1	Optic atrophy 1
OXPHOS	Oxidative phosphorylation
PARL	Presenilin-associated rhomboid-like
PBS	Phosphate buffered saline
PhS	Phenylsuccinate
Pi	Inorganic phosphate
PI	Propidium iodide
PKA	Protein kinase A
qPCR	Quantitative polymerase chain reaction
RNAi	Ribonucleic acid interference
rRNA	Ribosomal ribonucleic acid
S-OPA1	Short OPA1 isoforms
SDS	Sodium dodecyl sulfate
SDS-PAGE	Sodium dodecyl sulfate polyacrylamide gel electrophoresis
shCont	Control short hairpin ribonucleic acid
shATAD3A	Short hairpin ribonucleic acid targeting ATAD3A
siATAD3A	Short-interfering ribonucleic acid targeting ATAD3A
siCtr	Control short-interfering ribonucleic acid

siOGC	Short-interfering ribonucleic acid targeting the oxoglutarate carrier
siRNA	Short-interfering ribonucleic acid
SLC25 protein	Solute-linked carrier 25 protein
SUMO	Small ubiquitin-like modifier
T-PBS	Tween 20 phosphate buffered saline
TBS	Tris-buffered saline
TM	Transmembrane domain
tRNA	Transfer ribonucleic acid
WA	Walker A domain
WB	Walker B domain

ACKNOWLEDGMENTS

I would first like to thank Dr. Ruth Slack for all the support and guidance she has given me throughout my Master's project and during the writing of this thesis. I am truly grateful for being given the opportunity to work in her lab and to present my work at local and international conferences. I would also like to thank David Patten, a current PhD student within the lab, for all his help and advice over the past two years. It has been a pleasure to work with him on this project. In addition, I appreciate all the guidance and valuable discussions given by Dr. Marc Germain, a former senior post-doctoral fellow, and Dr. Mireille Khacho, a current senior post-doctoral fellow. Our lab manager, Jason MacLaurin, has also provided me with extensive training especially with respect to molecular cloning and for this I am thankful. I would also like to give a special thanks to Dr. David Park and Dr. Johnny Ngsee, members of my thesis advisory committee, for their critical assessment of my work during TAC meetings. The moral support given by my family and girlfriend, Erin, has also been invaluable throughout my degree and for this I am really appreciative. Lastly, I would like to thank all the members from the Slack lab for their scientific advice and for creating such a great work environment.

CHAPTER 1: INTRODUCTION

1.1 – Mitochondria:

During the evolution of eukaryotes, an endosymbiosis with purple, aerobic bacteria is believed to have formed leading to the creation of mitochondria (Sagan, 1967). Now within eukaryotic cells, mitochondrial number ranges from several hundred to several thousand where they serve a variety of functions (Garcia-Rodriguez, 2007). Their basic appearance includes a rod-shaped morphology with the presence of two lipid bilayers termed the outer and inner membrane, which are separated by an intermembrane space (IMS) and together enclose an electron-dense matrix (Fig.1). The best-described function of mitochondria is their role in energy metabolism. However, it is now clear that mitochondria are also important in other cellular processes. For instance, mitochondria participate in autophagy as well as apoptotic and calcium signaling (Bredesen, 2006; Bianchi, 2004). The involvement of mitochondria in these non-metabolic processes has generated extensive interest in mitochondrial function in the context of cellular physiology.

In the subsequent sections, I will describe oxidative phosphorylation, inner membrane structure and the mitochondrial genome. Afterwards, I will explain the concept of mitochondrial dynamics and how one of its regulators, optic atrophy 1 (OPA1), also maintains the mitochondrial genome and regulates inner membrane topology. Then I will detail the function of ATAD3A and the SLC25 protein family and how they may regulate OPA1 function.

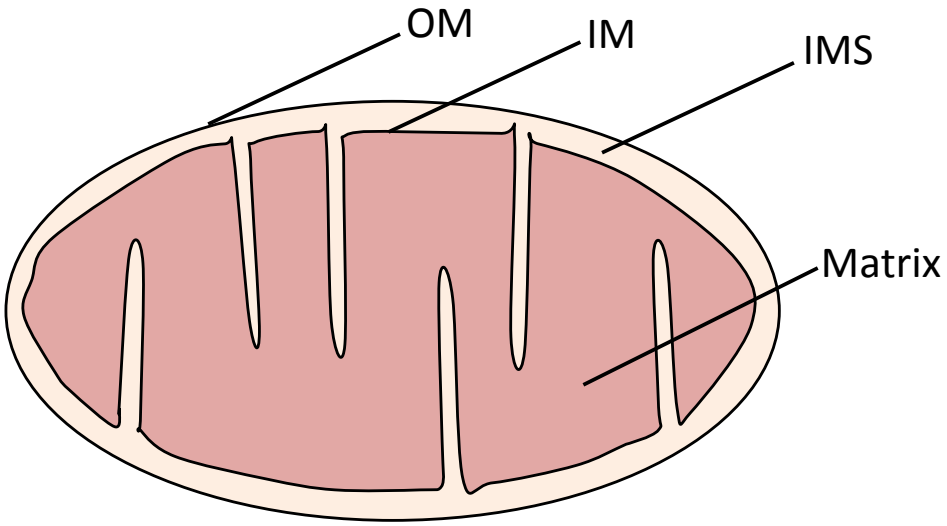

Figure 1: **The Mitochondrion.** Image displays the typical bean-shaped morphology of mitochondria and it's compartments. (OM) – outer membrane, (IM) – inner membrane, (IMS) – intermembrane space.

1.2 –Oxidative phosphorylation (OXPHOS):

There are two main pathways in which adenosine triphosphate (ATP) is generated within the cell. One pathway is called glycolysis where cytosolic glucose is broken down into pyruvate and the other pathway is called OXPHOS, which occurs within mitochondria and produces the bulk of cellular ATP (Fig.2). The electron transport chain and the ATP synthase are the machinery responsible for carrying out OXPHOS (Hatefi, 1985). There are a total of four respiratory chain complexes (complex I [CI], complex II [CII], complex III [CIII], and complex IV [CIV) within the electron transport chain displaying oxidoreductase activity (Fowler et al., 1962; Hatefi et al., 1962; Hatefi et al., 1961; Rieske et al., 1964; Ziegler & Doeg, 1962). During OXPHOS, electrons from reducing equivalents (eg. NADH, $FADH_2$), generated during glycolysis and the Kreb's cycle, enter the electron transport chain at either CI or CII (Cecchini, 2003; Hirst, 2005). Then the electron carrier, coenzyme Q, will transfer them to CIII (Crane et al., 1957; Ernster et al., 1969; Kröger & Klingenberg, 1970; Szarkowska, 1966). Another electron carrier called cytochrome c then shuttles these electrons to CIV, which reduces oxygen to water (Adams and Turnbull, 1996). The function of each respiratory chain complex (except CII) is to couple electron transport with subsequent proton export from the matrix to generate a proton gradient across the mitochondrial inner membrane (Leung & Hinkle, 1975; Sigel & Carafoli, 1978; Wikström, 1977; Wikström, 1984). The energy stored within this gradient, also known as proton motive force, is then used by ATP

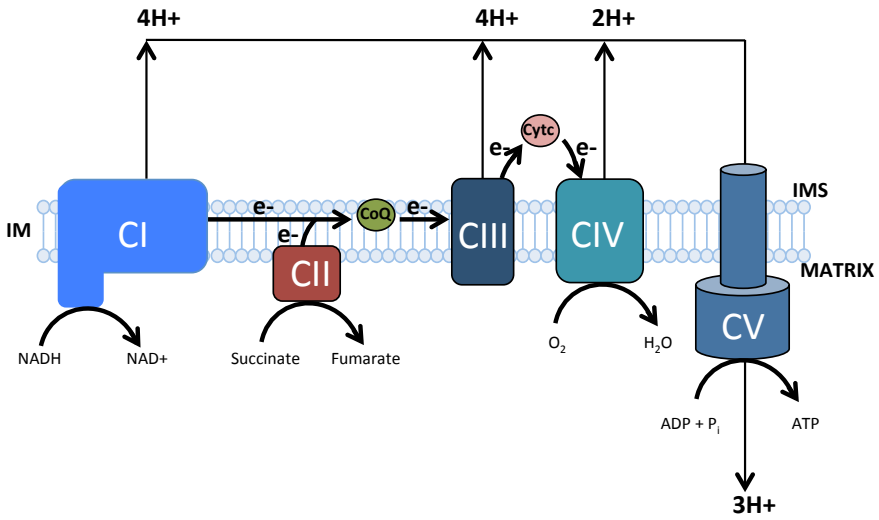

Figure 2: **Oxidative Phosphorylation.** Electrons from NADH or $FADH_2$, which originate from the breakdown of glucose, enter the electron transport chain and get transferred between respiratory chain complexes that couple electron transport with proton pumping. Complex I (CI), complex II (CII), complex III (CIII), and complex IV (CIV) comprise the respiratory chain whereas the ATP synthase (complex V [CV]) catalyzes ATP synthesis using the energy stored within the generated proton gradient. (Cytc) – cytochrome c, (CoQ) – coenzyme Q, (ADP) – adenosine diphosphate, (P_i) – inorganic phosphate, (IM) – inner membrane, and (IMS) – intermembrane space.

synthase (complex V) to generate ATP from adenosine diphosphate (ADP) and inorganic phosphate (Pi) (Mitchell, 1961; Smeitink et al., 2012).

1.3 –Electron transport chain organization:

Respiratory chain complexes are located within the mitochondrial inner membrane, but their organization has been a matter of debate (Chaban et al., 2013). Early studies provided evidence for two alternate models of electron transport chain organization (Chance & Williams, 1955; Fowler & Richardson, 1963; Hackenbrock, et al., 1986). One model was the “fluid-state” model that proposed an organization in which respiratory chain complexes randomly diffused within the mitochondrial inner membrane mediating electron transport through random collisions (Fig.3A) (Hackenbrock et al., 1986). The other model was the “solid-state” model stating that all the respiratory chain complexes interacted with one another in a large supramolecular complex (Chance & Williams, 1955; Fowler & Richardson, 1963). Successful isolation of fully functional respiratory chain complexes shed doubt onto the “solid-state” model leading to wide acceptance of the “fluid-state” model (Fig.3B) (Hackenbrock et al., 1986). Recent studies however, support the idea of respiratory chain supercomplexes.

Using digitonin for lysis and blue-native polyacrylamide gel electrophoresis (BN-PAGE) for separation, Schägger and Pfeiffer observed large protein

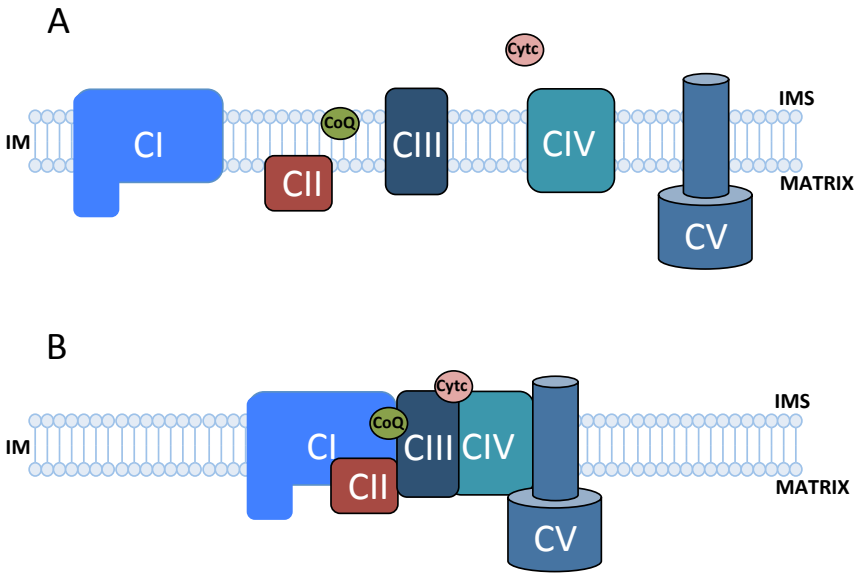

Figure 3: **Organization of the electron transport chain.** (A) Figure depicting the "fluid-state" model where cytochrome c (Cytc), coenzyme Q (CoQ) and respiratory chain complexes are free to diffuse within the mitochondrial inner membrane (IM). (B) Figure depicting the "solid-state" model where Cytc, CoQ, and respiratory chain complexes associate into large supramolecular complexes within the IM. (CI) – complex I, (CII) – complex II, (CIII) – complex III, (CIV) – complex IV, (CV) – complex V, and (IMS) – intermembrane space.

complexes containing different combinations of CI, CIII and CIV at varying stoichiometry (Schägger and Pfeiffer, 2000). Since this study, supercomplexes have been observed in many organisms from a variety of kingdoms (reviewed in Lenaz & Genova, 2012). The most commonly identified supercomplex combinations were CI + $CIII_2$, $CIII_2$ + CIV_n and CI + $CIII_2$ + CIV_n with some supercomplexes encasing the electron carriers, coenzyme Q and/or cytochrome c (Acín-Pérez et al., 2008; Chaban et al., 2013; Eubel et al., 2003; H Schägger & Pfeiffer, 2000). Generally respiratory chain supercomplexes lack CII, but one study did detect minimal amounts (Acín-Pérez et al., 2008; Chaban et al., 2013). The purpose of supercomplexes is predicted to improve electron transport efficiency by minimizing the distance between respiratory chain complexes and electron leak (Chaban et al., 2013). Not only this, but formation of different supercomplexes may also define separate electron transport routes that enable maximal use of available energy sources (Chaban et al., 2013; Lapuente-Brun et al., 2013). Some evidence also suggests supercomplex assembly confers stability to its components (Acín-Pérez et al., 2004, 2008; Diaz et al., 2006; Schägger et al., 2004). In light of these new findings, a new model of electron transport chain organization was proposed called the “plasticity” model, which combines aspects from both the “solid-state” and “fluid-state” models (Fig.4) (Acín-Pérez et al., 2008).

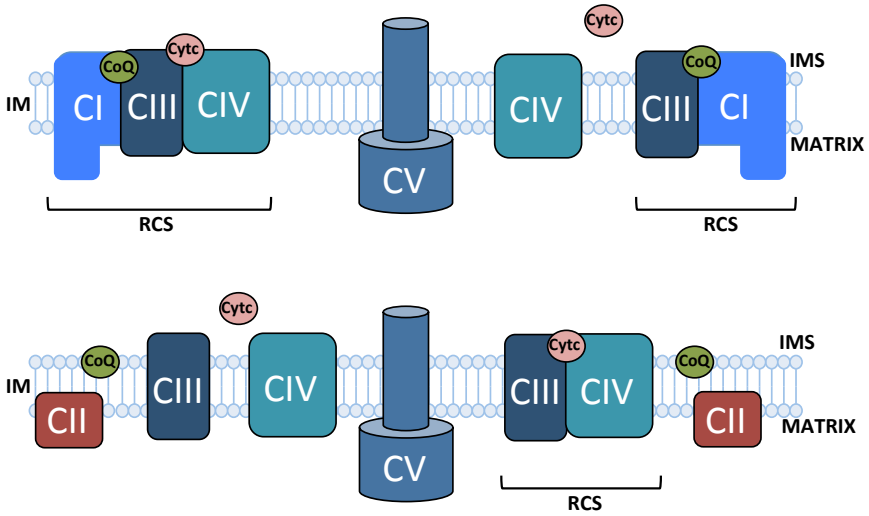

Figure 4: **"Plasticity" model of electron transport chain organization.** The "plasticity" model is a combination between the "fluid-state" and "solid-state" models where respiratory chain complexes and electron carriers either diffuse freely within the mitochondrial inner membrane (IM) or assemble into supercomplexes. (CI) – complex I, (CII) – complex II, (CIII) – complex III, (CIV) – complex IV, (CV) – complex V, (Cytc) – cytochrome c, (CoQ) – coenzyme Q, (RCS) – respiratory chain supercomplexes, and (IMS) – intermembrane space.

1.4 - ATP synthase oligomerization:

In addition to the respiratory chain supercomplexes, the ATP synthase also forms supramolecular arrangements (Arnold et al., 1998; Schägger & Pfeiffer, 2000; Wittig, et al., 2008). The basic functional unit of the ATP synthase is the monomer, which contains an F_1 and F_0 subunit (reviewed in Walker, 2012). The F_1 subunit faces the matrix and represents the catalytic subunit containing binding sites for both ADP and Pi (Harris, 1978; Penefsky, 1977). While the inner membrane-bound F_0 subunit is the motor subunit responsible for proton pumping (Hoppe and Sebald, 1984). Even though ATP synthase monomers are fully functional on their own, many studies show that the ATP synthase can assemble into dimers, which can further assemble into oligomers (Arnold et al., 1998; Krause et al., 2005; Schägger & Pfeiffer, 2000; Wittig et al., 2008). Formation of these ATP synthase dimers was shown to be required for maintenance of mitochondrial ultrastructure (Paumard et al., 2002). Indeed, rows of ATP synthase dimers are observed at the base of cristae by cryo-electron tomography (Strauss, et al., 2008). ATP synthase dimers are believed to induce inner membrane curvature, which could stimulate its activity by increasing local proton concentrations at the apex of cristae (Strauss, et al., 2008). Although their function is not completely understood, these structures seem to be implicated in the regulation of inner membrane topology and potentially metabolism.

1.5 – Mitochondrial inner membrane:

In contrast to the mitochondrial outer membrane, the inner membrane displays a complex topology with large invaginations that protrude into the mitochondrial matrix. These invaginations, referred to as cristae, and the regions that remain parallel to the outer membrane, termed the inner boundary membrane (IBM), are sub compartments of the inner membrane (Fig.5). Using traditional electron microscopy and modern electron tomographic analyses, the 'crista junction model' of inner membrane topology was proposed (Mannella et al., 1994; Mannella et al., 1997; Daems & Wisse, 1966). Rather than being simple, broad in folds of the inner membrane; cristae were shown to consist of long tubular or lamellar structures with small openings, termed crista junctions, that connect the cristal membrane to the IBM. Not only do the two compartments differ morphologically, their protein content is also different (Wurm and Jakobs, 2006). For instance, the electron transport chain is concentrated within cristae while the IBM is enriched with proteins involved with protein translocation (Wurm and Jakobs, 2006). Consistent with these findings, was the identification of cristae as the principal site of OXPHOS (Gilkerson et al., 2003). The function of crista junctions is predicted to act as a diffusional barrier to both membrane proteins and the contents enclosed by cristae (Frey et al., 2002; Mannella et al., 2001; Zick et al., 2009). Such contents include ions and metabolic substrates that support OXPHOS such as ADP, ATP and protons. Furthermore, the majority of cytochrome c, an electron carrier, was shown to reside within cristae (Scorrano et al., 2002). It is estimated that only 15-20% of the cytochrome c pool

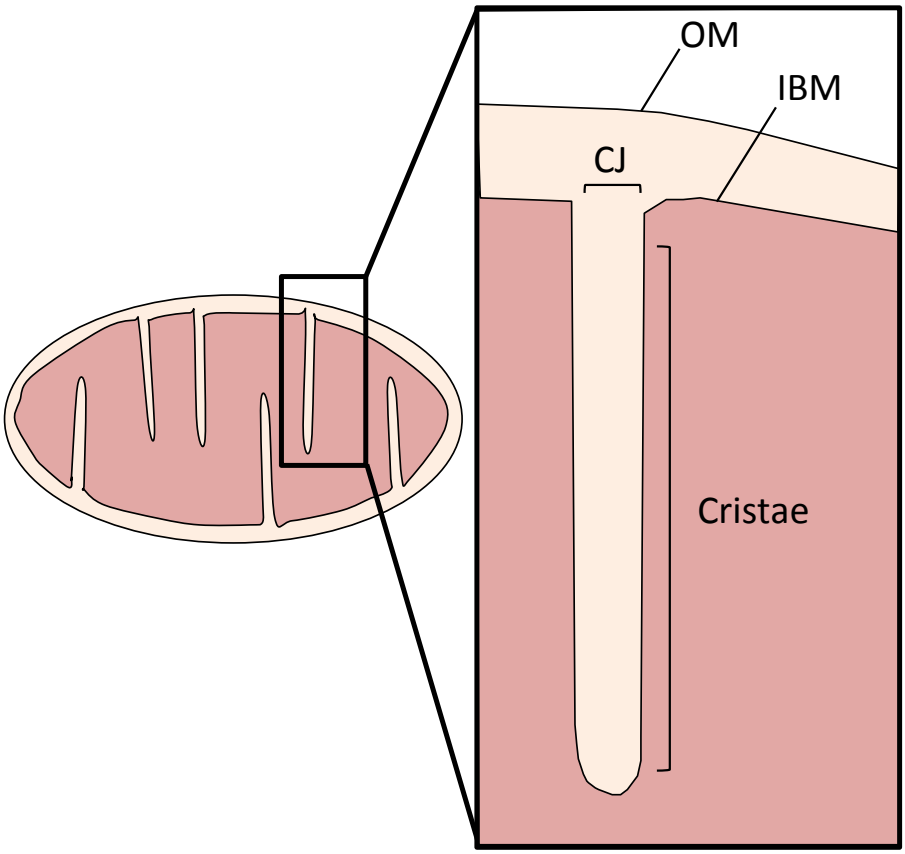

Figure 5: **Structure of the mitochondrial inner membrane.** The mitochondrial inner membrane is composed of two distinct compartments, the inner boundary membrane (IBM) and cristae. Cristae are the large invaginations present within the inner membrane and their openings are referred to as crista junctions (CJ). The IBM is the section of the mitochondrial inner membrane that remains in close proximity to the mitochondrial outer membrane (OM).

is present within the IMS with the remaining cytochrome c residing in cristae (Bernardi and Azzone, 1981; Scorrano et al., 2002). Taken together, it is clear that cristal membranes are key metabolic centers within mitochondria.

1.6 – Mitochondrial DNA (mtDNA):

In accordance with their prokaryotic origin, mitochondria contain their own genome (Fig.6) (Nass & Nass, 1963; Tuppy et al., 1964). The mitochondrial genome is circular and their numbers are typically in the thousands per cell (Garcia-Rodriguez, 2007; Nass, 1966; Sinclair & Stevens, 1966; Van Bruggen et al., 1966). In terms of size it is significantly smaller than its nuclear counterpart containing ~ 16,500 base pairs (Anderson et al., 1981; Andrews et al., 1999; Bibb et al., 1981). Despite its small size, the mitochondrial genome is able to encode 37 genes, of which there are two ribosomal RNA (rRNA) genes, thirteen protein-coding genes and twenty-two transfer RNA genes (Anderson et al., 1981; Bibb et al., 1981). Each protein-coding gene encodes subunits for respiratory chain (CI, CIII, and CIV) or the ATP synthase and mutations within these genes lead to a variety of pathology (Wallace, 2005). There is also a large non-coding region called the displacement loop (D-loop) (Anderson et al., 1981; Bibb et al., 1981). The D-loop region is triple stranded and contains an origin of replication site as well as two transcriptional promoters (Anderson et al., 1981; Chang & Clayton, 1984, 1985; Fish, et al., 2004; Kasamatsu 1971). Similar to bacterial DNA, mtDNA associates with a variety of proteins forming a nucleoprotein complex termed the mitochondrial nucleoid that associates with the mitochondrial

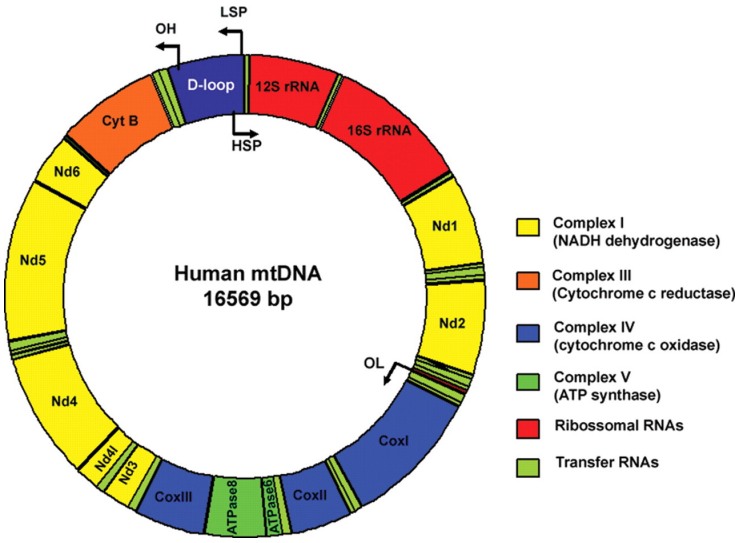

Figure 6: **The human mitochondrial genome**. From St John et al., 2010. Figure depicts the location of genes and non-coding elements within human mitochondrial DNA (mtDNA). In total, mtDNA contains 37 genes including 22 transfer RNA genes, 13 protein-coding genes and 2 ribosomal RNA genes. It also contains two regions of non-coding DNA termed the displacement-loop (D-loop) and the origin of light strand replication (OL). The D-loop harbors the origin of heavy strand replication (OH), the light strand promoter (LSP) and the heavy strand promoter (HSP).

inner membrane (Chen & Butow, 2005; Wang & Bogenhagen, 2006). The average size of human nucleoids is approximately 70nm and each nucleoid can contain up to 10 individual mtDNA molecules (Chen & Butow, 2005; Kukat et al., 2011). The mitochondrial transcription factor A, the Twinkle helicase, and polymerase γ 1 and 2 were amongst the proteins identified as associated with nucleoids (Alam et al., 2003; Bogenhagen et al., 2008; Garrido et al., 2003; Spelbrink et al., 2001; Wang & Bogenhagen, 2006). Mutations in these proteins lead to either complete mtDNA loss or mtDNA deletions demonstrating the importance of nucleoid structure in maintaining mtDNA (Larsson et al., 1998; Spelbrink et al., 2001; Van Goethem et al., 2001).

1.7 - Mitochondrial dynamics:

In contrast to the traditional rod-shaped morphology depicted in textbooks, mitochondria can adopt various morphologies ranging from small spheres to elongated tubules (Johnson et al., 1980). This dynamic nature is shaped by continuous fusion and fission events and the balance between these antagonistic forces ultimately determine mitochondrial morphology (Nunnari et al., 1997; Sesaki and Jensen, 1999). Key factors identified as being required for mitochondrial dynamics were the dynamin-related guanosine triphosphatases (GTPases), mitofusins (Mfns) 1 and 2, optic atrophy 1 (OPA1) and dynamin-related protein 1 (DRP1) (Chen et al., 2003; Chen et al., 2005; Olichon et al., 2003; Smirnova et al., 2001). A tremendous interest in mitochondrial dynamics came with its implication in various physiological processes (Itoh et al., 2013).

For example, an early event in apoptosis is mitochondrial fragmentation, which was shown to facilitate the release of proapoptotic factors from mitochondria (Breckenridge et al., 2003; Frank et al., 2001; Karbowski et al., 2002; Mancini et al., 1997; Pinton et al., 2001). Furthermore, loss of mitochondrial fusion leads to mitochondrial dysfunction including loss of membrane potential and reduced respiratory capacity (Chen et al., 2005). Mitochondrial fusion may preserve mitochondrial function by enabling content mixing thereby complementing dysfunctional mitochondria (Legros et al., 2004; Nunnari et al., 1997). Loss of fusion also sensitizes cells to apoptosis (Olichon et al., 2003; Sugioka et al., 2004). Regulated changes in mitochondrial structure seem to be a key determinant during development as well since loss of fusion or fission is embryonic lethal (Chen et al., 2007; Wakabayashi et al., 2009). Mutations in fusion genes are also linked to neurodegeneration (Alexander et al., 2000; Delettre et al., 2000; Zuchner et al., 2004). For instance, Charcot-Marie-Tooth neuropathy type 2A (CMT2A), a disease characterized by the progressive loss of peripheral neurons, was linked to mutations in the *Mfn2* gene (Zuchner et al., 2004). Furthermore, mutations in the *OPA1* gene were linked to the development of autosomal dominant optic atrophy (ADOA) (Alexander et al., 2000; Delettre et al., 2000). All together, it becomes clear that maintenance of mitochondrial morphology is important for mitochondrial function, cellular homeostasis and development.

1.8 - Mitochondrial fission:

The division of mitochondria primarily relies on DRP1, a protein that resides within the cytosol (Fig.7) (Shin et al., 1997; Smirnova et al., 2001; Smirnova et al., 1998). Being cytosolic, DRP1 must first be recruited to the mitochondrial OM to induce fragmentation (Oettinghaus et al., 2012). A key mechanism triggering DRP1 translocation to mitochondria is posttranslational modifications such as phosphorylation, ubiquitination and sumoylation (reviewed in Oettinghaus et al., 2012). The major phosphorylation sites identified are Ser637 and Ser616, which cause differential effects on DRP1 translocation (Cereghetti et al., 2008; Chang & Blackstone, 2007; Taguchi et al., 2007). Phosphorylation of Ser637 by PKA results in the sequestration of DRP1 within the cytosol and mitochondrial elongation while dephosphorylation by calcineurin induces the opposite effect (Cereghetti et al., 2008; Chang & Blackstone, 2007). On the contrary, phosphorylation at Ser616 by Cdk1/cyclinB promotes fission by inducing the translocation of DRP1 to mitochondria (Taguchi et al., 2007). In addition to phosphorylation, ubiquitination seems to be important as loss of MARCH5, an E3 ubiquitin ligase, decreases the amount of DRP1 at mitochondria (Karbowski et al., 2007). Addition of small ubiquitin-like modifier (SUMO) proteins yields similar results in that mitochondrial translocation of DRP1 is increased (Braschi et al., 2009; Wasiak et al., 2007). Once DRP1 is recruited, adaptor proteins located on the mitochondrial outer membrane will stabilize it (Otera et al., 2013). Many different adaptor proteins have been identified including Fis1, mitochondrial fission factor (Mff), mitochondrial elongation factor 1

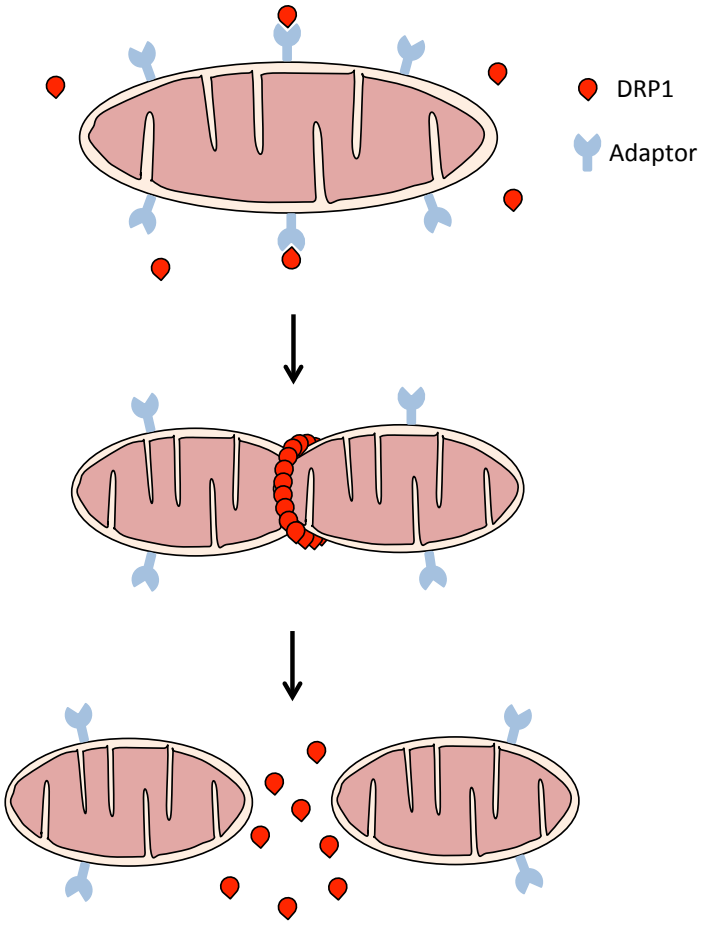

Figure 7: **Division of mitochondria**. Adaptor proteins (eg. fis1, Mff, etc.) located on the mitochondrial outer membrane bind DRP1. DRP1 then self-assembles forming a concentric ring at the site of fission that constricts the mitochondrion leading to cleavage of both membranes.

(Mief1), and mitochondrial dynamics factor 49 (MiD49) (Otera et al., 2010; Palmer et al., 2011; Yoon et al., 2003; Zhao et al., 2011). While Fis1 and Mff have been implicated in promoting fission, there are conflicting reports concerning the roles of Mief1 and MiD49 where both inhibitory and permissive roles have been described illustrating the complexity of DRP1 recruitment to mitochondria (Otera et al., 2010; Palmer et al., 2011; Yoon et al., 2003; Zhao et al., 2011). Mitochondrial division then proceeds via the self-assembly of DRP1 into large ring-like structures at puncta on mitochondria that mechanically constrict the mitochondrion in a GTPase-dependent manner until both membranes are severed (Ingerman et al., 2005; Lackner et al., 2009; Mears et al., 2011).

1.9 - Mitochondrial fusion:

Mitochondrial fusion in mammals involves the activity of the Mfns (1 and 2) and OPA1 (Fig.8) (Cipolat et al., 2004; Song et al., 2009). Mfn 1 and 2 are paralogous proteins localized to the mitochondrial outer membrane that mediate its fusion (Chen et al., 2003; Rojo et al., 2002). Mouse embryonic fibroblasts (MEFs) lacking both Mfns have no fusion activity and contain a completely fragmented mitochondrial reticulum (Chen et al., 2003, Chen et al., 2007). However, single Mfn knockouts do display low levels of fusion implying that one can compensate for the other and that both isoforms participate in fusion (Chen et al., 2003; Chen et al., 2005). Outer membrane fusion is initiated by the formation of homotypic and heterotypic Mfn complexes *in trans* via their heptad

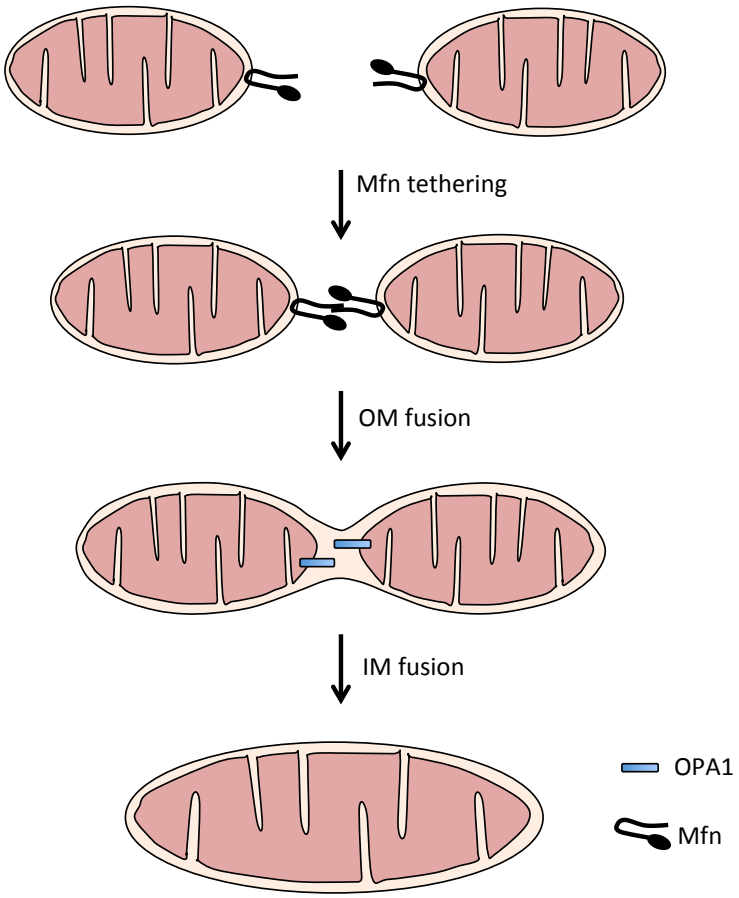

Figure 8: **Fusion of mitochondria**. For complete mitochondrial fusion, both the inner and outer membrane has to undergo fusion. Mitofusins (Mfn) on separate mitochondria initiate outer membrane fusion by forming homotypic or heterotypic interactions that ultimately leads to fusion of the outer membrane. Then OPA1 mediates inner membrane fusion to complete the process of mitochondrial fusion.

repeat regions (H. Chen et al., 2003; Koshiba et al., 2004). These interactions form a tether between adjacent mitochondria culminating in outer membrane fusion (Koshiba et al., 2004).

As two membranes enclose mitochondria, inner membrane fusion must follow for complete mitochondrial fusion and this process requires the inner membrane protein, OPA1 (Olichon et al., 2002, Olichon et al., 2003). Similarly to Mfn loss, mitochondria are fragmented and lack mitochondrial fusion following OPA1-silencing (Chen et al., 2005; Olichon et al., 2003). OPA1 overexpression studies have produced conflicting results concerning mitochondrial length, but elongation was observed in cells with more fragmented mitochondria (Chen et al., 2005; Cipolat et al., 2004; Misaka et al., 2002). Interestingly, this phenotype was not observed in cells lacking Mfns suggesting that fusion of each membrane are distinct events and that outer membrane fusion precedes inner membrane fusion (Cipolat et al., 2004). Further evidence for this notion came from a study showing that mitochondria from OPA1-knockout cells can fuse their outer membrane (Song et al., 2009). Although the mechanism linking OM and IM fusion has been discovered in yeast, no such link has been identified in mammals (Sesaki and Jensen, 2004).

1.10 – Mitochondrial IM dynamics:

The dynamic nature of mitochondria is not restricted to fusion and fission events rather mitochondria can also adopt diverse inner membrane topologies (reviewed in Mannella et al., 2013; Zick et al., 2009). For instance, dynamic

changes in cristae architecture are observed during apoptosis (Akao et al., 2003; Frezza et al., 2006; Germain et al., 2005; Kim et al., 2004; Scorrano et al., 2002; Sun et al., 2007). Mitochondria play a pivotal role in the intrinsic apoptosis pathway (reviewed in Bredesen et al., 2006). During apoptosis, proapoptotic factors such as cytochrome c are released from mitochondria triggering downstream apoptotic events. Scorrano and colleagues reported that upon induction of apoptosis cristae become wider and cytochrome c release increases (Frezza et al., 2006; Scorrano et al., 2002). One group also noted that cristae junction width can increase up to 3 fold (from 75nm to 250nm) in response to apoptotic stimuli (Germain et al., 2005). Since cristae contain the majority of cytochrome c, it is predicted that these changes are required for sufficient cytochrome c release and initiation of apoptosis (Frezza et al., 2006; Scorrano et al., 2002).

Before this observation during apoptosis, mitochondria were long known to remodel their ultrastructure in response to bioenergetic transitions (Hackenbrock, 1966). Specifically, a dynamic switch between two different morphologies was reported when isolated rat liver mitochondria transitioned between respiratory states III (high [ADP]) and IV (low [ADP]) (Fig.9) (Hackenbrock, 1966). Mitochondria in state IV had an enlarged matrix with narrow tubular cristae, which were called “orthodox” mitochondria (Hackenbrock, 1966). Whereas state III mitochondria were described as “condensed” containing a smaller matrix and wider cristae (Hackenbrock, 1966). The functional implications of these morphological changes are not known. However using

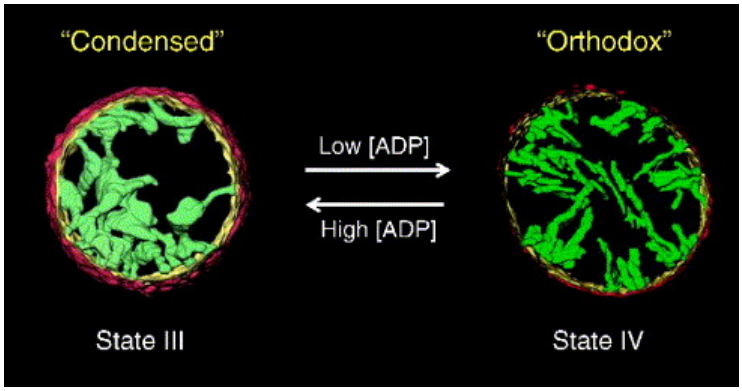

Figure 9: **Shifts in bioenergetics cause cristae remodeling**. From Mannella, 2006. Isolated rat liver mitochondria remodel their cristae as they transition between state III (high ADP) and state IV (low ADP). Specifically mitochondria display an "orthodox" morphology (enlarged matrix and narrow cristae) in state IV while mitohcondria in state III display a "condensed" morophology (condensed matrix and enlarged cristae).

computer simulations, it was found that [ADP] would become limiting within the enlarged cristae of state III mitochondria and its transport would diminish (Mannella et al., 2001). Therefore, the tightening of cristae under low [ADP] conditions could preserve ATP synthesis by increasing local concentrations of ADP (Mannella et al., 2013; Mannella, 2006; Mannella et al., 2001). Alterations in cristae morphology were also seen more recently under nutrient-poor conditions (Gomes et al., 2011a; Gomes et al., 2011b). Where MEFs grown in Hank's balanced salt solution (HBSS), a medium lacking amino acids, displayed an increase in the number of cristae per mitochondrial length (Gomes et al., 2011a; Gomes et al., 2011b). From the aforementioned studies, it is apparent that mitochondrial ultrastructure changes according to metabolic status, but whether this represents a form of metabolic regulation has yet to be seen.

1.11 –OPA1:

OPA1 is a ubiquitously expressed, highly conserved mitochondrial dynamin-related GTPase encoded by the *OPA1* gene on chromosome 3q28-q29 (Alexander et al., 2000; Delettre et al., 2000). Similar to dynamin, OPA1 contains the prototypical GTPase domain, middle domain and C-terminal GTPase effector domain (GED) as well as several coiled-coil (CC) domains termed, CC1, CC2 and CC0 (Fig.10A) (Belenguer and Pellegrini, 2013; Praefcke and McMahon, 2004). The CC1 and CC0 domains are located upstream of the GTPase domain while the CC2 domain is contained within the GED at the C-terminus. CC domains are known to self assemble and a previous study has shown that the

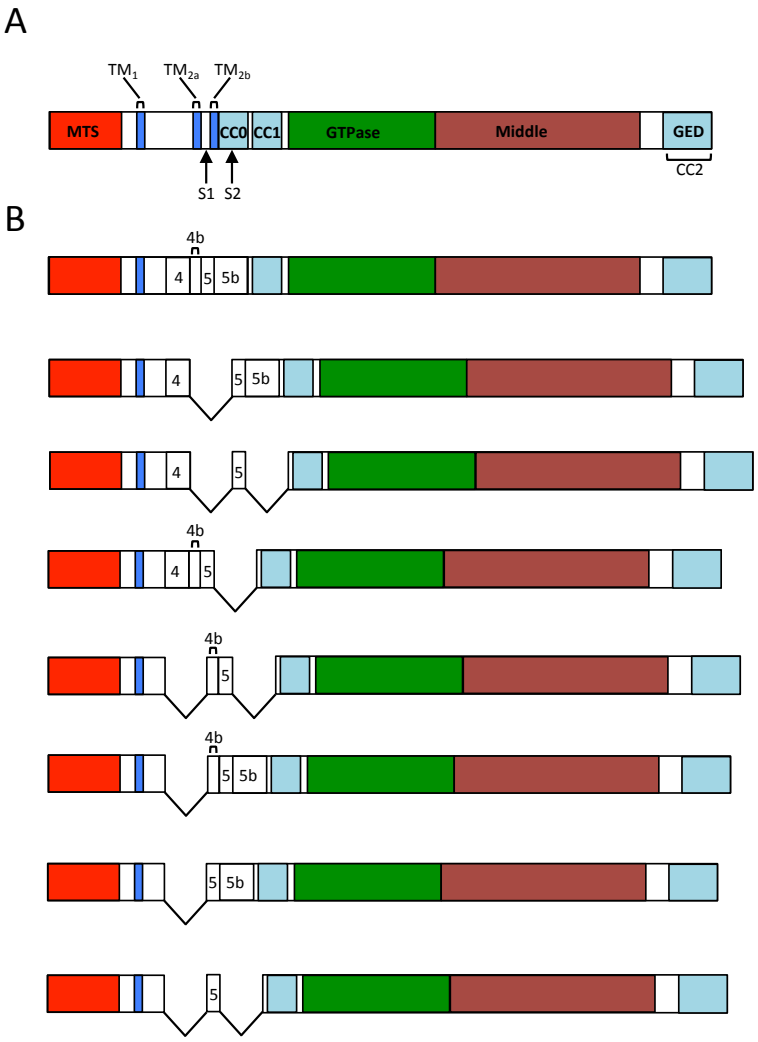

Figure 10: **OPA1 gene structure and splice variants.** (A) *OPA1* contains a GTPase domain, middle domain and GTPase-effector domain (GED). At its N-terminus, it also contains two coil-coiled domains (CC) involved with oligomerization and three transmembrane domains (TM) that enable interactions with the mitochondrial inner membrane. Being a mitochondrial protein, it also harbors a mitochondrial targeting sequence (MTS) that is cleaved by the mitochondrial processing peptidase upon entry within the mitochondrion. S1 and S2 are sites cleaved by mitochondrial proteases (paraplegin, PARL, etc.) causing the generation of both long-OPA1 and short-OPA1 (cleaved). (B) During transcription of the *OPA1* gene, exons 4, 4b and 5b are alternatively spliced leading to the generation of 8 different transcripts.

CC1 and CC2 domains of OPA1 can homo-oligomerize while the CC0 can hetero-oligomerize with CC1 (Akepati et al., 2008; Shin et al., 1999). Like most nuclear-encoded mitochondrial proteins, OPA1 contains a mitochondrial-targeting signal (MTS) at its N-terminus. It also harbors several transmembrane domains (TM1, 2a, and 2b) that enable interactions with the mitochondrial IM.

1.12 - OPA1 post-transcriptional and post-translational modifications:

Within the human *OPA1* gene, there are 30 coding exons (Delettre et al., 2001). Of these exons 4, 4b and 5b get alternatively spliced leading to the formation of 8 separate mRNA transcripts (Fig.10B) (Delettre et al., 2001). Following translation and import into mitochondria, the MTS of OPA1 is cleaved by the mitochondrial processing peptidase, giving rise to long OPA1 isoforms (L-OPA1). A subset of these L-OPA1 isoforms are processed further giving rise to short OPA1 isoforms (S-OPA1) (Cipolat et al., 2006; Ishihara et al., 2006; Song et al., 2007). Two cleavage sites, termed S1 and S2, were identified in exons 5 and 5b respectively (Ishihara et al., 2006). Thus far, four proteases are implicated in processing OPA1 at these sites (Cipolat et al., 2006; Head et al., 2009; Ishihara et al., 2006; Song et al., 2007). For instance, overexpression of the m-AAA protease, paraplegin, in HeLa cells increased OPA1 processing at S1 (Ishihara, et al, 2006). Also loss of the presenilin-associated rhomboid-like (PARL) protease impaired OPA1 processing (Cipolat, et al., 2006). Another metalloprotease, called OMA1 was also shown to cleave OPA1 at S1 when mitochondrial membrane potential is lost (Head et al., 2009). Furthermore,

Yme1L was shown to specifically process OPA1 at the S2 site (Song et al., 2007). The S-OPA1 isoforms, which lack TM domains, reside within the IMS whereas L-OPA1 remains associated with the IM with its N-terminus facing the matrix (Ishihara et al., 2006; Olichon et al., 2002; Satoh et al., 2003). Evidence suggests that proteolytic processing is necessary for OPA1 function (Song et al., 2007). For example, a combination of L-OPA1 and S-OPA1 are required to rescue mitochondrial morphology in OPA1-knockout cells (Song et al., 2007). One study employing transient OPA1 knockdown claimed that only L-OPA1 was required for fusion, but complete knockdown may not have been achieved (Ishihara et al., 2006). Taken together, it is clear that OPA1 is extensively processed both at the transcriptional and translational level affecting its localization and function.

1.13 - OPA1 and cristae structure regulation:

In addition to mitochondrial fragmentation, abnormalities in mitochondrial ultrastructure are observed following OPA1 knockdown (Olichon et al., 2003). This disorganization correlated with increased cytochrome c release and spontaneous apoptosis (Olichon et al., 2003). Later it was shown that OPA1 mediates cristae remodeling during apoptosis in a fusion-independent manner (Frezza et al., 2006). In their study they found that L-OPA1 and S-OPA1 isoforms assemble into oligomers whose disassembly correlates with apoptosis-induced crista junction dilation (Fig.11) (Frezza et al., 2006). Therefore, it was proposed that the oligomerization status of OPA1 correlated with crista junction width

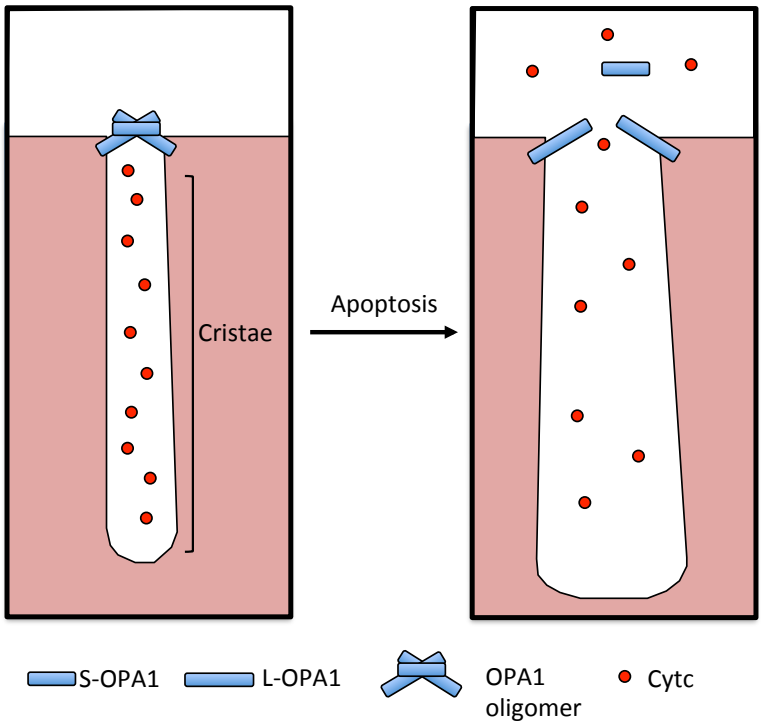

Figure 11: **Cristae remodeling during apoptosis correlates with changes in OPA1 oligomerization**. Adapted from Frezza et al., 2006. During apoptosis, crista junction width increases leading to the release of proapoptotic factors (eg cytochrome c [Cytc]). This remodeling of mitochondrial ultrastructure correlates with a decrease in OPA1 oligomers presumed to be present at crista junctions.

(Frezza et al., 2006). Further support for this model came from a study by Newmeyer and colleagues demonstrating that a disassembly-resistant OPA1 mutant (Q297V), that mimics the GTP-bound state and hyperoligomerizes, prevents cristae remodeling and cytochrome c release during apoptosis (Yamaguchi et al., 2008). These findings implicate OPA1 as a dynamic regulator of cristae structure.

1.14 - Metabolic OPA1-dependent cristae remodeling:

As mentioned before, Hackenbrock observed cristae remodeling in response to changes in bioenergetics (orthodox vs. condensed mitochondria) (Hackenbrock, 1966), however the role of OPA1-dependent cristae remodeling in this transition is not known. Therefore, our lab tested whether dynamic changes in OPA1 oligomerization occur in response to changes in bioenergetics. To investigate this, our lab assessed cristae architecture under nutrient-poor conditions. To simulate low nutrient conditions, MEFs were starved with Earl's balanced salt solution (EBSS), a medium lacking essential amino acids. Similar to the "orthodox" morphology of class IV mitochondria (low [ADP]), crista tightening was observed during starvation (Fig.12A-B) (Patten unpublished). Under the same conditions, an increase in OPA1 oligomerization was also observed suggesting that OPA1 may be involved (Fig.12C). A previous study demonstrated that OPA1-knockout MEFs are sensitized to starvation-induced cell death and have impaired mitochondrial respiration during starvation (Gomes et al., 2011). Findings from our lab show that expression of a fusion-incompetent,

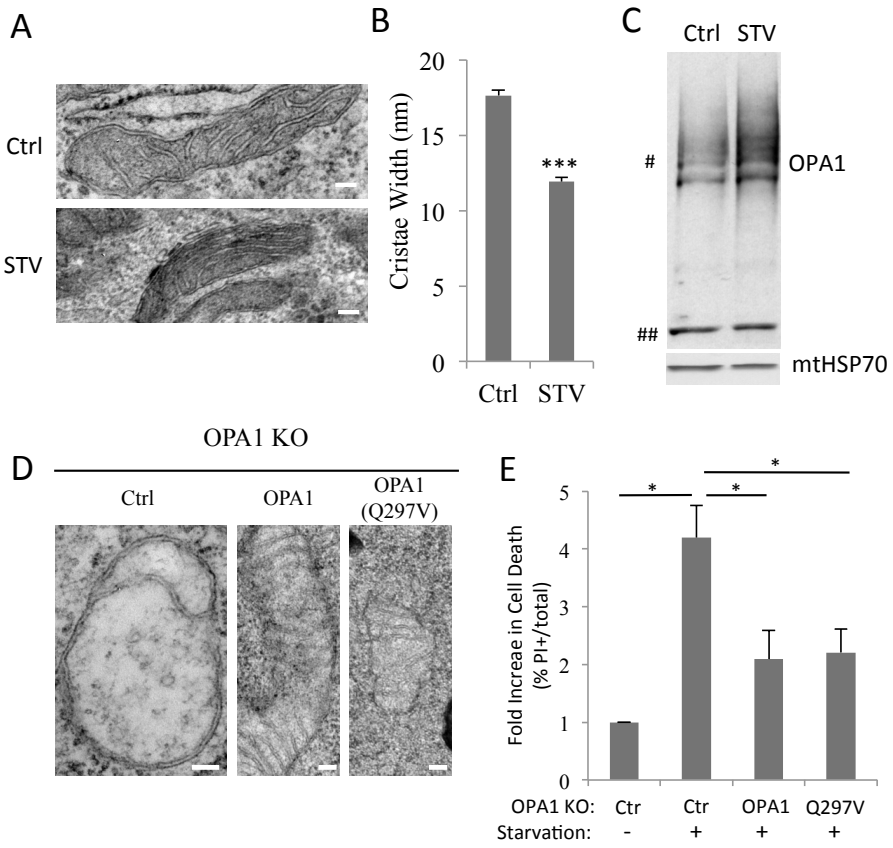

Figure 12: **Cristae remodeling during starvation is required for protection against starvation-induced cell death.** (A) Mitochondrial ultrastructure of mouse embryonic fibroblasts (MEF) either starved for 2 hours with EBSS (STV) or not (Ctrl) were visualized by transmission electron microscopy (TEM) following fixation with 2% paraformaldehyde and 1.6% glutaraldehyde. Scale bars represent 100nm. (B) Cristae width from all mitochondria in 20 cells (10 cells from two independent cultures) from (A) was measured (n = 20). (C) MEFs either starved for 2hrs with EBSS (Starved) or not (Control) were cross-linked with BMH and lysates were analyzed by western blot with the indicated antibodies to assess OPA1 oligomerization. (D) Representative TEM images of OPA1 knockout (KO) MEFs transiently transfected with GFP (Ctrl), OPA1, or OPA1-Q297V for 48hrs. Scale bars represent 100nm. (E) OPA1 KO MEFs were transiently transfected with GFP (Ctrl), OPA1, or OPA1-Q297V for 48hrs and either starved with EBSS for 6hrs or not. The cells were then stained with Hoechst and propidium iodide (PI) to measure cell death (n = 4). Error bars represent ±SEM and statistical significance was assessed using two-tailed student's t-tests (α = 0.05). (*) – $p<0.05$, (***) – $p<0.005$, (#) – OPA1 oligomers, and (##) – OPA1 monomers.

OPA1 mutant (Q297V) in OPA1 knockout MEFs rescues cristae structure (Fig.12D), sensitivity to starvation-induced cell death (Fig.12E), and oxygen consumption (Patten and Slack, unpublished). Recent findings from Scorrano's group also show that manipulating OPA1 oligomerization and cristae structure affects cellular respiration and assembly of respiratory chain supercomplexes (Cogliati et al., 2013). These findings combined present strong evidence for the involvement of OPA1-dependent cristae structure changes in regulating metabolism. For this to be possible however, OPA1 would have to sense changes in cellular bioenergetics to trigger changes in ultrastructure accordingly. The mechanism by which OPA1 senses the bioenergetic state of cell remains unknown.

1.15 – OPA1 and mtDNA maintenance:

Early studies examining the yeast homologues of OPA1, revealed that it was required for mtDNA maintenance (Diot et al., 2009; Jones & Fangman, 1992). Despite these findings in yeast, the link between OPA1 and mtDNA maintenance was only recently established (Chen et al., 2007). The original observation was made in OPA1 knockout MEFs where it was noted that many mitochondria lacked mitochondrial nucleoids (Chen et al, 2007; Chen et al, 2010). Further evidence came from studies on "ADOA-plus" patients harboring mutations in OPA1 (Amati-Bonneau et al., 2008; Hudson et al., 2008). The authors reported that these individuals had multiple deletions in their mtDNA (Amati-Bonneau et al., 2008; Hudson et al., 2008). It was later shown that

transient knockdown of OPA1 also lead to drastic decreases in mtDNA copy number suggesting that it served a direct role in mtDNA maintenance (Elachouri et al., 2011; Kushnareva et al., 2013). Support for this hypothesis came recently in a study where specific OPA1 transcripts containing exon 4, 4b or 5 were targeted via RNAi (Elachouri et al, 2011). They found that only knockdown of exon 4b transcripts lead to decreased mtDNA content and replication (Elachouri et al, 2011). Typically these transcripts are fully processed yielding S-OPA1 and a small N-terminal peptide (Song et al, 2007). Interestingly, they demonstrated that re-introduction of this N-terminal peptide was sufficient to rescue the mtDNA phenotype (Elachouri et al, 2011). From these findings, they proposed that the N-terminal fragment of OPA1 ensures maintenance of mtDNA through direct interactions with the mitochondrial nucleoid (Elachouri et al, 2011). To date, the molecular link between the nucleoid and OPA1 has not been identified.

1.16 – Validation of OPA1 interacting partners:

To gain further insight into OPA1 function, our lab globally identified OPA1-interacting partners using stable isotope labeling of amino acids in cell culture (SILAC) coupled with co-immunoprecipitation and mass spectroscopy (Patten and Slack unpublished). Using this approach we identified many putative OPA1 interactors including the AAA+ adenosine triphosphatase (ATPase), ATAD3A, and several solute-linked carrier 25 (SLC25) proteins (SLC25a10, SLC25a11, SLC25a12, and SLC25a13). Here I will elaborate on their function and how they may regulate OPA1 function, which is the subject of my thesis.

1.17 – ATPase Family AAA+ domain-containing protein 3A (ATAD3A):

ATAD3A is a ubiquitously expressed, mitochondrial AAA+ ATPase exclusively found in multicellular eukaryotes such as plants, mammals, and insects (Rousseau and Li, 2012). In humans, ATAD3A is encoded by the *Atad3A* gene on 1p36.33 and has undergone gene duplication events generating two paralogous genes termed ATAD3B and ATAD3C (Rousseau and Li, 2012). Like OPA1, it contains CC domains enabling oligomerization and a TM domain that anchors it within the mitochondrial inner membrane (Fig.13) (Gilquin et al., 2010a; Hubstenberger et al., 2010). However unlike most nuclear-encoded mitochondrial proteins, it lacks the prototypical MTS at its N-terminus (Gilquin et al., 2010a). Instead its mitochondrial localization was shown to depend on its C-terminus (Gilquin et al., 2010a). Topological analyses have confirmed that the C-terminus of ATAD3A faces the mitochondrial matrix, whereas its N-terminus is located in the IMS where it can interact with the mitochondrial outer membrane (Hubstenberger et al., 2010; Gilquin et al, 2010a). At the C-terminal end of ATAD3A there is a classical ATPase domain with Walker A and B domains involved with ATP binding and hydrolysis, respectively (Walker et al., 1982).

1.18 - ATAD3A function:

Since its identification, there have been several studies conducted to determine the function of ATAD3A (Gilquin et al., 2010a; Goller, 2013; J He et al., 2012; He et al., 2007; Hoffmann et al., 2009; Rone et al., 2012). For example, a role for ATAD3A in development has been identified as ATAD3A silencing

Figure 13: ***Atad3a*** **protein structure.** At its C-terminus, ATAD3A contains an ATPase domain with the classical Walker A (WA) and B (WB) domains that confer ATP binding and hydrolysis, respectively. Further upstream, it contains a transmembrane domain (TM) that enables interactions with the mitochondrial inner membrane. Closer to its N-terminus there are two coil-coiled (CC) domains that mediate protein-protein interactions.

causes growth defects and/or embryonic lethality (Gilquin et al., 2010a; Goller et al., 2013; Hoffmann et al., 2009). Several lines of evidence also suggest that it is important for steroidogenesis (Gilquin et al., 2010a; Rone et al., 2012). While other studies implicated ATAD3A in mitochondrial dynamics since its knockdown and mutation causes mitochondrial fragmentation (Gilquin et al., 2010a; Rone et al., 2012). In addition, there are several reports indicating that ATAD3A is important for mtDNA metabolism (He et al., 2007; 2012; Wang and Bogenhagen, 2006). Originally it was identified as a nucleoid-associated protein in two separate mtDNA nucleoid preparations (He et al., 2007; Wang & Bogenhagen, 2006). In one of those studies, the authors noted that nucleoid number was drastically reduced following transient knockdown of ATAD3A in 143B osteocarcinoma cells (He et al., 2007). However, only minimal changes in mtDNA copy number was observed leading them to conclude that the topology of mtDNA was being altered in the absence of ATAD3A (He et al., 2007). Nonetheless, a direct interaction between the D-loop of mtDNA and ATAD3A was established substantiating a direct role for ATAD3A in mtDNA metabolism (He et al., 2007). More recent findings indicate that ATAD3A interacts with mitochondrial ribosome and is required for mtDNA-specific gene translation (He et al., 2012). Due to its role in mtDNA metabolism, I was interested in examining the function of ATAD3A and OPA1 interactions in the context of mtDNA maintenance. These studies constitute part 1 of my thesis.

1.19 – The SLC25 protein family:

The SLC25 protein family also known as the mitochondrial carrier family is a large protein family containing more than 50 nuclear-encoded genes in humans (reviewed in Palmieri, 2004; 2011; 2013). The SLC25 proteins are primarily localized within the mitochondrial inner membrane. Their main function is to catalyze the transport of a wide variety of metabolites across the mitochondrial inner membrane (Palmieri, 2004; 2011; 2013). These metabolites serve important roles in a variety of metabolic processes such as OXPHOS, Kreb's cycle, gluconeogenesis, fatty acid synthesis, ketone body synthesis and many more (Palmieri, 2004; 2011; 2013). Typically transport is dependent on concentration gradients or the electrochemical gradient and the vast majority of transporters utilize an antiport mechanism (Palmieri, 2004; 2011; 2013). A tripartite structure defines the primary amino acid sequence of SLC25 proteins where three repeated domains of ~100 amino acids are arranged in tandem (Fig.14) (Aquila et al., 1987; F Palmieri, 1994; Runswick et al., 1987). Within each repeated domain there are two membrane-spanning hydrophobic alpha helices connected by a matrix linker (Saraste and Walker, 1982). Small cytosolic loops connect each repeated domain to one another leaving the N- and C-terminus facing the IMS (Capobianco et al., 1991; Saraste & Walker, 1982). From analyses with the ADP/ATP transporter, it was determined that the structure of SLC25 proteins dynamically transition between a "cytosolic" (c-) and "matrix" (m-) state during transport (Erdelt et al., 1972; Klingenberg & Buchholz, 1973; Klingenberg, 1979). In the c-state, the binding cavity faces the cytosol and

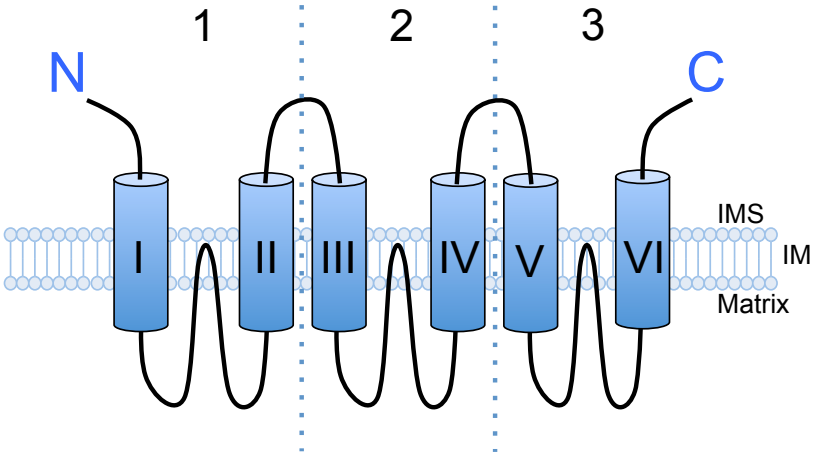

Figure 14: **Generic secondary structure of SLC25 proteins**. Cartoon depicting the classical tripartate structure of SLC25 proteins where three segments of ~100 amino acids are repeated in tandem (1-3). Each segment is connected to one another via a cytosolic loop and within each segments there are two hydrophobic α-helices (I-VI) connected by matrix linker sequences. (IMS) – intermembrane space, (IM) – mitochondrial inner membrane, (N) – N-terminus, and (C) – C-terminus.

allows entry of a cytosolic substrate (Klingenberg, 1979). Then the transporter will change conformation and adopt the “matrix” (m) state allowing release of the substrate into the matrix and binding of a matrix substrate (Klingenberg, 1979). This same transition in opposite order then occurs to complete the exchange. From this OPA1 interaction screen, the dicarboxylate carrier (DIC), 2-oxoglutarate carrier (OGC), and both aspartate- glutamate carrier isoforms (AGC1 and 2) were identified as putative OPA1 targets, which I will describe in further detail. The role of SLC25 proteins in OPA1 function constitutes part 2 of my thesis.

1.20 - The dicarboxylate and 2-oxoglutarate carrier (DIC and OGC):

In the human genome, the *SLC25A10* (DIC) and *SLC25A11* (OGC) genes are localized on chromosome 17q25.3 and 17p13.3, respectively (Gutiérrez-Aguilar & Baines, 2013; Palmieri, 2013). Both transporters are members of SLC25 protein subfamily responsible for transporting either di-/tri-carboxylates or keto-acids (Palmieri et al., 2011). Specifically, the DIC mediates the electroneutral exchange of malate or succinate from the matrix for cytosolic Pi or inorganic sulfur-containing compounds (Indiveri et al., 1989; Palmieri et al., 1971; Palmieri, 2004). The OGC imports malate or other dicarboxylates into the matrix in exchange for 2-oxoglutarate (Indiveri 1991; Palmieri et al., 1972; Palmieri, 2004). Physiologically, the DIC participates in gluconeogenesis, ureogenesis and fatty acid synthesis. Alternatively, the OGC serves an important role in the malate-aspartate shuttle, a mechanism that shuttles electrons from glycolysis into

mitochondria for use in the electron transport chain (Indiveri et al., 1987; Palmieri, 2004). In addition to the aforementioned substrates, genetic studies and transporter blockade have implicated both carriers in the transport of glutathione, an important antioxidant (Chen & Lash, 1998; Kamga et al., 2010; Lash et al., 2002; Wilkins et al., 2013; Zhong et al., 2008). Due to their potential interaction with OPA1 and involvement with diverse metabolic processes, it is possible that these transporters confer metabolic sensing to OPA1.

1.21 – The aspartate-glutamate carriers 1 and 2 (AGC1 and 2):

The *SLC25A12* (AGC1 or aralar1) and *SLC25A13* (AGC2 or citrin) genes are localized on chromosome 2q24 and 7q21.3 of the human genome, respectively (Gutiérrez-Aguilar & Baines, 2013; F. Palmieri, 2013). Both transporters belong to the subfamily of SLC25 proteins responsible for transporting amino acids across the mitochondrial inner membrane. There is ~78% sequence similarity between the two AGC isoforms and each display tissue-specific expression patterns (Kobayashi et al., 1999). For instance, AGC2 is widely expressed in many tissues whereas AGC1 expression is prevalent in the brain, heart and skeletal muscle (del Arco and Satrústegui, 1998; Kobayashi et al., 1999). Typically the AGCs catalyze the electrogenic co-transportation of glutamate and H+ from the cytosol to the matrix in exchange for aspartate (LaNoue et al., 1974; Palmieri, 2004; Palmieri et al., 2001). Like the OGC, the AGCs are a major molecular determinant of the malate-aspartate shuttle (Indiveri et al., 1987; Palmieri, 2004). They are also important for amino acid synthesis,

nucleotide synthesis and for the urea cycle (Palmieri, 2004). Unlike most SLC25 proteins, AGC1 and AGC2 contain several EF hand domains responsible for calcium binding at their N-terminus and previous studies show that their activity is indeed calcium-dependent (Palmieri et al., 2001). For this reason, they also belong to the Ca^{2+}-sensitive mitochondrial carrier subfamily (Gutiérrez-Aguilar and Baines, 2013). Genetic studies indicate that the AGCs are important for neuronal homeostasis and human disease (Jalil et al., 2005; Kobayashi et al., 1999; Palmieri, 2008; Yasuda et al., 2000). For instance, AGC1 knockout mice display various abnormalities including stunted growth, poor motor coordination, tremors, decreased myelination in the central nervous system, and shortened life span (Jalil et al., 2005). Deficiency of AGC2 caused by mutations in the *SLC25A13* gene is linked to the development of adult-onset type II citrullinemia and neonatal intrahepatic cholestasis (Kobayashi et al., 1999; Palmieri, 2008; Yasuda et al., 2000). Like the DIC and OGC, these transporters could also represent a metabolic sensor that regulates OPA1.

Part 1: The role of ATAD3A and OPA1 interactions in mtDNA maintenance.

Given that ATAD3A is implicated in mtDNA metabolism (He et al., 2007, 2012; Wang and Bogenhagen, 2006) and that it was identified in our OPA1 interaction screen (Patten and Slack, unpublished), I hypothesize ATAD3A and OPA1 interactions are required for mtDNA maintenance. I have three main objectives to address this hypothesis. 1) I would validate the interactions between ATAD3A and OPA1 by co-immunoprecipitation. 2) Then I would analyze

the function of ATAD3A in mitochondrial dynamics and mtDNA maintenance using overexpression and knockdown approaches. 3) Finally, I would determine if disrupting ATAD3A and OPA1 interactions is sufficient to impair mtDNA maintenance.

Part 2: The role of OPA1 and SLC25 protein interactions in sensing cellular bioenergetics.

Our lab has shown that changes in OPA1 oligomerization and cristae structure are triggered by nutrient availability (eg. starvation) and that several SLC25 proteins, which are responsible for nutrient transport, were identified as OPA1 interactors (Patten and Slack, unpublished). Given these findings, I hypothesize that OPA1 senses the bioenergetics state of the cell through interactions with SLC25 proteins and alters cristae structure to modulate metabolism according to nutrient availability. To address this hypothesis, I have three main objectives. 1) I would validate the interactions between OPA1 and the SLC25 proteins (DIC, OGC, AGC1, and AGC2) identified in our screen by co-immunoprecipitation. 2) Then I would assess the consequence of SLC25 protein inhibition and knockdown on OPA1 oligomerization and cristae structure. 3) Finally, I would correlate changes in OPA1 oligomerization and cristae structure to changes in respiratory chain supercomplexes and ATP synthase assembly.

CHAPTER 2: MATERIALS AND METHODS

2.1 - Plasmids and molecular cloning:

ATAD3A-FLAG was generated from cDNA amplified via polymerase chain reaction (PCR) from the CMV-Sport6-ATAD3A expression vector (Thermo scientific). A NotI and EcoRI restriction site was added to the forward and reverse primer, respectively. The reverse primer also contained the coding sequence for 1XFLAG (Asp-Tyr-Lys-Asp-Asp-Asp-Asp-Lys-Stop). Mito-YFP-FLAG and DIC-FLAG were also generated from cDNA PCR amplified from the pCMV-OCT-YFP vector (generous gift from Dr. Heidi Mcbride (Harder et al., 2004)) and CMV-Sport6-DIC (Thermo scientific), respectively. The amplicons from each reaction were then separated via gel electrophoresis on 1% agarose gels and purified with the Illustra GFX PCR DNA and gel band purification kit (GE Healthcare). For ATAD3A-FLAG, the amplicon and empty pcDNA3.1+ expression vector (Invitrogen) were incubated with both EcoRI (New England BioLabs) and NotI (New England BioLabs) restriction enzymes overnight at 37^{o}C. After purification, the resulting fragment and linearized vector were ligated together with T4 DNA ligase (New England BioLabs). For the other vectors, each amplicon was ligated into the pGEM-T-easy vector (Promega) and cleaved with EcoRI (New England BioLabs) alone overnight at 37^{o}C. The resulting fragments were then resolved on a 1% agarose gel, purified and finally ligated via T4 DNA ligase (New England BioLabs) into EcoRI-cleaved 3XFLAG-CMV-14 expression vector (Sigma-Aldrich). Directionality of the inserts was validated using restriction analysis. The StemCore DNA sequencing and Microarray Facility (http://www.stemcore.ca) sequenced the final vector.

Other plasmids used were the pLKO.1-puro-shCont (Sigma-Aldrich) and the pLKO.1-puro-shATAD3A (Sigma-Aldrich) vectors used for the generation of stable cell lines, analysis of mtDNA and mitochondrial length. Also the CMV-Sport6-ATAD3A (Thermo Scientific) and pcDNA3.1+ vectors (Invitrogen) were used to test the effect of ATAD3A overexpression on mitochondrial length. Lastly, OGC-FLAG, AGC1-FLAG and AGC2-FLAG were previously generated by D. Patten in our lab and utilized in the co-immunoprecipitation experiments.

2.2 - Cell Culture and transfection:

MEFs (generous gift from Dr. Scorrano (Gomes et al., 2011a)), highly transfectable MEFs (HT-MEFs) and HeLa cells were propagated in cell culture at 37^{o}C and 5% CO_2. The culture medium used was high glucose, Dulbecco's modified Eagle's medium (DMEM) (Wisent) containing 10% heat inactivated fetal bovine serum (FBS) (Wisent, Cat.#: 080-150), 50 u/mL penicillin/streptomycin (Gibco), and 2 mM glutamine (Gibco). To transfect expression or shRNA constructs, MEFs were plated at 90-95% confluency and transfected using Lipofectamine 2000 transfection reagent (Invitrogen) according to the manufacturer's specifications. For generation of shRNA stable cell lines, growth medium was replaced with DMEM containing puromycin (2 µg/mL) 24hrs post-transfection and maintained for 2 weeks. These cells were then split into 96-well dishes and clones stably expressing shRNA were selected over the span of 3-4 weeks. To generate HT-MEFs, the pLKO.1-puro-shCont construct was transfected into MEFs and single clones were selected with puromycin as

described above. To transfect siRNA oligonucleotides, MEFs and HeLa cells were grown to ~50% confluency and the siLentfect transfection (Bio-Rad) reagent was used according to the manufacturer's specifications. Each siRNA oligonucleotide was used at a final concentration of 20nM. Silencer Select siRNA control #1 (siCtr) (Ambion, Cat.#: 4390843), Silencer Select OGC siRNA s85783 (siOGC) (Ambion, Cat.#: 4390771), ATAD3A siRNA (siATAD3A) (Dharmacon custom siRNA, GAAGUUGCUCCAUUUGUCC[dTdT] (Gilquin et al., 2010b)) and a scrambled Control siRNA-A (siCtr) (Santa Cruz, sc37007) were used.

2.3 - Immunofluorescence Analysis:

MEF lines were plated onto coverslips and incubated for 48 hrs at 37°C. For the serum starvation experiments, growth medium was replaced with DMEM lacking FBS 24 hrs after plating onto coverslips and then incubated for 16 hrs at 37°C. The cells were then fixed with 4% PFA for 30 min at room temperature. Primary antibodies were diluted into 1° antibody solution (phosphate-buffered saline (PBS), 1% triton X100, and 1% bovine serum albumin) and applied onto coverslips for 1 hr. Coverslips were then washed with PBS three times and incubated with fluorophore-conjugated secondary antibodies diluted in PBS for 1 hr. Finally, the coverslips were mounted onto slides with Shandon Immu-Mount (Thermo Scientific) and dried overnight. Images were taken with a 63X objective using a LSM 510 META/AxioVert 200 confocal microscope (Zeiss) and Zen imaging software (Zeiss). Mitochondrial length measurements were performed with ImageJ software (National Institutes of Health; http://rsb.info.nih.gov/ij/).

2.4 - Western Blot Analysis:

Whole-cell protein lysates were prepared by mechanically breaking apart cells with 10 strokes of a 25-gauge syringe in lysis buffer (10 mM Tris-HCl pH 7.4, 150 mM NaCl, 1 mM EDTA, and 0.5% Triton X-100) containing CLAAP protease inhibitors (Sigma-Aldrich). Cellular debris was cleared by centrifugation at 12,900 x g for 10 min at 4^{o}C. For mitochondrial lysates, protein was extracted from isolated mitochondria using the above lysis buffer containing CLAAP protease inhibitors (Sigma-Aldrich). Protein concentration was measured using the Bradford assay (Bio-Rad). SDS loading buffer (31.25 mM tris pH 6.8, 1% SDS, 5% glycerol, 0.025% bromophenol blue and 312.5 mM BME) was then diluted into each sample, boiled for 10min and separated by SDS-PAGE. BLUeye prestained protein ladder (FroggaBio) was used as a size reference. Separated protein was transferred onto 0.2 µm nitrocellulose membranes (Bio-Rad), blocked with tween 20 phosphate buffered saline (T-PBS) containing 5% skim milk, washed with T-PBS and immunoblotted with the indicated primary antibodies. For protein detection, secondary antibodies conjugated with horseradish peroxidase (HRP) and Immobilon HRP chemiluminescent substrate (Millipore) were applied. Densitometric analyses were performed using ImageJ software (National Institutes of Health; http://rsb.info.nih.gov/ij/).

2.5 - Antibodies:

For immunofluorescence analysis and/or western blot analysis the following primary antibodies were used: polyclonal rabbit anti-TOM20 (Santa

Cruz Biotech), monoclonal mouse anti-mtHsp70 (ABR Bioreagents), M2 monoclonal mouse anti-FLAG (Sigma Aldrich), monoclonal mouse anti-OPA1 (BD Biosciences), polyclonal rabbit anti-OPA1 (Abcam), polyclonal rabbit anti-ATAD3A (generous gift from Dr. Jacques-Baudier (Gilquin et al., 2010a)), monoclonal mouse anti-actin (Sigma-Aldrich), monoclonal mouse anti-NDUFA9 (Life Technologies), polyclonal rabbit anti-OGC (Abcam), monoclonal mouse anti-ATP5A (Abcam) and monoclonal mouse anti-complex II 70 kDa Fp subunit (Life Technologies). For Immunofluorescence, DyLight 594 AffiniPure donkey anti-mouse IgG (H+L) (Jackson Immuno), Alexa Fluor 594-AffiniPure Donkey anti-rabbit IgG (H+L) (Jackson Immuno), and Alexa Fluor 488-AffiniPure Donkey anti-rabbit IgG (H+L) (Jackson Immuno) secondary antibodies were used. For Western blot analysis, HRP-conjugated goat anti-mouse (H+L) (Pierce) and HRP-conjugated goat anti-rabbit (H+L) (Pierce) secondary antibodies were used.

2.6 - Co-immunoprecipitation with whole-cell lysates:

HT-MEFs were transiently transfected with OCT-YFP-FLAG, DIC-FLAG, OGC-FLAG, AGC1-FLAG, AGC2-FLAG, or ATAD3A-FLAG constructs. Protein was harvested 24hrs post-transfection with lysis buffer (50 mM Tris-HCl pH 7.4, 150 mM NaCl, 1 mM EDTA, and 1% TRITON X-100) containing CLAAP protease inhibitors (Sigma-Aldrich). Immunoprecipitations were performed with ANTI-FLAG M2 magnetic beads (Sigma-Aldrich) using 2mg of protein lysate. Samples were incubated overnight and the beads were washed 4 times with Tris-buffered saline (TBS) (50 mM Tris-HCl pH 7.4, and 150 mM NaCl) containing CLAAP

protease inhibitors. Immunoprecipitated protein was then eluted from the magnetic beads twice with 20µl of elution buffer (50 mM Tris-HCl pH 7.4, 150 mM NaCl, and 150 ng/µl FLAG peptides [Sigma Aldrich]). The elutions were then analyzed by western blot with the indicated antibodies.

2.7 - Co-immunoprecipitations with mitochondrial lysates:

MEF mitochondrial extracts from two confluent 150 mm dishes (~3.0 X 10^7 cells) were used per sample for the endogenous OPA1 immunoprecipitation. The extracts were lysed with lysis buffer (50 mM Tris-HCl pH 7.4, 150 mM NaCl, 1 mM EDTA, and 1% 3-[(3-Cholamidopropyl)dimethylammonio]-1-propanesulfonate hydrate (CHAPs)) containing CLAAP protease inhibitors (Sigma-Aldrich), and incubated at 4^{o}C overnight with no antibody, normal mouse IgG (Santa Cruz), or mouse monoclonal anti-OPA1 (BD Biosciences). After which, 20µl of protein A/G magnetic beads (Pierce) were added to each sample and incubated at room temperature (RT) for 1hr. Afterwards, the beads were separated with a magnetic stand and washed 4 times with TBS (50 mM Tris-HCl pH 7.4, and150 mM NaCl). Protein was eluted from the beads by incubating them with SDS loading buffer for 20 min at room temperature and then analyzed by western blot.

2.8 - DNA extraction and quantitative PCR (q-PCR):

DNA was isolated from shCont and shATAD3A MEFs using a phenol-chloroform extraction protocol adapted from (Guo et al., 2009). Confluent 35mm

plates (~1.60 X 10^5 cells) of shCont or shATAD3A MEFs were lysed with 500µl of DNA extraction buffer (10 mM Tris-HCl pH 8.0, 1 mM EDTA, and 0.1% SDS) and vortexed vigorously. Each sample was then treated with 50 µl of 20 mg/ml proteinase K (Invitrogen) and incubated overnight at 55^{o}C. The samples were then vigorously vortexed again and centrifuged at 10,600 x g for 15 min at room temperature. The supernatants were then transferred to new microcentrifuge tubes and 500 µl of phenol/chloroform/isoamyl alcohol (25:4:1 v/v) was added to each sample. After extensive vortexing, the samples were centrifuged again at 10,600 x g for 15min. An equal volume of chloroform was then added to the supernatants of each sample and vortexed. Following centrifugation at 10,600 x g for 15 min, 400 µl of the supernatant was transferred to new microcentrifuge tubes and 40 µl of 3 M sodium acetate and 440 µl of pure isopropanol were added. The samples were then incubated at -20^{o}C for 30 min. Precipitated DNA was pelleted by centrifugation at 10,600 x g for 15 min and the DNA pellet was washed 2X with 70% ethanol. Each pellet was then air dried, re-suspended in nuclease-free water and incubated at 55^{o}C for 10 min. DNA concentrations were determined using a Nanodrop 2000 spectrophotometer (Thermo Scientific). QPCR was carried out in a Rotor-Gene-Q Real-time PCR cycler (Qiagen) using 50 ng of DNA and the PerfeCta SyBr Green FastMix kit (Qiagen). The data was then analyzed using Rotor Gene Q series software (Qiagen). The PCR program was comprised of 40 cycles of 10 sec at 95^{o}C for DNA denaturation, 30 sec at 57^{o}C for primer annealing and 30 sec at 72^{o}C for primer elongation. Each PCR reaction was carried out in triplicate and levels of the cytochrome c oxidase

subunit I (COI) and NADH dehydrogenase subunit 6 gene (complex I) were normalized to 18S rRNA gene abundance. The primer sequences used for qPCR are listed in table 1. The complex I primer sequences came from (Furda et al., 2012) and both the COI and 18S rRNA primer sequences came from (Tal et al., 2009).

2.9 - Mitochondrial nucleoid quantification:

MEFs and HeLa cells were plated onto coverslips and grown for 48 hrs at 37^{o}C. To visualize mtDNA nucleoids, the Quant-iT PicoGreen dsDNA reagent (Invitrogen) stock was added to the cells at a 1:500 dilution and incubated for either 50 min (MEFs) or 40 min (HeLa cells) at 37^{o}C. To stain mitochondria, MitoTracker Red CM-H_2XROS (Invitrogen) was prepared according to manufacturers specifications and added to the cells at a 1:500 dilution following PicoGreen incubation and incubated for an additional 10 min at 37^{o}C. Then the DMEM containing the stains were washed out with PBS, replaced with phenol red-free DMEM (Wisent, Cat.# 319-050-CL) and incubated again for 10 min at 37^{o}C. Live cells were mounted onto coverslips with phenol red-free DMEM and visualized through a 63X objective with an Axio Imager M2 fluorescence microscope (Zeiss). Z-stack images were obtained with an AxioCam MRm camera (Zeiss) and Axio Image software (Zeiss). Image J software (National

qPCR primers	Nucleotide sequence (5’ to 3’)
COI - F	GCCCCAGATATAGCATTCCC
COI - R	GTTCATCCTGTTCCTGCTCC
Complex I - F	CCCAGCTACTACCATCATTCAAGT
Complex I - R	GATGGTTTGGGAGATTGGTTGATGT
18s rRNA - F	TAGAGGGACAAGTGGCGTTC
18s rRNA - R	CGCTGAGCCAGTCAGTGT

Table 1: **Primers used for mtDNA quantification by qPCR.** (F) – forward, (R) – reverse, (rRNA) – ribosomal RNA, and (COI) – cytochrome c oxidase subunit 1.

Institutes of Health; http://rsb.info.nih.gov/ij/) was then used to generate image stacks and to count nucleoid number. In figure 21, cells were visualized with an Axioskop 2 MOT fluorescence microscope using a 100X objective and images were taken with a QICAM Fast 1394 camera.

2.10 - Cell fractionation:

Liver extracted from either CD1 or C57/B6 mice were suspended in HIM buffer (200 mM mannitol, 70 mM sucrose, 10 mM HEPES, 1 mM EDTA, pH 7.5) and lysed in a 2 ml dounce with 8 strokes. MEFs and HT-MEFs were pelleted, resuspended in HIM buffer and lysed with 15 strokes in a 25-gauge syringe. Lysates from both HT-MEFs and mouse liver were then centrifuged at 110 x g for 9 min at 4^{o}C to pellet nuclei and cellular debris. Afterwards, the supernatants were transferred to new microcentrifuge tubes and centrifuged again at 8600 x g for 9 min at 4^{o}C to pellet mitochondria. The mitochondrial pellet was then resuspended with HIM buffer and the previous spin steps were repeated to remove contaminating nuclei and cellular debris. Finally, the mitochondrial pellet was resuspended with HIM buffer again and protein concentration was measured using the Bradford assay (Bio-Rad).

2.11 - Mitochondrial cross-linking and analysis of OPA1 oligomerization:

OPA1 oligomerization was analyzed using a protocol adapted from (Frezza et al., 2006). Isolated mitochondria were pelleted and re-suspended in sucrose buffer (0.2 M sucrose, 10 mM Tris-MOPS pH 7.4, and 10 μM EGTA)

containing phenylsuccinate (15 mM or 50 mM), butylmalonate (15 mM or 50 mM), complex I substrates (5 mM malate, 5 mM glutamate, 0.08 mM ADP, and 2 mM K_2HPO_4), complex II substrates (5 mM succinate, 0.08 mM ADP, and 2 mM K_2HPO_4), no substrates (0.08 mM ADP and 2 mM K_2HPO_4), or no additives with or without 2 μM rotenone. Once re-suspended, the mitochondria were incubated for 30 min or 1 hr at 37^{o}C. Mitochondria were then cross-linked with 1 mM (liver mitochondria) or 0.4 mM (MEF mitochondria) 1-Ethyl-3-[3-dimethylaminopropyl] carbodiimide hydrochloride (EDC) for 30 min at room temperature to crosslink protein. The crosslinking reaction was quenched with 100 mM (liver mitochondria) or 80 mM (MEF mitochondria) β-mercapto-ethanol (BME) and the samples were centrifuged at 8600 x g for 9 min at 4^{o}C to pellet mitochondria. The cross-linked mitochondrial pellets were then re-suspended in 1X NuPAGE LDS sample buffer (Invitrogen), boiled for 10 min, resolved on NuPAGE Novex 3-8% tris-acetate protein gels (Invitrogen) and analyzed by western blot.

2.12 - Cytochrome c distribution assay:

Cytochrome c distribution was analyzed according to a protocol adapted from (Wasilewski et al., 2012). Isolated mouse liver or HT-MEF mitochondria were incubated with sucrose buffer containing substrates, inhibitors, no substrates or no additives as described above. Then the mitochondria were treated with 0.1% digitonin (1 μg:1 μg mitochondria) and rocked for 30 min at 4^{o}C. Subsequently, the samples were centrifuged at 10,000 x g for 10 min at 4^{o}C

to separate the supernatant (IMS contents) and pellets (mitoplasts). Each fraction was then analyzed by western blot with the indicated antibodies.

2.13 - Blue native polyacrylamide gel electrophoresis (BN-PAGE):

Supramolecular ATP synthase and respiratory chain assemblies were examined using a BN-PAGE protocol adapted from (Wittig et al., 2006). Isolated mouse liver mitochondria were incubated with sucrose buffer containing substrates, inhibitors, no substrates or no additives as described above. Mitochondria were then pelleted by centrifugation at 8600 x g and lysed with digitonin lysis buffer (50 mM imidiazole/HCl pH 7.0, 50 mM NaCl, 5 mM 6-aminohexanoic acid, 1 mM EDTA and 1% digitonin [8 µg:1 µg of mitochondria]) for 30 min on ice with light pipetting every 10 min. The lysates were then centrifuged at 20,800 x g for 30 min and the supernatants were supplemented with coomassie brilliant blue G-250 loading dye at a detergent:dye ratio of 10 (loading dye stock: 250 mM 6-aminohexanoic acid, 50% glycerol, and 2.5% coomassie brilliant blue G-250). Gradient gels (3-13%) were casted and 75 µg of each sample were loaded. For the first 2 hrs, the gels were run at 150 V with cathode buffer B (50 mM tricine, 7.5 mM Imidazole, and 0.02% coomassie brilliant blue G-250) at 4^{o}C. Afterwards, the buffer was replaced with cathode buffer B/10 (50 mM tricine, 7.5 mM imidazole and 0.002% coomassie brilliant blue G-250) and run overnight at 200 V at 4^{o}C. The gels were then transferred onto 0.2 µm nitrocellulose membranes (Bio-Rad) for 2 hrs at room temperature at

500 mA. Membranes were blocked with T-PBS containing 5% skim milk, washed with T-PBS and analyzed by western blot.

2.14 - Statistical analysis:

A two-tailed unpaired student's t-test or one-way analysis of variance (ANOVA) with Tukey's post-hoc test was used to determine statistical significance between means ($\alpha=0.05$).

CHAPTER 3: RESULTS

Part 1: The role of ATAD3A and OPA1 interactions in mtDNA maintenance

3.1 - OPA1 and ATAD3A interact in MEFs:

In the following experiments I sought to validate the interaction between OPA1 and ATAD3A by co-immunoprecipitation. To achieve this, I constructed and overexpressed both FLAG-tagged ATAD3A and mito-YFP in HT-MEFs. After 24hrs, the cells were lysed and these exogenously expressed proteins were immunoprecipitated to determine if OPA1 co-immunoprecipitates with ATAD3A-FLAG (Fig.15A). As previously shown in our laboratory (Patten and Slack unpublished), OPA1 specifically co-immunoprecipitates with overexpressed ATAD3A-FLAG with minimal OPA1 signal detected in the mito-YFP-FLAG overexpression sample. Interaction of endogenous proteins was also confirmed by immunoprecipitating endogenous OPA1 from isolated MEF mitochondria and probing for endogenous ATAD3A. Endogenous ATAD3A signal was observed in the sample containing immunoprecipitated OPA1, whereas the no antibody and normal mouse IgG controls completely lacked ATAD3A signal (Fig.15B). These results confirm that ATAD3A and OPA1 do form a complex in MEFs and validate the findings from the SILAC screen, in search of OPA1 targets (Patten and Slack, unpublished).

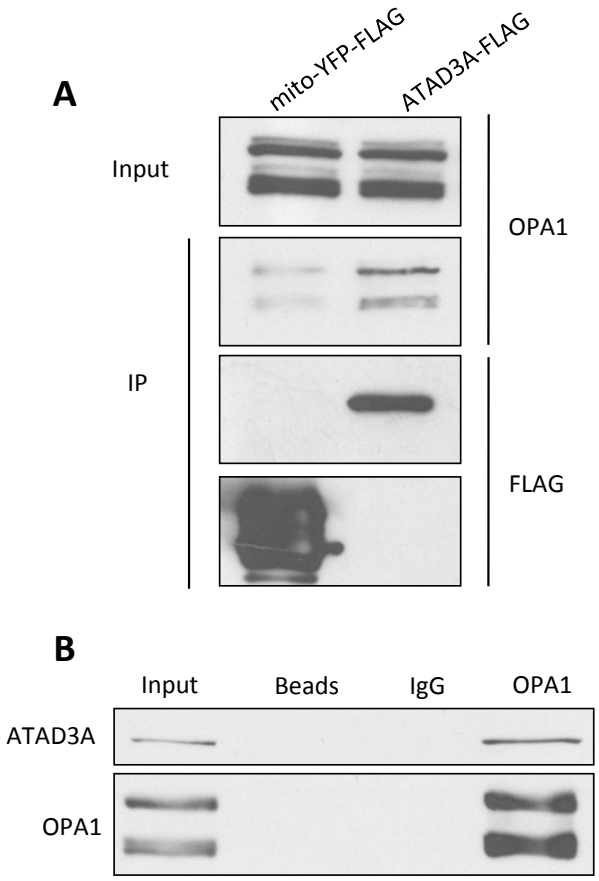

Figure 15: **OPA1 interacts with ATAD3A in MEFs.** (A) ATAD3A-FLAG and mito-YFP-FLAG were transiently transfected into HT-MEFs. 24 hrs post-transfection, the cells were lysed and the FLAG-tagged proteins were immunoprecipitated. The eluted samples and 25 µg of input were then analyzed by western blot for OPA1. (B) Endogenous OPA1 was immunoprecipitated from MEF mitochondrial lysates and eluted with SDS loading buffer. The eluted samples and 2% input were analyzed by western blot. (IP) – corresponds to immunoprecipitates.

3.2 - Alterations in ATAD3A expression has minimal effect on mitochondrial length in MEFs:

Following validation, I examined the function of ATAD3A. Given that ATAD3A knockdown was shown to modify mitochondrial structure, I asked whether manipulations of ATAD3A expression affects mitochondrial length (Gilquin et al., 2010a; Rone et al., 2012a). I assessed the effects of ATAD3A overexpression by co-transfecting MEFs with either CMV-Sport6-ATAD3A or pcDNA3.1+ (empty vector) (2.5 µg), and limiting amounts of mito-YFP-FLAG (0.5 µg) to serve as a marker of overexpression for 48hrs. ATAD3A overexpression was confirmed by western blot 48hrs post-transfection, where an ~ 2 fold increase in expression was observed in a band between 63 kDa and 75 kDa (Fig.16C). Using TOM20 and mtHsp70 antibodies, mitochondria were visualized by immunofluorescence with a confocal microscope. Mitochondrial length was then measured with ImageJ software using all mitochondria from YFP-positive cells and each measurement was binned into different categories based on their length (<1 µm, 1-2 µm, 2-3 µm and >3 µm). The number of mitochondria in each category was then expressed as a percentage per cell. Overexpression of ATAD3A did not significantly alter the proportion of mitochondria in any of the categories suggesting that an elevated level of ATAD3A does not affect mitochondrial length (Fig.16A and B, $n = 3$). To assess whether knockdown of ATAD3A affected mitochondrial length, MEFs were transfected with a scrambled short hairpin RNA (shCont-1 and -2) or an shRNA

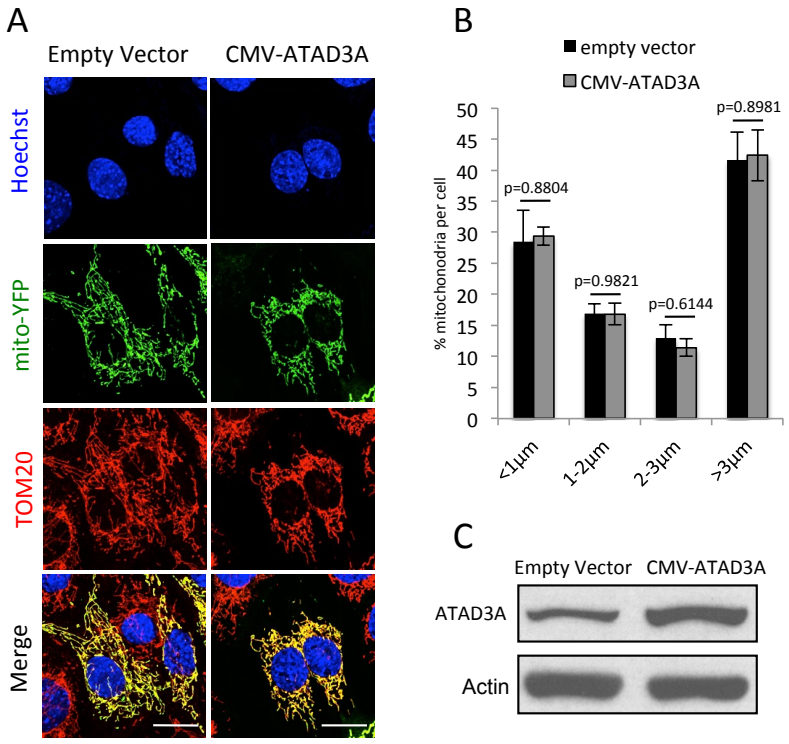

Figure 16: **Overexpression of ATAD3A in MEFs does not affect mitochondrial length**. MEFs were co-transfected at 5:1 with either ATAD3A-CMV-sport-6 (CMV-ATAD3A) or empty pcDNA3.1+ (empty vector), and mito-YFP-FLAG. Cells were then analyzed by immunofluorescence for the indicated markers 72 hrs post-transfection. (A) Representative images displaying mitochondrial morphology of MEFs transfected with the indicated vectors. Scale bars represent 20 µm. (B) The length of mitochondria from (A) were measured, binned into the indicated categories, and presented as a percentage per cell. (C) ATAD3A expression in cells transfected with empty vector or CMV-ATAD3A was validated by western blot analysis. Bars represent the average ± SEM (n = 3). Statistical significance was assessed using a two-tailed student's t-test ($\alpha = 0.05$) and non-significant p-values are displayed.

targeting ATAD3A (shATAD3A-1) and stable clones were selected with puromycin. Almost complete ATAD3A knockdown was confirmed by western blot in parallel samples (Fig.17C). As before, mitochondria were stained with TOM20 and mtHsp70, however, mitochondria from all cells in a given field were measured, binned into categories and expressed as a percentage per cell. In contrast to previous findings (Gilquin et al., 2010a; Rone et al., 2012a), the proportion of mitochondria in each category was not significantly different indicating that reduced ATAD3A expression also has no effect on mitochondrial morphology (Fig.17A and B, *n = 3*).

Previous findings have shown that mitochondrial morphology changes at various points within the cell cycle (Mitra et al., 2009). Given that, my previous measurements were performed on an unsynchronized population of cells, I asked if differences could be detected if cells were serum-starved. These experiments were, therefore, repeated as before, but following 16hrs serum-starvation. After serum-starvation, the proportion of mitochondria in each category remained unaltered in MEFs transfected with CMV-Sport6-ATAD3A substantiating that ATAD3A overexpression has no effect on mitochondrial length (Fig.18, *n = 3*). Serum-starved shATAD3A MEFs also displayed no significant difference in any of the size categories when compared to shCont MEFs (Fig.19, *n = 3*). Taken together, it is clear that alterations in ATAD3A expression have minimal effect on mitochondrial length.

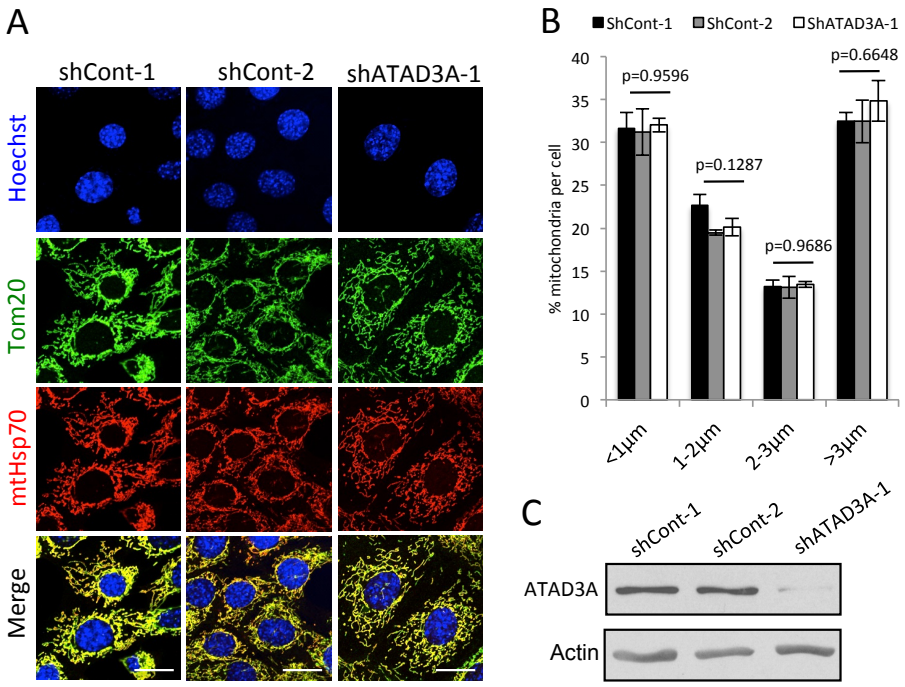

Figure 17: **Stable knockdown of ATAD3A does not affect mitochondrial length in MEFs.** ShCont and shATAD3A MEFs were analyzed by immunofluorescence for the indicated markers 48 hrs after plating onto coverslips. (A) Representative images displaying mitochondrial morphology of shCont and shATAD3A MEFs. Scale bars represent 20 µm. (B) The length of mitochondria from (A) were measured, binned into the indicated categories, and presented as a percentage per cell. (C) Whole cell lysates from shCont and shATAD3A MEFs were analyzed by western blot. Bars represent the average ± SEM (n = 3). Statistical significance was assessed using a one-way ANOVA (α = 0.05) and and non-significant p-values are shown.

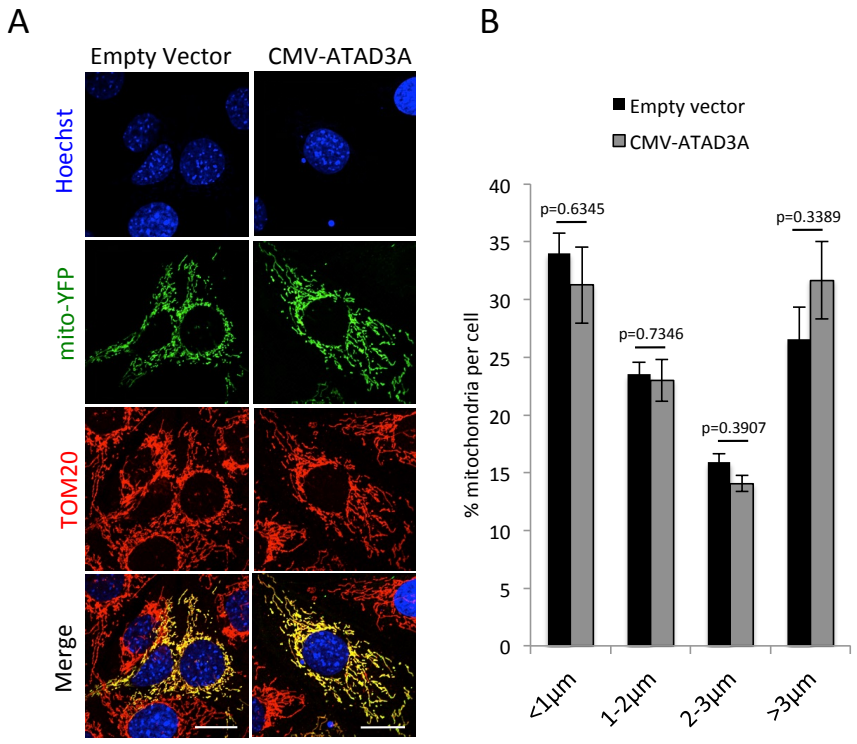

Figure 18: **Mitochondrial length remains unchanged in MEFs overexpressing ATAD3A following serum starvation.** MEFs were co-transfected at a 5:1 with either CMV-Sport6-ATAD3A (CMV-ATAD3A) or empty pcDNA3.1+ (empty vector), and mito-YFP-FLAG. 24 hrs post-transfection, cells were plated onto coverslips and grown for additional 24 hrs. The cells were then serum starved for 16 hrs prior to fixation and analyzed by immunofluorescence for the indicated markers. (A) Representative images displaying mitochondrial morphology of MEFs transfected with the indicated vectors. Scale bars represent 20 µm. (B) Mitochondria from (A) were measured, binned into the indicated categories, and presented as a percentage per cell. Bars represent the average ± SEM (n = 3). Statistical significance was assessed using a two-tailed student's t-test (α = 0.05) and non-significant p-values are displayed.

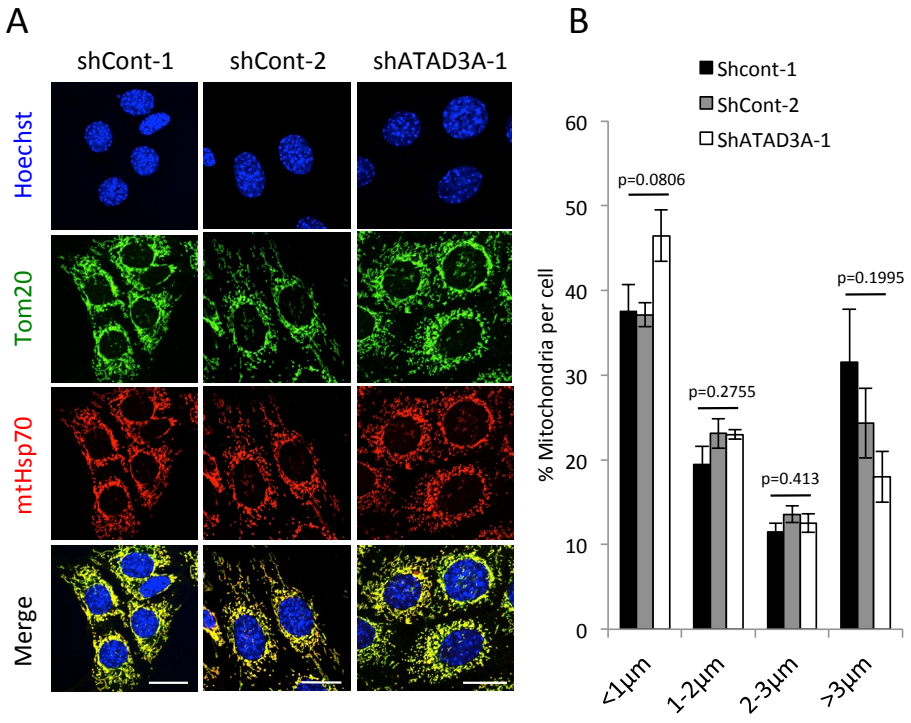

Figure 19: **Mitochondrial length remains unchanged in MEFs with reduced ATAD3A expression following serum starvation.** ShCont and shATAD3A MEFs were grown for 24 hrs on coverslips, serum starved for 16 hrs prior to fixation and analyzed by immunofluorescence for the indicated markers. (A) Representative images displaying mitochondrial morphology of shCont and shATAD3A MEFs. Scale bars represent 20 µm. (B) The length of mitochondria from (A) were measured, binned into the indicated categories, and presented as a percentage per cell. Bars represent the average ± SEM (n = 3). Statistical significance was assessed using a one-way ANOVA (α = 0.05) and non-significant p-values are shown.

3.3 - ATAD3A knockdown has minimal effects on mtDNA levels

Several studies have presented findings implicating ATAD3A in mtDNA maintenance and expression of mtDNA-encoded genes (He et al., 2012; He et al., 2007). To determine whether ATAD3A has a role in maintaining mtDNA, I measured mtDNA content and nucleoid number in both shCont and shATAD3A MEFs. To quantify mtDNA, I performed qPCR on DNA extracts from shCont (clone 1 and 2) and shATAD3A (clone 1 and 2) MEFs using primers specific for either the cytochrome c oxidase subunit I (COI) or the NADH dehydrogenase subunit 6 gene of complex I. The quantity of each gene was then normalized to that of the nuclear 18S ribosomal RNA gene. Although ATAD3A expression was barely detectable in shATAD3A MEFs (Fig.20A), there was no decrease in the quantity of either gene rather an increasing trend was apparent (Fig.20B and C, *n = 3*). This increase did not reach statistical significance using the COI gene, but was significant when the complex I gene was measured using a one-way ANOVA ($p = 0.0408$). After applying the Tukey's HSD post-hoc test, however, there was no significant difference between any of the shCont or shATAD3A clones implying that reduced ATAD3A expression has minimal effect on mtDNA levels.

MtDNA was further analyzed in these cells by counting the number of mitochondrial nucleoids per cell. To visualize nucleoids, I stained live shCont and shATAD3A MEFs with Picogreen, a double-stranded DNA stain, and imaged them by fluorescence microscopy. To ensure that Picogreen signal was mitochondrial, cells were previously co-stained with the fluorescent dye,

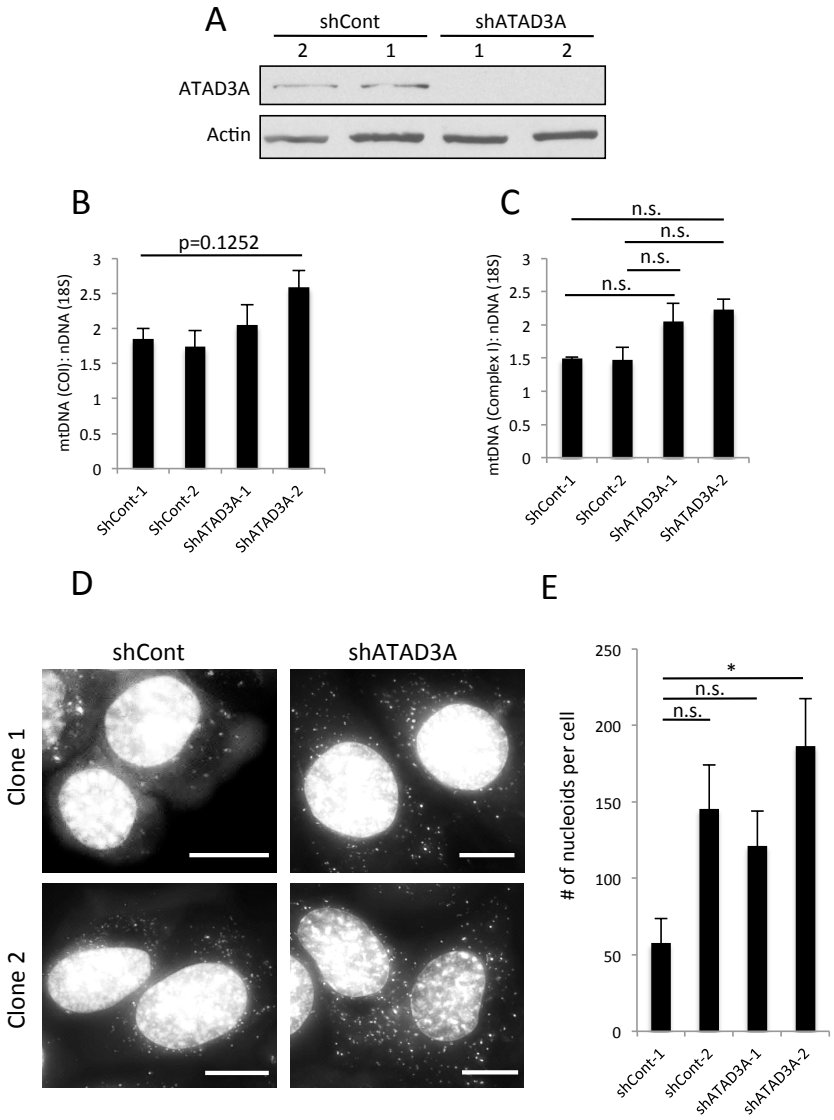

Figure 20: **ATAD3A knockdown does not alter nucleoid number or mtDNA content in MEFs**. (A) Whole cell lysates from shCont and shATAD3A MEFs were analyzed by western blot with the indicated antibodies. DNA from shCont and shATAD3A MEFs were harvested and mtDNA was quantified via qPCR using primers specific to the cytochrome c oxidase subunit I (COI) (B) (n = 3) and NADH dehydrogenase subunit 6 (Complex I) gene (C) (n = 3). Levels of each mtDNA marker were normalized to the quantity of the 18S rRNA gene (nuclear DNA [nDNA]). (D) Representative images of live shCont and shATAD3A MEFs stained with Picogreen. Scale bars represent 10 μm. (E) Quantification of nucleoid number from (D) normalized per cell (n = 3). Bars represent average ± SEM. Statistical significance was assessed using a one-way ANOVA (α = 0.05) and a Tukey HSD post-hoc test was performed when necessary. (*) - $p<0.05$, (n.s) – non-significant.

MitoTracker (Fig.21) (Patten and Slack, unpublished). Like overall mtDNA, no decrease in nucleoid number per cell was observed in shATAD3A MEFs, but shCont-1 (~58 ± 16.05) MEFs did contain significantly less nucleoids per cell than shATAD3A-2 MEFs (~186 ± 31.27) (Fig.20D and E, *n* = *3*). As a result, ATAD3A silencing does not appear to decrease mtDNA content nor nucleoid number as previously described.

The previous findings with ATAD3A and mtDNA were observed in human cell lines and following transient knockdown (He et al., 2012; He et al., 2007). Since I did not reproduce these results in MEFs, I counted the number of mitochondrial nucleoids per cell in live HeLa cells treated with either siCtrl or siATAD3A. Mitochondrial nucleoids were stained as described earlier and their mitochondrial localization was confirmed (Fig.22A). ATAD3A expression was barely detectable after 72hrs siATAD3A treatment as shown by western blot (Fig.22B). In agreement with our results with shATAD3A MEFs, no significant difference in nucleoid number was observed between siCtr and siATAD3A HeLa cells (Fig.22C and D, *n* = *4*). In summary, it is clear from my data that ATAD3A interacts with OPA1, but these interactions do not seem to be required for mtDNA maintenance or mitochondrial morphology. I then went on to pursue other OPA1 interacting partners identified in our SILAC OPA1 interaction screen.

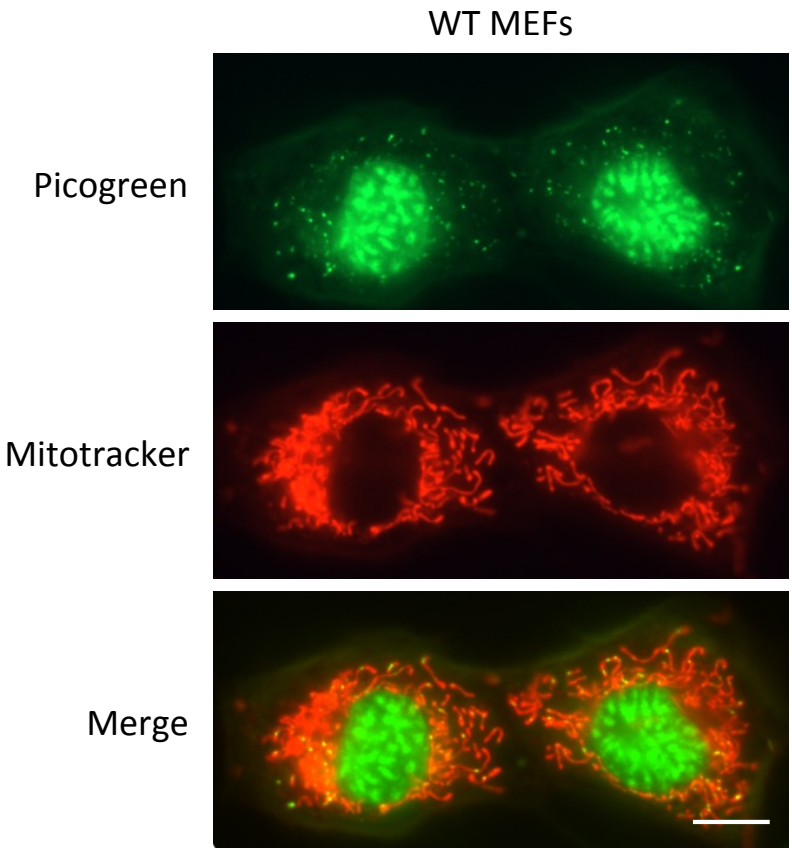

Figure 21: **Mitochondrial localization of nucleoid staining in MEFs.** Live MEFs were double labeled with Mitotracker and Picogreen to confirm mitochondrial localization of nucleoid staining. Scale bar represents 10 μm.

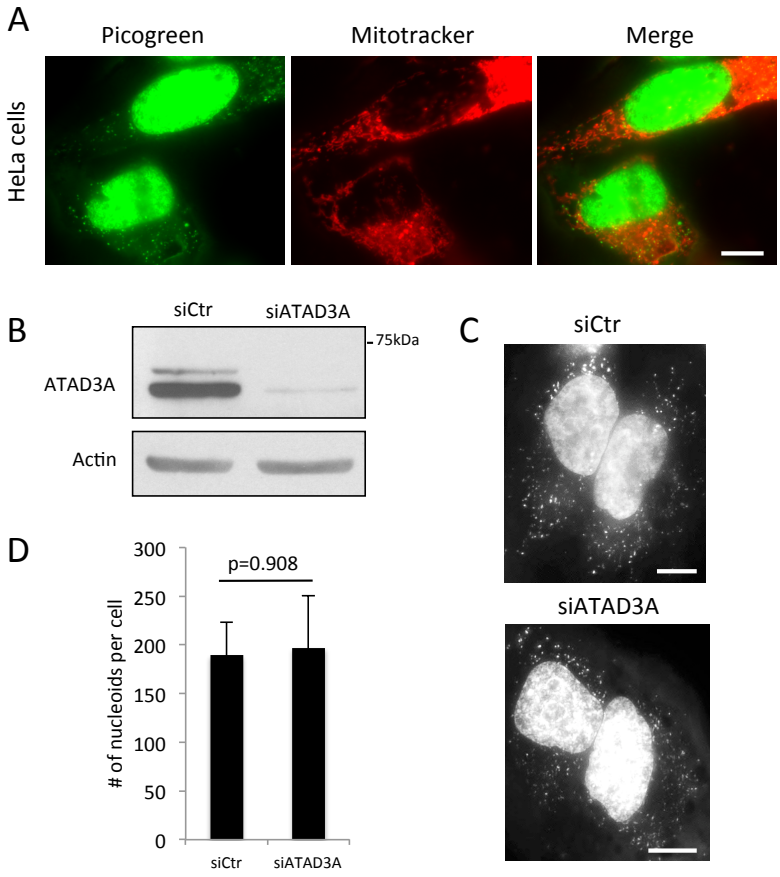

Figure 22: **The number of mitochondrial nucleoids are unaffected by transient ATAD3A knockdown in HeLa cells.** (A) Live HeLa cells were double labeled with Mitotracker and Picogreen to confirm mitochondrial localization of Picogreen staining. Scale bar represents 10 μm. (B) Western blot analysis of whole cell lysates from HeLa cells transiently transfected with either scrambled siRNA (siCtr) or ATAD3A siRNA (siATAD3A) for 72 hrs. (C) Representative images of live siCtr and siATAD3A HeLa cells stained with Picogreen 72 hrs post-transfection. Scale bars represent 10 μm. (D) Quantification of nucleoid number from (C) normalized per cell. Bars represent the average ± SEM (n = 4). Statistical significance was assessed using a two-tailed student's t-test (α = 0.05) and non-significant p-value is shown.

Part 2: **The role of OPA1 and SLC25 protein interactions in sensing cellular bioenergetics.**

3.4 - OPA1 oligomerization decreases and cristae widen under nutrient-rich conditions:

Data from our lab shows that OPA1 responds to starvation conditions (low nutrient conditions) by increasing its oligomerization (Patten and Slack, unpublished). Not only this, but OPA1 oligomerization was also shown to decrease when isolated mitochondria were treated with substrates that stimulate either complex I (malate and glutamate) or complex II (succinate) of the electron transport chain (Patten and Slack, unpublished). From this data, it seems that OPA1 can sense changes in nutrient levels and alter its oligomerization. In our SILAC OPA1 interaction screen, several SLC25 proteins, which catalyze metabolite transport, were identified as OPA1 interacting partners. Due to their role in nutrient transport, I decided to characterize the interactions between OPA1 and SLC25 proteins as they may regulate these nutrient-dependent changes in OPA1 oligomerization. However, I first wanted to reproduce the results showing that OPA1 can respond to complex I and II substrates. To accomplish this, I isolated mitochondria from mouse liver, incubated them with substrates that stimulate either complex I or complex II of the electron transport chain and cross-linked them with EDC. Following chemical crosslinking and analysis by western blot, large OPA1 oligomers between 245 kDa and 180 kDa could be observed, which decreased in the presence of complex I or II substrates

as shown previously (Fig.23A) (Patten and Slack, unpublished). This same observation was also made when mitochondria were simultaneously treated with rotenone, a complex I poison, indicating that OPA1's response was independent of electron transport chain function (Fig.23A) (Patten and Slack, unpublished). To correlate these changes to changes in cristae structure, a cytochrome c distribution assay was performed. The majority of cytochrome c is localized within cristae and mobilization of this pool to the IMS is indicative of cristae remodeling (Scorrano et al., 2002). Therefore, comparing the relative amount of cytochrome c in the IMS and cristae can provide an indication of cristae remodeling. To measure cytochrome c in these compartments, isolated liver mitochondria were incubated with either complex I or II substrates as before, but then treated with 0.1% digitonin (1 μg:1μg protein) to permeabilize the mitochondrial outer membrane (Fig.23B). The mitochondria were then centrifuged to separate the IMS (supernatant) and mitoplasts (pellet) and each were probed for cytochrome c by western blot (Fig.23B). As expected, almost no cytochrome c was detected in the supernatants of mitochondria not treated with digitonin (Fig.23C) (Patten and Slack, unpublished). Upon digitonin treatment, minimal amounts of cytochrome c were detected in supernatant of mitochondria incubated with no substrate buffer and this amount drastically increased when mitochondria were treated with either complex I or II substrates (Fig.23C) (Patten and Slack, unpublished). These findings show that decreased nutrient levels causes a reduction in OPA1 oligomerization and induces cristae widening

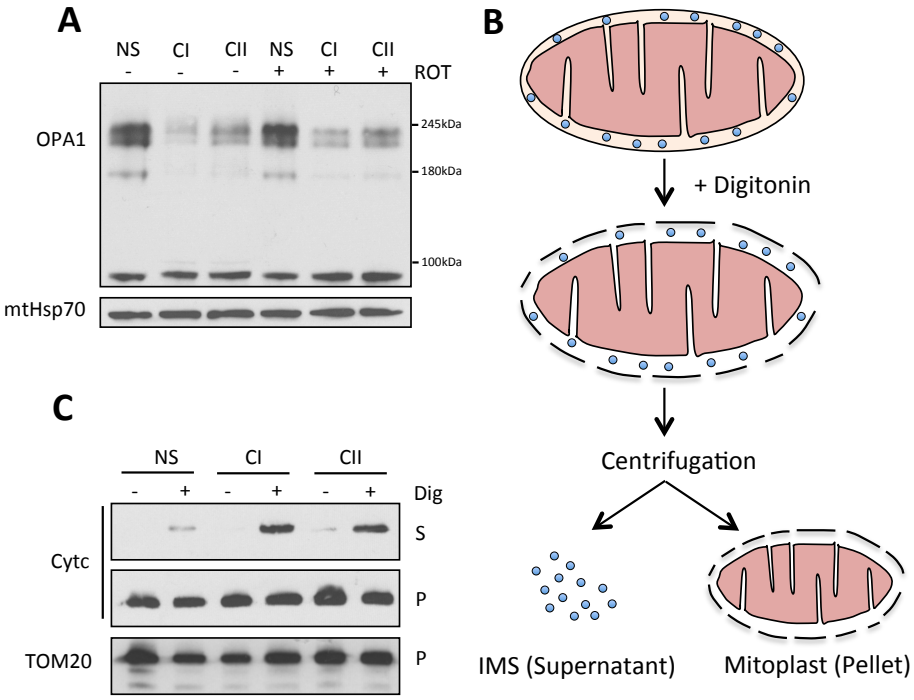

Figure 23: **Complex I and II substrates decrease OPA1 oligomerization and induce cytochrome c redistribution.** (A) Isolated mouse liver mitochondria were incubated with no substrates, complex I substrates (CI) or complex II substrates (CII) for 1hr at 37°C. Samples were then cross-linked with EDC and analyzed by western blot with the indicated antibodies. (B) Diagram describing cytochrome c (Cytc) distribution assay. (C) Isolated mouse liver mitochondria were treated as in (A) followed by treatment with 0.1% digitonin (Dig) (1 µg/µg protein) for 30 min at 4°C. The pellets (P) and supernatants (S) were then separated by centrifugation and analyzed by western blot with the indicated antibodies. (NS) – No substrate, (ROT) – rotenone, (IMS) – intermembrane space.

(increased IMS cytochrome c) suggesting that OPA1 responds to nutrient availability.

3.5 - OPA1 interacts with SLC25 proteins:

To determine how OPA1 may sense changes in nutrient availability, I sought to characterize OPA1 and SLC25 protein interactions. Results from our SILAC screen indicate that OPA1 may interact with the DIC, OGC, AGC1, and AGC2, which are nutrient transporters. Interestingly, these carriers are responsible for transporting the substrates that affect OPA1 oligomerization and cristae structure. For example, both the DIC and OGC transport malate (complex I substrate) while the DIC carrier also transports succinate (complex II substrate). In our starvation paradigm cells are deprived of amino acids, which are transported by the AGC carriers. Glutamate was also used in combination with malate to stimulate complex I. I therefore hypothesized that interactions between OPA1 and SLC25 proteins regulate OPA1 oligomerization according to nutrient availability. As with ATAD3A, I first validated these interactions by co-immunoprecipitation. To accomplish this, FLAG-tagged mito-YFP, DIC, OGC, AGC1, and AGC2 were constructed, overexpressed in HT-MEFs, and immunoprecipitated 24rs post-transfection. OPA1 co-immunoprecipitated with each tagged SLC25 protein, but was absent from the sample in which mito-YFP-FLAG was immunoprecipitated (Fig.24A). A robust interaction between OPA1 and OGC-FLAG was detected suggesting that it may form a stronger interaction with OPA1. This interaction was also shown endogenously in isolated MEF

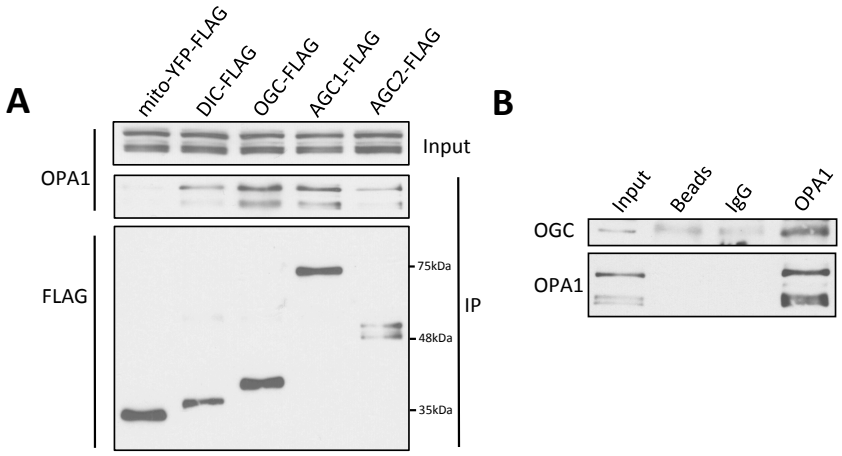

Figure 24: **OPA1 interacts with the DIC, OGC, AGC1, and AGC2 in MEFs.** (A) Mito-YFP-FLAG, DIC-FLAG, OGC-FLAG, AGC1-FLAG and AGC2-FLAG were transiently transfected into HT-MEFs. 24 hrs post-transfection, the MEFS were lysed and the FLAG-tagged proteins were immunoprecipitated. The elutions and 25 µg of input were then analyzed by western blot with the indicated antibodies. (B) Endogenous OPA1 was immunoprecipitated from MEF mitochondrial lysates and eluted with SDS loading buffer. The eluted samples and 2% input were analyzed by western blot with the indicated antibodies. (IP) –immunoprecipitates.

mitochondria, where more OGC signal was detected in the immunoprecipitated OPA1 sample than the no antibody and normal IgG control samples (Fig.24B). All together, these results validate the findings from the SILAC screen (Patten and Slack, unpublished) and reveal a novel interaction between OPA1 and SLC25 proteins.

3.6 - SLC25 protein inhibitors decrease OPA1 oligomerization and widen cristae:

To further investigate the role of SLC25 proteins and whether simply substrate binding is sufficient to change OPA1 oligomerization and cristae structure; we treated isolated mouse liver mitochondria with competitive inhibitors for SLC25 proteins in the absence of substrates and cross-linked them with EDC. Specifically mitochondria were treated with increasing amounts of either phenylsuccinate (PhS) or butylmalonate (BM), which are competitive inhibitors of the OGC and DIC, respectively (LaNoue and Schoolwerth, 1979). Similar to the complex I and II substrates, each inhibitor caused drastic decreases in OPA1 oligomerization and increasing their concentrations seemed to cause a slight dose-dependent response (Fig.25A). To determine whether changes in cristae also occur, cytochrome c distribution was measured as before, but the isolated mouse liver mitochondria were incubated with either 50 mM PhS or BM. In the absence of digitonin, the supernatants of the no substrate and BM sample displayed minimal cytochrome c signal as expected, however, mitochondria incubated with PhS did contain substantial cytochrome c in their supernatants (Fig.25B). Nonetheless, strong cytochrome c signal was still present in the

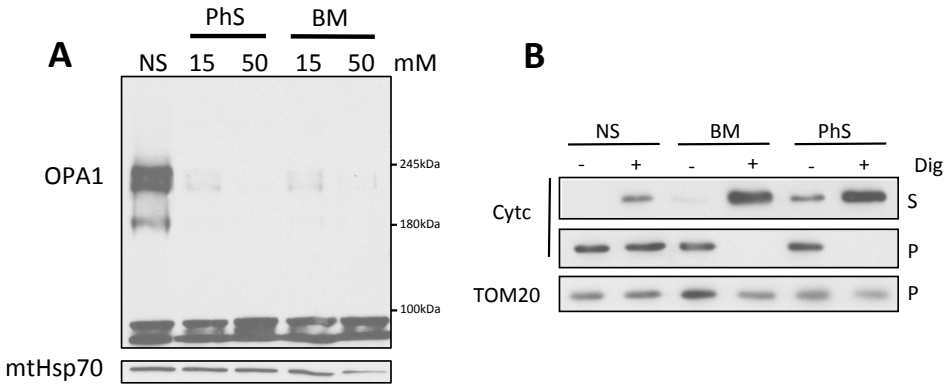

Figure 25: **Butylmalonate and phenylsuccinate reduce OPA1 oligomerization and cause massive redistribution of cytochrome c.** (A) Mouse liver mitochondria were incubated with the indicated amounts of phenylsuccinate (PhS) or butylmalonate (BM) for 30 min at 37^{o}C, cross-linked with EDC and analyzed by western blot using the indicated antibodies. (B) Mouse liver mitochondria were incubated with 50 mM PhS or BM for 1hr at 37^{o}C followed by treatment with 0.1% digitonin (1 µg/1µg protein) for 30 min at 4^{o}C. The pellets (P) and supernatants (S) were then separated by centrifugation and analyzed by western blot with the indicated antibodies. (NS) – no substrate buffer, and (Cytc) – cytochrome c.

mitochondrial pellet indicating that these mitochondria could still retain cytochrome c and were not completely compromised. In the presence of digitonin, the supernatants of mitochondria treated with either inhibitor contained substantially more cytochrome c than the no substrate control indicating that cristae became enlarged releasing its store of cytochrome c (Fig.25B). In fact, cytochrome c was barely detectable in the mitoplasts (pellets) of mitochondria suggesting that most of the cytochrome c pool redistributed to the IMS. Thus, SLC25 protein inhibitors decrease OPA1 oligomers and induce cristae widening (increased IMS cytochrome c) consistent with the hypothesis that transporter binding alone triggers changes in OPA1 oligomerization and cristae structure.

3.7 - OGC knockdown also causes decreased OPA1 oligomerization and cristae widening:

A previous study showed that OGC knockdown causes alterations in cristae structure (Gallo et al., 2011). Given this observation and that both its substrate (malate) and inhibitor (PhS) cause decreased OPA1 oligomerization and ultrastructural changes; we wanted to assess whether OGC knockdown alone could alter OPA1 oligomerization and cristae structure. To examine this, I transfected HT-MEFs with siRNA targeting OGC (siOGC), which almost completely reduced its expression (band between 25 kDa and 35 kDa) 72 hrs post-transfection (Fig.26A). Mitochondria were then isolated from these cells, incubated in no substrate buffer mimicking starvation and cross-linked with EDC to measure OPA1 oligomerization. Like the substrates and inhibitors, OGC

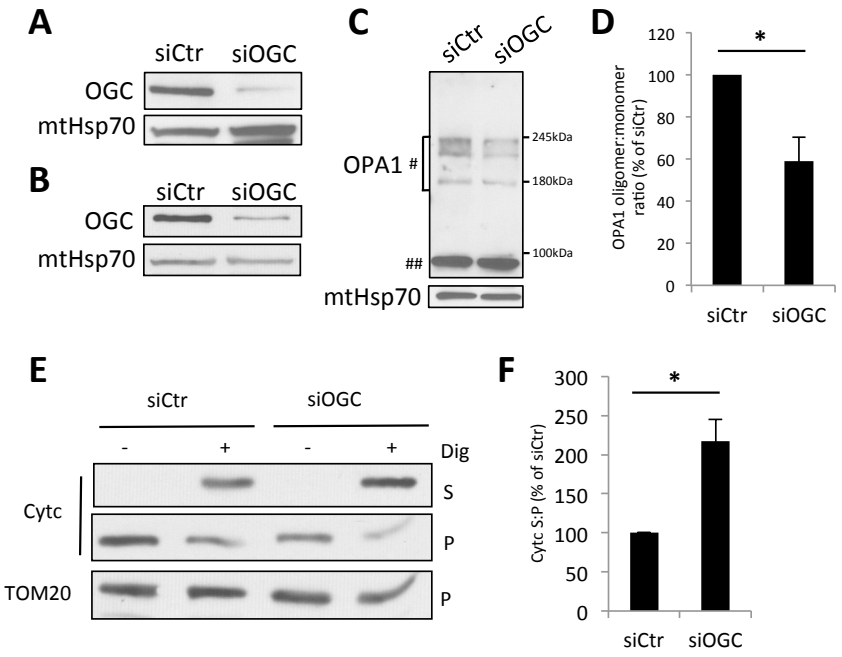

Figure 26: **OGC knockdown decreases OPA1 oligomerization and increases cytochrome c redistribution.** HT-MEFs were transfected with siOGC for 72hrs (A) or 120hrs (B) and mitochondrial lysates were analyzed by western blot with the indicated antibodies. (C) – 72 hrs post-transfection, isolated mitochondria from siRNA-treated HT-MEFs were incubated with no substrate buffer (NS) for 30 min at 37oC, cross-linked with EDC and analyzed by western blot with the indicated antibodies. (D) Densitometric analysis of (C) was performed and the ratio of OPA1 oligomers (#) to monomers (##) was computed (n = 3). (E) 120hrs post-transfection, isolated mitochondria from siRNA-treated HT-MEFs were incubated as in (C) and then treated with 0.1% digitonin (Dig) (1µg/1µg protein) for 30min at 4oC. The pellets (P) and supernatants (S) were separated by centrifugation and analyzed by western blot with the indicated antibodies. (F) Densitometric analysis of (E) was performed and the ratio of cytochrome c (Cytc) in the supernatant (S) to pellet (S) was calculated (n = 3). The bars represent the average ± SEM. Statistical significance was assessed using a two-tailed student's t-test where *p<0.05.

knockdown caused a significant decrease in OPA1 oligomers in starvation conditions (58.96 ± 11.35% of siCont) (Fig.26C and D, *n* = *3*). To assess cristae structure, the cytochrome c distribution assay was employed as before, but HT-MEFs were transfected twice over 120hrs to ensure sufficient knockdown. Western blot analysis was performed to confirm OGC knockdown and almost complete OGC silencing was observed in siOGC-treated cells (Fig.26B). In accordance with the oligomerization data, OGC knockdown caused a significant increase (217.49 ± 27.12% of siCont) in cytochrome c signal in the supernatants of mitochondria incubated with no substrate buffer suggesting that cristae became wider in starvation conditions (Fig.26E and F, *n* = *3*). All together, these data show that reduced OGC expression mimics the effects of substrates and inhibitors during starvation suggesting that OGC is required for oligomer stability during starvation.

3.8 - SLC25 protein substrates and inhibitors reduce ATP synthase monomers and oligomers:

The previous data demonstrates that cristae structure changes according to nutrient levels, but how these structural changes affect metabolism is not known. A previous study showed that OPA1 loss impairs ATP synthase assembly and mitochondrial ATP production (Gomes et al., 2011). Considering that SLC25 protein substrates and inhibitors affect cristae structure (based on OPA1 oligomerization and cytochrome c distribution assays), I asked if these compounds also affected ATP synthase assembly. To address this question I

incubated isolated mouse liver mitochondria with either complex I substrates or SLC25 protein inhibitors (BM and PhS) and analyzed their lysates by BN-PAGE to measure ATP synthase monomer and oligomer levels. For visualization of ATP synthase, I probed mitochondrial lysates for ATP5A, a component of the catalytic F_1 subunit, by western blot. The abundance of ATP synthase oligomers (37.22 ± 4.66% of no substrate) and monomers (52.98 ± 16.89% of no substrate) were decreased by the presence of complex I substrates (Fig.27A and B, *n* = *5*). Treatment with PhS and BM caused almost complete loss of ATP synthase oligomers and large reductions in monomer levels (29.41 ± 11.15% and 16.30 ± 7.34% of no substrate, respectively) (Fig. 27D and E, *n* = *6*). These findings imply that cristae remodeling induced by transporter binding decreases the abundance of ATP synthase monomers and oligomers.

3.9 - Only SLC25 protein inhibitors reduce respiratory chain supercomplexes:

A recent study showed that alterations in cristae structure impair respiratory chain supercomplex assembly and respiration (Cogliati et al., 2013). Since both SLC25 protein inhibitors and substrates induce cristae remodeling, I wanted to measure their effect on respiratory chain supercomplexes. Respiratory chain supercomplex abundance was analyzed by BN-PAGE using isolated mouse liver mitochondria incubated with complex I substrates or SLC25 protein inhibitors (BM and PhS). For visualization of respiratory chain supercomplexes, the mitochondrial lysates were probed for NDUFA9, a complex I component, by western blot. Unlike the results for the ATP synthase, complex I substrates had

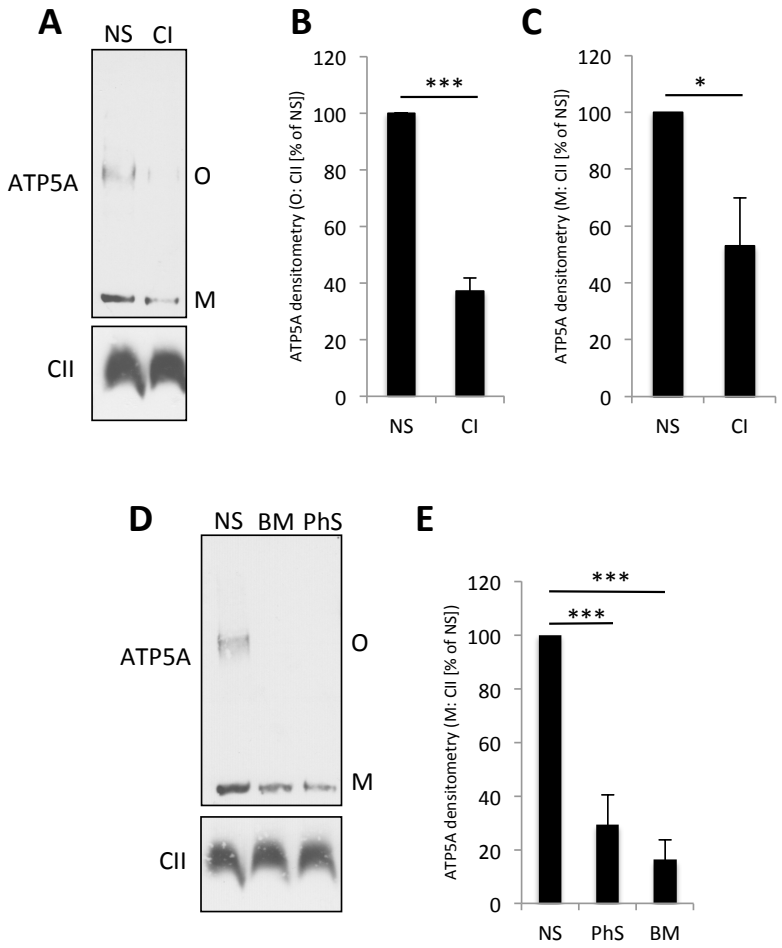

Figure 27: **The abundance of ATP synthase oligomers and monomers is lowered by SLC25 protein substrates and inhibitors.** (A) Mouse liver mitochondria were incubated with complex I substrates (CI) for 1 hr at 37^{o}C, lysed and analyzed by BN-PAGE. (B and C) ATP synthase oligomers (O) and monomers (M) from (A) were quantified by densitometry and normalized to CII abundance. Bars represent the average ± SEM (n = 5). (D) Mouse liver mitochondria were incubated with either 50 mM phenylsuccinate (PhS) or butylmalonate (BM) for 1 hr at 37oC, lysed and analyzed by BN-PAGE. (E) M from (D) were quantified by densitometry and normalized to CII abundance. The bars represent the average ± SEM (n = 6). Statistical significance was assessed using a two-tailed student's t-test and non-significant p-values are displayed. (*) - $p<0.05$, (***) - $p<0.005$, and (NS) – no substrate buffer.

no significant effect on respiratory chain supercomplex levels (Fig.28A and B, *n* = *5*). Complex I substrates, however, did cause a significant decrease (32.10 ± 8.67% of no substrate) in the complex I monomer (Fig.28A and C, *n* = *5*). Meanwhile, treating isolated liver mitochondria with PhS or BM caused a strong reduction (47.61 ± 17.32% and 40.56 ± 15.87% of no substrate, respectively) in respiratory chain supercomplexes (Fig.28D and E, *n* = *5*). PhS and BM also extensively decreased (16.68 ± 9.65% and 8.72 ± 2.24% of no substrate, respectively) the abundance of complex I monomers (Fig.28D and F, *n* = *5*). Therefore, these results demonstrate that only SLC25 protein inhibitors affect the abundance of respiratory chain supercomplexes. Since the inhibitors caused the most robust changes in cristae structure and OPA1 oligomerization, assembly of respiratory chain supercomplexes may only be sensitive to large-scale cristae alterations. In summary, the data presented in this section shows that several SLC25 proteins interact with OPA1 and ligands for these transporters induce changes in OPA1 oligomerization, cristae structure and ATP synthase assembly.

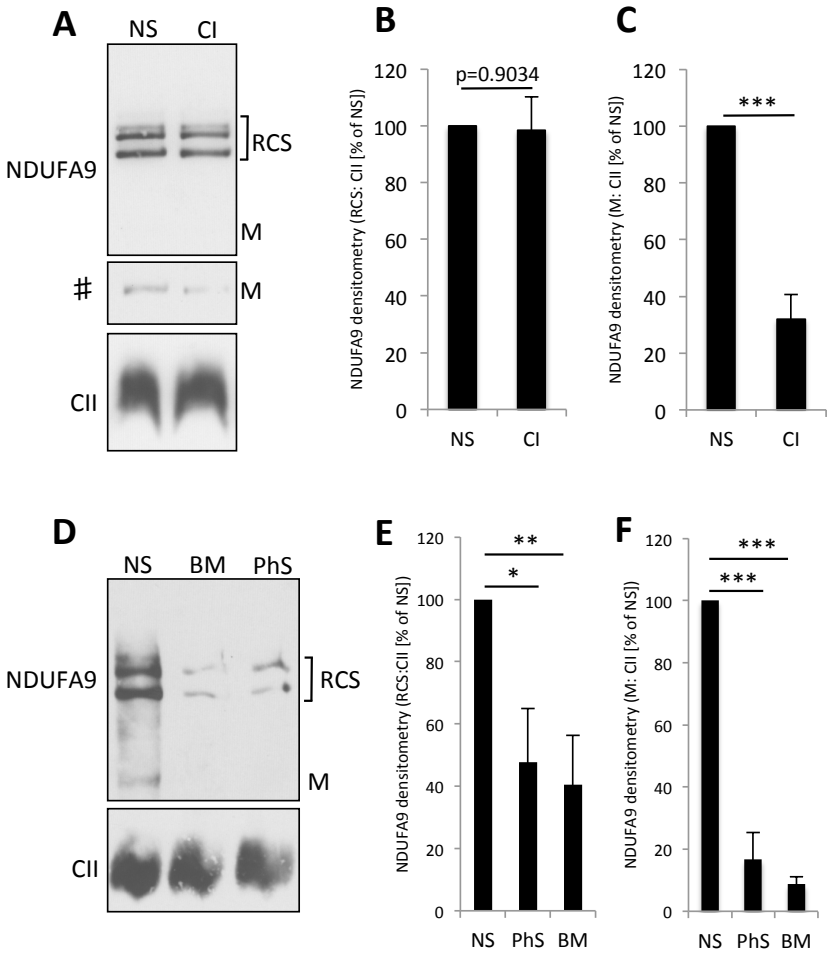

Figure 28: **Respiratory chain supercomplexes are differentially affected by SLC25 protein inhibitors and complex I substrates.** (A) Mouse liver mitochondria were incubated with either complex I substrates (CI) for 1 hr at 37^{o}C, lysed and analyzed by BN-PAGE. (B-C) Respiratory chain supercomplexes (RCS) and CI monomers (M) from (A) were quantified by densitometry and normalized to CII abundance. (D) Mouse liver mitochondria were incubated with either 50 mM phenylsuccinate (PhS) or butylmalonate (BM) for 1 hr at 37^{o}C, lysed and analyzed by BN-PAGE. (E-F) RCS and M from (D) were quantified by densitometry and normalized to CII abundance. The bars represent the average ± SEM (n = 5). Statistical significance was assessed using a two-tailed student's t-test and non-significant p-values are displayed. (*) - $p<0.05$, (**) - $p<0.01$, and (***) - $p<0.005$, (NS) – no substrate buffer, (♯) – darker exposure.

CHAPTER 4: DISCUSSION

4.1 - Summary of key findings:

In this work, the role of OPA1 interacting partners (ATAD3A and SLC25 proteins) was studied with regards to different facets of OPA1 function. My first goal was to validate these interactions using co-immunoprecipitation. Both endogenous and overexpression approaches revealed that OPA1 does interact with ATAD3A and SLC25 proteins (DIC, OGC, AGC1 and AGC2) (Fig. 15 and 24). Then I examined the role of ATAD3A in mtDNA maintenance and regulation of mitochondrial morphology, both functions shared by OPA1. Using stable shATAD3A MEF lines and HeLa cells, no appreciable alterations in mitochondrial morphology or mtDNA content were observed (Fig. 16-22). Afterwards, I pursued the role of the SLC25 proteins in the regulation of OPA1-dependent cristae remodeling. Treating isolated mitochondria with SLC25 protein substrates decreases OPA1 oligomerization and widens cristae reproducing previous findings from our lab (Fig. 23A and C) (Patten and Slack, unpublished). Not only this, but the response was unchanged by rotenone treatment suggesting that substrate binding may be important (Fig.23A) (Patten and Slack, unpublished). Indeed, competitive inhibitors for the DIC (BM) and OGC (PhS) alone produced similar results (Fig.25). Transient OGC knockdown also reduced OPA1 oligomerization and remodeled cristae in nutrient-poor conditions implying that the OGC is required for oligomer stability during starvation conditions (Fig.26). In addition to changes in OPA1 oligomerization and cristae structure, binding of SLC25 protein substrates or inhibitors also induced changes in ATP synthase assembly (Fig.27). Respiratory chain supercomplex assembly, however, was not

altered by SLC25 protein substrates or inhibitors suggesting that cristae remodeling induced by transporter binding only appreciably affects ATP synthase assembly (Fig.28).

4.2 –ATAD3A Knockdown does not affect mitochondrial morphology:

Previous genetic studies implicate ATAD3A as a regulator of mitochondrial dynamics (Gilquin et al., 2010a; Rone et al., 2012). Specifically, ATAD3A knockdown in MA-10 cells and *D. melanogaster* lead to fragmentation of the mitochondrial network (Gilquin et al., 2010a; Rone et al., 2012). Not only this, but dominant negative ATAD3A mutants cause mitochondrial fragmentation when overexpressed in U373 cells (Gilquin et al., 2010a). Similar observations were made following overexpression of ATAD3A with a N-terminal truncation (Gilquin et al., 2010a). Nevertheless, in our studies using stable shATAD3A MEFs, mitochondrial fragmentation was not observed (Fig.17 and 19). Although the previous studies highlight clear defects in mitochondrial morphology, there are other studies that report no change in mitochondrial morphology following ATAD3A silencing. For instance, He et al. documented that mitochondrial morphology was normal in 143B osteocarcinoma cells treated with ATAD3A-siRNA (He et al., 2007). Also *C. elegans* fed with ATAD3A-siRNA displayed disorganization of their mitochondrial reticulum, but no fragmentation (Hoffmann et al., 2009). In addition, no change in mitochondrial morphology was observed in the steroidogenic cell line, NCI-H295R, following ATAD3A knockdown (Gilquin et al., 2010a). More recently, trophoblasts taken from mice with stably inactivated

ATAD3A also displayed no gross alterations in mitochondrial morphology (Goller et al., 2013). A potential reason for the discrepancies could be that mitochondrial morphology is affected by ATAD3A loss in a cell-type/cell-line dependent manner. This would suggest that certain cell types/cell lines rely more heavily on ATAD3A function for mitochondrial structure. Another explanation could be that ATAD3A loss or loss-of-function causes mitochondrial dysfunction in certain cells leading to fragmentation as a secondary effect. In fact, loss of mitochondrial membrane potential is known to inactivate OPA1 leading to mitochondrial fragmentation (Griparic et al., 2007). Therefore, based on these results it is unlikely that ATAD3A is a direct regulator of mitochondrial morphology.

4.3 – ATAD3A knockdown does not affect mtDNA:

There are several lines of evidence also linking ATAD3A to mtDNA metabolism (He et al., 2012; He et al., 2007; Wang & Bogenhagen, 2006). For example, an ~15% reduction in mtDNA levels and a severe loss in Picogreen staining was observed following ATAD3A knockdown (He et al., 2007). As with mitochondrial morphology, however, we did not detect any alterations in mtDNA levels using qPCR and Picogreen staining in either shATAD3A MEFs or siATAD3A-treated HeLa cells (Fig.20 and 22). One possibility for the differences could be that we performed our siRNA treatments over 72hrs in HeLa cells while He et al. did their treatment for six days. This difference could have produced the discrepancies, as they reported no change after three days of knockdown (He et al., 2007). In addition to technical differences, new findings shed doubt on the

role of ATAD3A in mtDNA metabolism (Bogenhagen et al., 2008). The original screen identifying ATAD3A as associated with nucleoids was performed using mild lysis conditions (Wang & Bogenhagen, 2006). In a newer study from the same group, the screen was repeated with cross-linked mitochondria lysed with a more stringent detergent (SDS) and ATAD3A was not identified as a nucleoid-bound protein (Bogenhagen et al., 2008). Previously, however, He et al. found that N-terminal ATAD3 fragments bound directly to synthetic D-loop sequences (He et al., 2007). It is known from several topological studies that the N-terminus of ATAD3A faces the IMS (Bogenhagen et al., 2008; Gilquin et al., 2010a; Hubstenberger et al., 2010). Therefore interactions with the N-terminus of ATAD3A would be impossible questioning the biological significance of such interactions. As a result, Bogenhagen et al. speculated that ATAD3A interacts with the nucleoid indirectly (Bogenhagen et al., 2008). These findings do not exclude, however, the possibility that ATAD3A serves other functions in mtDNA metabolism. In fact, one group found that ATAD3A bound to the transcription termination sequence of one of the major precursor mtDNA transcripts suggesting that it may affect mtDNA gene expression (Sondheimer et al., 2010). Moreover, a recent study found that ATAD3A binds to mitochondrial ribosomes and is required for mtDNA-gene translation (He et al., 2012). All together, it seems that ATAD3A is not required for maintaining the mitochondrial genome, but other functions with respect to mtDNA cannot be excluded.

The model originally proposed by Elachouri et al. states that the N-terminal fragment of OPA1 interacts directly with the mitochondrial nucleoid

thereby ensuring its maintenance (Elachouri et al., 2011). The findings presented in this work present evidence against ATAD3A being this molecular link. Since ATAD3A likely interacts with the nucleoid indirectly, OPA1 may require interactions with a different unknown core nucleoid-associated protein to anchor mtDNA and ensure its maintenance. Another possible nonexclusive mechanism could be that maintenance of mtDNA depends primarily on mitochondrial fusion. In fact, loss of both Mfns was also shown to cause mtDNA loss (Chen et al., 2007b; Chen et al., 2010). Another study in yeast reported that mtDNA loss and mitochondrial fragmentation caused by the loss of fusion could be rescued by disruption of fission (Sesaki et al., 2003). In addition, reintroduction of the fusion-incompetent OPA1-Q297V mutant into OPA1 knockout MEFs rescues cristae structure, but not mtDNA (Patten and Slack, unpublished). Mitochondrial fusion is believed to enable content mixing, which could allow functional complementation of dysfunctional mtDNA molecules (Chen & Chan, 2010; Legros et al., 2004; Nunnari et al., 1997). Therefore, OPA1's role in mtDNA maintenance is independent of ATAD3A and may require direct interactions with another nucleoid protein and/or mitochondrial fusion.

4.4 – Part 1: Future directions:

Although ATAD3A and OPA1 interactions were not required for either mtDNA maintenance or mitochondrial morphology, they may still serve another role within mitochondria. Recent studies have identified ATAD3A and OPA1 as regulators of steroidogenesis (Rone et al., 2012; Wasilewski et al., 2012). During

steroidogenesis, cholesterol is imported into mitochondria by a large protein complex termed the “transduceosome” which shuttles cholesterol from the outer mitochondrial membrane to the inner mitochondrial membrane (Liu et al., 2006; Rone et al., 2009). Then the cytochrome P450 enzyme, CYP11A1, catalyzes the production of pregnenalone from cholesterol, which serves as a precursor for all steroids (Rone et al., 2009). Interestingly, ATAD3A has been identified as a component of the “transduceosome” and its silencing lead to decreased production of several steroids (Rone et al., 2012). OPA1 was also identified in this complex and later work demonstrated that changes in OPA1 expression influenced the production of pregnenalone and cholesterol transport to the inner mitochondrial membrane (Wasilewski et al., 2012). Given their overlapping roles in steroidogenesis and that they interact, it would be interesting to determine whether these interactions regulate steroidogenesis or cholesterol import. The role of OPA1 in steroidogenesis is believed to involve inner membrane restructuration (Wasilewski et al., 2012). Knockdown of ATAD3A has also been shown to alter mitochondrial ultrastructure (Rone et al., 2012). Since altered cristae structure and decreased OPA1 expression enhances steroidogensis (Wasilewski et al., 2012), an attractive hypothesis could be that ATAD3A within the transduceosome regulates cholesterol shuttling through dynamic interactions with OPA1 that alter inner membrane topology. To test this, mitochondrial ultrastructure could be analyzed during steroidogenesis and fluorescence resonance energy transfer (FRET) could be used to assess dynamic interactions between fluorescently tagged ATAD3A and OPA1 following induction of

steroidogenesis. Once the nature of the interactions is deciphered, the interaction domains in ATAD3A and OPA1 could be mapped and peptides could be generated to disrupt their interactions during steroidogenesis. After the interactions are disrupted, effects on cholesterol shuttling, steroidogenesis, OPA1 oligomerization and cristae remodeling could be measured. I would also be curious to know whether ATAD3A regulates OPA1 oligomerization.

4.5 – SLC25 proteins as metabolic sensors:

In this work, I demonstrated that OPA1 interacts with SLC25 proteins and that their inhibitors and substrates decrease OPA1 oligomerization and induce cristae widening (Fig. 23-25). These findings suggest that the substrate-bound state of SLC25 proteins regulate OPA1-mediated cristae remodeling during shifts in bioenergetics. How substrate binding translates into changes in OPA1 oligomerization, however, is not known. One mechanism could be that conformational changes in SLC25 proteins during transport dynamically alter their interactions with OPA1 or OPA1 oligomerization. Indeed, it is known that these carriers transition between a c-state and m-state during transport (Klingenberg, 1979). Also Cys184 of OGC becomes more accessible to sulphydryl reagents in the presence of 2-oxoglutarate suggestive of a conformational change (Capobianco et al., 1996). These changes in topology could expose or hide certain residues required for interactions with OPA1 or OPA1 oligomer stability. I also showed that OGC knockdown was sufficient to reduce OPA1 oligomerization and induce cristae widening (Fig.25). From these

results, it is tempting to speculate that interactions with OPA1 are lost following substrate/inhibitor binding causing OPA1 oligomer disassembly, but this would require further testing. All together, I report a novel functional interaction between OPA1 and SLC25 proteins, but the nature and dynamics of these interactions require further investigation.

4.6 – Discrepancies between SLC25 protein inhibitors and substrates:

Both SLC25 protein substrates and inhibitors decrease OPA1 oligomerization and induce cristae widening, but to different extents (Fig. 23 and 25). The effects of each compound also differ with respect to their effects on respiratory chain supercomplexes and the ATP synthase (Fig. 27-28). Specifically, only the inhibitors drastically reduced respiratory chain supercomplexes whereas both inhibitors and substrates affect ATP synthase oligomerization to varying extents. We do not fully understand why differences exist, especially since Scorrano's group recently reported aberrant respiratory chain supercomplex assembly following cristae remodeling (Cogliati et al., 2013). Also direct interactions between OPA1 and respiratory chain complexes have been observed (Zanna et al., 2008). One explanation could be that OPA1 oligomer loss (or cristae widening) must surpass a particular threshold before respiratory chain supercomplex or monomer levels are affected. Indeed, the inhibitors almost completely ablate OPA1 oligomers, while complex I substrates induce a smaller effect (Fig.23A and 25A). Also Scorrano and colleagues used cleaved BID (a proapoptotic factor) and acute OPA1 loss in their study,

conditions that cause large reductions in or complete loss of OPA1 oligomers (Cogliati et al., 2013; Frezza et al., 2006). Therefore, the abundance of respiratory chain supercomplexes may only be sensitive to large-scale cristae alterations.

Both the inhibitors and substrates reduce OPA1 and ATP synthase oligomerization, but the inhibitors induce a much larger effect (Fig.23, 25 and 27). A reason for this could be that a higher concentration of inhibitors was used compared to the substrates (50mM versus 5mM). This could result in more substrate-bound transporters at any one time causing an enhanced OPA1 response. Another reason could be that these inhibitors are impermeable (Palmieri et al., 2001b). So once the inhibitor binds, it may lock the transporter into an intermediary conformation that could inhibit interactions with OPA1 or alter OPA1 oligomer stability for prolonged periods. Although the inhibitors and substrates produced varying responses, their effects seem to correlate with their relative effects on OPA1 oligomerization.

4.7 – Regulation of metabolism through changes in OPA1 and ATP synthase oligomerization:

The findings presented here show that cristae remodeling correlates with OPA1 and ATP synthase oligomerization (Fig.23, 25-27). The relationship between the ATP synthase and cristae structure is in line with a previous study showing that ATP synthase dimerization is required for cristae morphogenesis (Paumard et al., 2002). In addition, loss of OPA1 is known to affect ATP

synthase assembly and cristae structure (Gomes et al., 2011; Olichon et al., 2003). Results from our SILAC OPA1 interaction screen also show that components of the ATP synthase are putative OPA1 interactors suggesting that they form a complex (Patten and Slack unpublished). The impact of ATP synthase oligomer levels on mitochondrial function, however, is not fully understood. One study found that ATP synthase dimers induce inner membrane curvature at the apex of cristae, where it is believed to increase the local proton concentration and ATP synthesis (Strauss et al., 2008). In our no substrate (nutrient-poor) conditions, we do observe more ATP synthase oligomers and monomers (Fig.27). Under a similar condition (low [ADP]), Hackenbrock observed “orthodox” mitochondria with tight, narrow cristae (Hackenbrock, 1966). Since dimers may promote ATP synthase function, increasing ATP synthase oligomerization may represent a mechanism that preserves OXPHOS when nutrients are scarce. Indeed, expression of the e subunit of the ATP synthase, which is required for dimerization, was shown to increase under nutrient-poor conditions *in vivo* (Elliott et al., 1993). Therefore, OPA1 and the ATP synthase may together mediate dynamic cristae remodeling to maintain energy production when supply is perturbed. Thus, It is tempting to propose a model whereby OPA1 senses changes in cellular bioenergetics via interactions with SLC25 proteins and modulates metabolism accordingly through changes in cristae structure and ATP synthase oligomerization (Fig.29). This model, however, would require further experimentation.

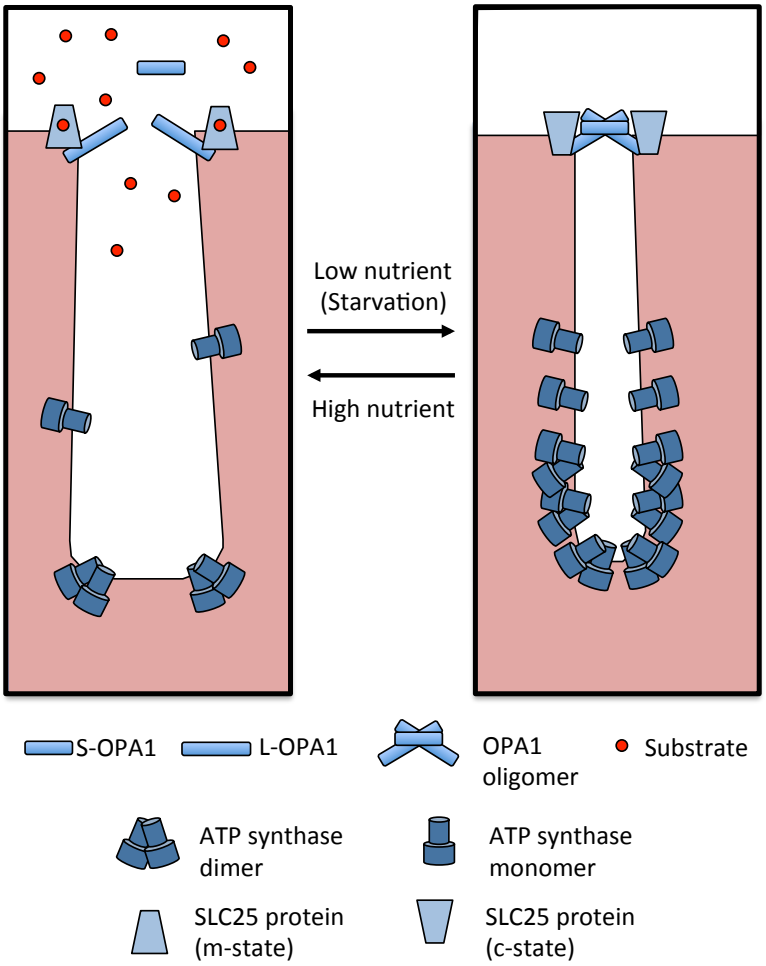

Figure 29: **OPA1 senses cellular bioenergetics through interactions with SLC25 proteins and modulates metabolism via cristae remodeling.** Cartoon depicting how metabolic sensing by SLC25 proteins may regulate OPA1 oligomerization, cristae structure and ATP synthase assembly. Under high nutrient conditions (Left panel), substrates bind SLC25 proteins leading to decreased OPA1 oligomerization potentially through dynamic protein-protein interactions or conformational changes. Alterations in OPA1 oligomerization then cause widening of cristae and decreased ATP synthase monomers and oligomers. However, during nutrient-poor conditions (right panel), the majority of SLC25 proteins become unbound leading to increased OPA1 oligomerization, cristae tightening and increased ATP synthase assembly (monomers and oligomers). Tightening of cristae and enhanced ATP synthase oligomerization may then act to maintain ATP synthesis when nutrients are scarce.

4.8 – Part 2: future directions:

The data presented in this work provide strong evidence for a functional relationship between SLC25 proteins, OPA1 and the ATP synthase, but some questions remain unanswered. For instance, cristae remodeling was only measured using the cytochrome c distribution assay outlined in figure 23B. Although measuring cytochrome c distribution does provide an indication of cristae remodeling (Scorrano et al., 2002), electron microscopy should also be performed on isolated mitochondria treated with substrates or inhibitors to verify that they similarly induce formation of "condensed" mitochondria as observed by Hackenbrock in nutrient-rich conditions (Hackenbrock, 1966). SLC25 protein substrates and inhibitors also affect OPA1 oligomerization, but how transporter binding induces these changes is not known. Therefore, it would be intriguing to know if OPA1 and SLC25 protein interactions dynamically change in response to substrate binding. One way to examine this could be to perform the same co-immunoprecipitation experiments as described earlier, but in the presence of either substrates or inhibitors to determine if these interactions become altered. Interaction dynamics could also be assayed in cells using fluorescence resonance energy transfer (FRET) where OPA1 and an SLC25 protein (eg. OGC) are fused with fluorescent markers. Changes in interactions could then be monitored using live-cell imaging following EBSS treatment or growth in galactose media, which forces energy production through mitochondria (Aguer et al., 2011; Cogliati et al., 2013). SLC25 protein substrates and inhibitors also decrease ATP synthase oligomerization, but the function of ATP synthase

oligomers is still a matter of debate. As a result, future experiments should examine what implication these supramolecular structures have on metabolism. This could be accomplished by growing cells in either galactose or EBSS media following transient knockdown of subunit e of the ATP synthase. Abnormalities in ATP production, oxygen consumption, cell growth and viability can then be measured. The model described above implies that the ATP synthase functions downstream of OPA1 oligomerization. Therefore, another potential experiment could be to overexpress the e subunit of ATP synthase in MEFs lacking OPA1 expression to determine if this is sufficient to rescue metabolic defects during starvation with EBSS or cell growth in galactose media.

4.9 – Concluding remarks:

The discovery of mitochondrial dynamics and its molecular determinants have revolutionized how we view mitochondria. The subsequent linkage of mitochondrial dynamic genes in diseases, development and cellular function demonstrated that these proteins are paramount for cellular homeostasis. However, the exact role that these proteins serve in cellular function is not completely understood. In this thesis, interacting partners of OPA1, a key regulator of mitochondrial dynamics, were characterized to determine if they regulate OPA1 function. Specifically, I investigated the role of ATAD3A and the SLC25 proteins (OGC, DIC, AGC1 and AGC2) in relation to OPA1's function in mtDNA maintenance and cristae remodeling, respectively. Using genetic studies, I found that ATAD3A is not required for mtDNA maintenance suggesting that

OPA1 maintains the mitochondrial genome independently of ATAD3A. Evidence for a functional interaction between OPA1 and SLC25 proteins however, was identified. Particularly, my data supports a model whereby SLC25 proteins sense changes in cellular bioenergetics and regulate OPA1 oligomerization causing cristae remodeling and altered ATP synthase oligomerization. These changes in cristae structure and ATP synthase assembly may then modulate metabolism further strengthening the link between mitochondrial structure and function. Studies aimed at elucidating the function of mitochondrial dynamic proteins are important as they may reveal novel disease mechanisms and potential therapeutic targets in diseases with aberrant mitochondrial dynamics or mutations in these genes, most notably the neurodegenerative diseases, ADOA or CMT2A.

CHAPTER 5: REFERENCES

Acín-Pérez, R., Bayona-Bafaluy, M.P., Fernández-Silva, P., Moreno-Loshuertos, R., Pérez-Martos, A., Bruno, C., Moraes, C.T., and Enríquez, J.A. (2004). Respiratory complex III is required to maintain complex I in mammalian mitochondria. Mol Cell *13*, 805–815.

Acín-Pérez, R., Fernández-Silva, P., Peleato, M.L., Pérez-Martos, A., and Enriquez, J.A. (2008). Respiratory active mitochondrial supercomplexes. Mol Cell *32*, 529–539.

Adams, P.L., and Turnbull, D.M. (1996). Disorders of the electron transport chain. J Inherit Metab Dis *19*, 463–469.

Aguer, C., Gambarotta, D., Mailloux, R.J., Moffat, C., Dent, R., McPherson, R., and Harper, M.-E. (2011). Galactose Enhances Oxidative Metabolism and Reveals Mitochondrial Dysfunction in Human Primary Muscle Cells. PLoS One *6*, e28536.

Akao, M., O'Rourke, B., Teshima, Y., Seharaseyon, J., and Marbán, E. (2003). Mechanistically distinct steps in the mitochondrial death pathway triggered by oxidative stress in cardiac myocytes. Circ Res *92*, 186–194.

Akepati, V.R., Muller, E.C., Otto, A., Strauss, H.M., Portwich, M., and Alexander, C. (2008). Characterization of OPA1 isoforms isolated from mouse tissues. J Neurochem *106*, 372–383.

Alam, T.I., Kanki, T., Muta, T., Ukaji, K., Abe, Y., Nakayama, H., Takio, K., Hamasaki, N., and Kang, D. (2003). Human mitochondrial DNA is packaged with TFAM. Nucleic Acids Res *31*, 1640–1645.

Alexander, C., Votruba, M., Pesch, U.E., Thiselton, D.L., Mayer, S., Moore, A., Rodriguez, M., Kellner, U., Leo-Kottler, B., Auburger, G., et al. (2000). OPA1, encoding a dynamin-related GTPase, is mutated in autosomal dominant optic atrophy linked to chromosome 3q28. Nat Genet *26*, 211–215.

Amati-Bonneau, P., Valentino, M.L., Reynier, P., Gallardo, M.E., Bornstein, B., Boissière, A., Campos, Y., Rivera, H., de la Aleja, J.G., Carroccia, R., et al. (2008). OPA1 mutations induce mitochondrial DNA instability and optic atrophy "plus" phenotypes. Brain *131*, 338–351.

Anderson, S., Bankier, A.T., Barrell, B.G.G., Bruijn, M. De, De Bruijn, M.H., Coulson, A.R., Drouin, J., Eperon, I.C., Nierlich, D.P., Roe, B.A., et al. (1981a). Sequence and organization of the human mitochondrial genome. Nature *290*, 457–465.

Anderson, S., Bankier, A.T., Barrell, B.G., de Bruijn, M.H., Coulson, A.R., Drouin, J., Eperon, I.C., Nierlich, D.P., Roe, B.A., Sanger, F., et al. (1981b). Sequence and organization of the human mitochondrial genome. Nature *290*, 457–465.

Andrews, R.M., Kubacka, I., Chinnery, P.F., Lightowlers, R.N., Turnbull, D.M., and Howell, N. (1999). Reanalysis and revision of the Cambridge reference sequence for human mitochondrial DNA. Nat Genet *23*, 147.

Aquila, H., Link, T.A., and Klingenberg, M. (1987). Solute carriers involved in energy transfer of mitochondria form a homologous protein family. FEBS Lett *212*, 1–9.

Del Arco, A., and Satrústegui, J. (1998). Molecular cloning of Aralar, a new member of the mitochondrial carrier superfamily that binds calcium and is present in human muscle and brain. J Biol Chem *273*, 23327–23334.

Arnold, I., Pfeiffer, K., Neupert, W., Stuart, R.A., and Schägger, H. (1998). Yeast mitochondrial F1F0-ATP synthase exists as a dimer: identification of three dimer-specific subunits. EMBO J *17*, 7170–7178.

Belenguer, P., and Pellegrini, L. (2013). The dynamin GTPase OPA1: more than mitochondria? Biochim Biophys Acta *1833*, 176–183.

Bernardi, P., and Azzone, G.F. (1981). Cytochrome c as an electron shuttle between the outer and inner mitochondrial membranes. J Biol Chem *256*, 7187–7192.

Bianchi, K., Rimessi, A., Prandini, A., Szabadkai, G., and Rizzuto, R. (2004). Calcium and mitochondria: mechanisms and functions of a troubled relationship. Biochim Biophys Acta *1742*, 119–131.

Bibb, M.J., Van Etten, R.A., Wright, C.T., Walberg, M.W., and Clayton, D.A. (1981). Sequence and gene organization of mouse mitochondrial DNA. Cell *26*, 167–180.

Bogenhagen, D.F., Rousseau, D., and Burke, S. (2008). The Layered Structure of Human Mitochondrial DNA Nucleoids. J Biol Chem *283*, 3665–3675.

Braschi, E., Zunino, R., and McBride, H.M. (2009). MAPL is a new mitochondrial SUMO E3 ligase that regulates mitochondrial fission. EMBO Rep *10*, 748–754.

Breckenridge, D.G., Stojanovic, M., Marcellus, R.C., and Shore, G.C. (2003). Caspase cleavage product of BAP31 induces mitochondrial fission through endoplasmic reticulum calcium signals, enhancing cytochrome c release to the cytosol. J Cell Biol *160*, 1115–1127.

Bredesen, D.E., Rao, R. V, and Mehlen, P. (2006). Cell death in the nervous system. Nature *443*, 796–802.

Van Bruggen, E.F.J., Borst, P., Ruttenberg, G.J.C.M., Gruber, M., and Kroon, A.M. (1966). Circular mitochondrial DNA. Biochim Biophys Acta *119*, 437–439.

Capobianco, L., Brandolin, G., and Palmieri, F. (1991). Transmembrane topography of the mitochondrial phosphate carrier explored by peptide-specific antibodies and enzymatic digestion. Biochemistry *30*, 4963–4969.

Capobianco, L., Bisaccia, F., Mazzeo, M., and Palmieri, F. (1996). The mitochondrial oxoglutarate carrier: sulfhydryl reagents bind to cysteine-184, and this interaction is enhanced by substrate binding. Biochemistry *35*, 8974–8980.

Cecchini, G. (2003). Function and structure of complex II of the respiratory chain. Annu Rev Biochem *72*, 77–109.

Cereghetti, G.M., Stangherlin, A., de Brito, O.M., Chang, C.R., Blackstone, C., Bernardi, P., and Scorrano, L. (2008). Dephosphorylation by calcineurin regulates translocation of Drp1 to mitochondria. Proc Natl Acad Sci U S A *105*, 15803–15808.

Chaban, Y., Boekema, E.J., and Dudkina, N. V (2013). Structures of mitochondrial oxidative phosphorylation supercomplexes and mechanisms for their stabilisation. Biochim Biophys Acta - Bioenerg -.

Chance, B. and W.G. (1955). A method for the localization of sites for oxidative phosphorylation. Nature *176*, 250–254.

Chang, C.R., and Blackstone, C. (2007). Cyclic AMP-dependent protein kinase phosphorylation of Drp1 regulates its GTPase activity and mitochondrial morphology. J Biol Chem *282*, 21583–21587.

Chang, D.D., and Clayton, D.A. (1984). Precise identification of individual promoters for transcription of each strand of human mitochondrial DNA. Cell *36*, 635–643.

Chang, D.D., and Clayton, D.A. (1985). Priming of human mitochondrial DNA replication occurs at the light-strand promoter. Proc Natl Acad Sci U S A *82*, 351–355.

Chen, H., and Chan, D.C. (2010). Physiological functions of mitochondrial fusion. Ann N Y Acad Sci *1201*, 21–25.

Chen, X.J., and Butow, R.A. (2005). The organization and inheritance of the mitochondrial genome. Nat Rev *6*, 815–825.

Chen, Z., and Lash, L.H. (1998). Evidence for mitochondrial uptake of glutathione by dicarboxylate and 2-oxoglutarate carriers. J Pharmacol Exp Ther *285*, 608–618.

Chen, H., Detmer, S.A., Ewald, A.J., Griffin, E.E., Fraser, S.E., and Chan, D.C. (2003). Mitofusins Mfn1 and Mfn2 coordinately regulate mitochondrial fusion and are essential for embryonic development. J Cell Biol *160*, 189–200.

Chen, H., Chomyn, A., and Chan, D.C. (2005). Disruption of fusion results in mitochondrial heterogeneity and dysfunction. J Biol Chem *280*, 26185–26192.

Chen, H., McCaffery, J.M., and Chan, D.C. (2007a). Mitochondrial fusion protects against neurodegeneration in the cerebellum. Cell *130*, 548–562.

Chen, H., McCaffery, J.M., and Chan, D.C. (2007b). Mitochondrial fusion protects against neurodegeneration in the cerebellum. Cell *130*, 548–562.

Chen, H., Vermulst, M., Wang, Y.E., Chomyn, A., Prolla, T.A., McCaffery, J.M., and Chan, D.C. (2010). Mitochondrial fusion is required for mtDNA stability in skeletal muscle and tolerance of mtDNA mutations. Cell *141*, 280–289.

Cipolat, S., de Brito, O.M., Zilio, B.D., and Scorrano, L. (2004). OPA1 requires mitofusin 1 to promote mitochondrial fusion. Proc Natl Acad Sci U S A *101*, 15927–15932.

Cipolat, S., Rudka, T., Hartmann, D., Costa, V., Serneels, L., Craessaerts, K., Metzger, K., Frezza, C., Annaert, W., D'Adamio, L., et al. (2006). Mitochondrial rhomboid PARL regulates cytochrome c release during apoptosis via OPA1-dependent cristae remodeling. Cell *126*, 163–175.

Cogliati, S., Frezza, C., Soriano, M.E., Varanita, T., Quintana-Cabrera, R., Corrado, M., Cipolat, S., Costa, V., Casarin, A., Gomes, L.C., et al. (2013). Mitochondrial cristae shape determines respiratory chain supercomplexes assembly and respiratory efficiency. Cell *155*, 160–171.

Crane, F.L., Hatefi, Y., Lester, R.L., and C, W. (1957). Isolation of a quinone from beef heart mitochondria. Biochim Biophys Acta *25*, 220–221.

Delettre, C., Lenaers, G., Griffoin, J.M., Gigarel, N., Lorenzo, C., Belenguer, P., Pelloquin, L., Grosgeorge, J., Turc-Carel, C., Perret, E., et al. (2000). Nuclear gene OPA1, encoding a mitochondrial dynamin-related protein, is mutated in dominant optic atrophy. Nat Genet *26*, 207–210.

Delettre, C., Griffoin, J.M., Kaplan, J., Dollfus, H., Lorenz, B., Faivre, L., Lenaers, G., Belenguer, P., and Hamel, C.P. (2001). Mutation spectrum and splicing variants in the OPA1 gene. Hum Genet *109*, 584–591.

Diaz, F., Fukui, H., Garcia, S., and Moraes, C.T. (2006). Cytochrome c Oxidase Is Required for the Assembly/Stability of Respiratory Complex I in Mouse Fibroblasts. Mol Cell Biol *26* , 4872–4881.

Diot, A., Guillou, E., Daloyau, M., Arnauné-Pelloquin, L., Emorine, L.J., and Belenguer, P. (2009). Transmembrane segments of the dynamin Msp1p uncouple its functions in the control of mitochondrial morphology and genome maintenance. J Cell Sci *122*, 2632–2639.

Elachouri, G., Vidoni, S., Zanna, C., Pattyn, A., Boukhaddaoui, H., Gaget, K., Yu-Wai-Man, P., Gasparre, G., Sarzi, E., Delettre, C., et al. (2011). OPA1 links human mitochondrial genome maintenance to mtDNA replication and distribution. Genome Res *21*, 12–20.

Elliott, T.S., Swartz, D.A., Paisley, E.A., Mangian, H.J., Visek, W.J., and Kaput, J. (1993). F1Fo-ATPase subunit e gene isolated in a screen for diet regulated genes. Biochem Biophys Res Commun *190*, 167–174.

Erdelt, H., Weidemann, M.J., Buchholz, M., and Klingenberg, M. (1972). Some principle effects of bongkrekic acid on the binding of adenine nucleotides to mitochondrial membranes. Eur J Biochem *30*, 107–122.

Ernster, L., Lee, I., Norling, B., and Persson, B. (1969). Studies with ubiquinone-depleted submitochondrial particles. Essentiality of ubiquinone for the interaction of succinate dehydrogenase, NADH dehydrogenase, and cytochrome b. Eur J Biochem *9*, 299–310.

Eubel, H., Jänsch, L., and Braun, H.-P. (2003). New insights into the respiratory chain of plant mitochondria. Supercomplexes and a unique composition of complex II. Plant Physiol *133*, 274–286.

Fish, J., Raule, N., and Attardi, G. (2004). Discovery of a major D-loop replication origin reveals two modes of human mtDNA synthesis. Science *306*, 2098–2101.

Fowler, L.R., and Richardson, S.H. (1963). Studies on the Electron Transfer System: L. ON THE MECHANISM OF RECONSTITUTION OF THE MITOCHONDRIAL ELECTRON TRANSFER SYSTEM . J Biol Chem *238* , 456–463.

Fowler, L.R., Richardson, S.H., and Hatefi, Y. (1962). A rapid method for the preparation of highly purified cytochrome oxidase. Biochim Biophys Acta *64*, 170–173.

Frank, S., Gaume, B., Bergmann-Leitner, E.S., Leitner, W.W., Robert, E.G., Catez, F., Smith, C.L., and Youle, R.J. (2001). The role of dynamin-related protein 1, a mediator of mitochondrial fission, in apoptosis. Dev Cell *1*, 515–525.

Frey, T.G., Renken, C.W., and Perkins, G.A. (2002). Insight into mitochondrial structure and function from electron tomography. Biochim Biophys Acta *1555*, 196–203.

Frezza, C., Cipolat, S., Martins de Brito, O., Micaroni, M., Beznoussenko, G. V, Rudka, T., Bartoli, D., Polishuck, R.S., Danial, N.N., De Strooper, B., et al. (2006). OPA1 controls apoptotic cristae remodeling independently from mitochondrial fusion. Cell *126*, 177–189.

Furda, A.M., Marrangoni, A.M., Lokshin, A., and Van Houten, B. (2012). Oxidants and not alkylating agents induce rapid mtDNA loss and mitochondrial dysfunction. DNA Repair (Amst) *11*, 684–692.

Gallo, M., Park, D., Luciani, D.S., Kida, K., Palmieri, F., Blacque, O.E., Johnson, J.D., and Riddle, D.L. (2011). MISC-1/OGC links mitochondrial metabolism, apoptosis and insulin secretion. PLoS One *6*, e17827.

Garcia-Rodriguez, L.J. (2007). Appendix 1. Basic properties of mitochondria. Methods Cell Biol *80*, 809–812.

Garrido, N., Griparic, L., Jokitalo, E., Wartiovaara, J., van der Bliek, A.M., and Spelbrink, J.N. (2003). Composition and dynamics of human mitochondrial nucleoids. Mol Biol Cell *14*, 1583–1596.

Germain, M., Mathai, J.P., McBride, H.M., and Shore, G.C. (2005). Endoplasmic reticulum BIK initiates DRP1-regulated remodelling of mitochondrial cristae during apoptosis. EMBO J *24*, 1546–1556.

Gilkerson, R.W., Selker, J.M.L., and Capaldi, R.A. (2003). The cristal membrane of mitochondria is the principal site of oxidative phosphorylation. FEBS Lett *546*, 355–358.

Gilquin, B., Taillebourg, E., Cherradi, N., Hubstenberger, A., Gay, O., Merle, N., Assard, N., Fauvarque, M.-O., Tomohiro, S., Kuge, O., et al. (2010a). The AAA+ ATPase ATAD3A controls mitochondrial dynamics at the interface of the inner and outer membranes. Mol Cell Biol *30*, 1984–1996.

Gilquin, B., Cannon, B.R., Hubstenberger, A., Moulouel, B., Falk, E., Merle, N., Assard, N., Kieffer, S., Rousseau, D., Wilder, P.T., et al. (2010b). The calcium-dependent interaction between S100B and the mitochondrial AAA ATPase ATAD3A and the role of this complex in the cytoplasmic processing of ATAD3A. Mol Cell Biol *30*, 2724–2736.

Van Goethem, G., Dermaut, B., Löfgren, A., Martin, J.J., and Van Broeckhoven, C. (2001). Mutation of POLG is associated with progressive external ophthalmoplegia characterized by mtDNA deletions. Nat Genet *28*, 211–212.

Goller, T., Seibold, U.K., Kremmer, E., Voos, W., and Kolanus, W. (2013). Atad3 Function Is Essential for Early Post-Implantation Development in the Mouse. PLoS One *8*, e54799.

Gomes, L.C., Benedetto, G. Di, and Scorrano, L. (2011a). During autophagy mitochondria elongate, are spared from degradation and sustain cell viability. Nat Cell Biol *13*, 589–598.

Gomes, L.C., Di Benedetto, G., and Scorrano, L. (2011b). Essential amino acids and glutamine regulate induction of mitochondrial elongation during autophagy. Cell Cycle *10*, 2635–2639.

Griparic, L., Kanazawa, T., and van der Bliek, A.M. (2007). Regulation of the mitochondrial dynamin-like protein Opa1 by proteolytic cleavage. J Cell Biol *178*, 757–764.

Guo, W., Jiang, L., Bhasin, S., Khan, S.M., and Swerdlow, R.H. (2009). DNA extraction procedures meaningfully influence qPCR-based mtDNA copy number determination. Mitochondrion *9*, 261–265.

Gutiérrez-Aguilar, M., and Baines, C.P. (2013). Physiological and pathological roles of mitochondrial SLC25 carriers. Biochem J *454*, 371–386.

Hackenbrock, C.R. (1966). Ultrastructural bases for metabolically linked mechanical activity in mitochondria. I. Reversible ultrastructural changes with change in metabolic steady state in isolated liver mitochondria. J Cell Biol *30*, 269–297.

Hackenbrock, C.R., Chazotte, B., and Gupte, S.S. (1986). The random collision model and a critical assessment of diffusion and collision in mitochondrial electron transport. J Bioenerg Biomembr *18*, 331–368.

Harder, Z., Zunino, R., and McBride, H. (2004). Sumo1 conjugates mitochondrial substrates and participates in mitochondrial fission. Curr Biol *14*, 340–345.

Harris, D.A. (1978). The interactions of coupling ATPases with nucleotides. Biochim Biophys Acta *463*, 245–273.

Hatefi, Y. (1985). THE MITOCHONDRIAL ELECTRON TRANSPORT AND OXIDATIVE PHOSPHORYLATION SYSTEM. Annu Rev Biochem *54*, 1015–1069.

Hatefi, Y., Haavik, A.G., and Jurtshuk, P. (1961). Studies on the electron transport system. XXX. DPNH-cytochrome c reductase I. Biochim Biophys Acta *52*, 106–118.

Hatefi, Y., Haavik, A.G., and Griffiths, D.E. (1962). Studies on the electron transfer system. XLI. Reduced coenzyme Q (QH2)-cytochrome c reductase. J Biol Chem *237*, 1681–1685.

He, J., Mao, C.-C., Reyes, A., Sembongi, H., Di Re, M., Granycome, C., Clippingdale, A.B., Fearnley, I.M., Harbour, M., Robinson, A.J., et al. (2007). The AAA+ protein ATAD3 has displacement loop binding properties and is involved in mitochondrial nucleoid organization. J Cell Biol *176*, 141–146.

He, J., Cooper, H.M., Reyes, a, Di Re, M., Sembongi, H., Litwin, T.R., Gao, J., Neuman, K.C., Fearnley, I.M., Spinazzola, a, et al. (2012). Mitochondrial nucleoid interacting proteins support mitochondrial protein synthesis. Nucleic Acids Res *40*, 6109–6121.

Head, B., Griparic, L., Amiri, M., Gandre-Babbe, S., and van der Bliek, A.M. (2009). Inducible proteolytic inactivation of OPA1 mediated by the OMA1 protease in mammalian cells. J Cell Biol *187*, 959–966.

Hirst, J. (2005). Energy transduction by respiratory complex I--an evaluation of current knowledge. Biochem Soc Trans *33*, 525–529.

Hoffmann, M., Bellance, N., Rossignol, R., Koopman, W.J.H., Willems, P.H.G.M., Mayatepek, E., Bossinger, O., and Distelmaier, F. (2009). C. elegans ATAD-3 is essential for mitochondrial activity and development. PLoS One *4*, e7644.

Hoppe, J., and Sebald, W. (1984). The proton conducting F0-part of bacterial ATP synthases. Biochim Biophys Acta *768*, 1–27.

Hubstenberger, A., Merle, N., Charton, R., Brandolin, G., and Rousseau, D. (2010). Topological analysis of ATAD3A insertion in purified human mitochondria. J Bioenerg Biomembr *42*, 143–150.

Hudson, G., Amati-Bonneau, P., Blakely, E.L., Stewart, J.D., He, L., Schaefer, A.M., Griffiths, P.G., Ahlqvist, K., Suomalainen, A., Reynier, P., et al. (2008). Mutation of OPA1 causes dominant optic atrophy with external ophthalmoplegia, ataxia, deafness and multiple mitochondrial DNA deletions: a novel disorder of mtDNA maintenance. Brain *131*, 329–337.

Indiveri, C., Krämer, R., and Palmieri, F. (1987). Reconstitution of the malate/aspartate shuttle from mitochondria. J Biol Chem *262*, 15979–15983.

Indiveri, C., Capobianco, L., Krämer, R., and Palmieri, F. (1989). Kinetics of the reconstituted dicarboxylate carrier from rat liver mitochondria. Biochim Biophys Acta *977*, 187–193.

Indiveri, C., Dierks, T., Krämer, R., and Palmieri, F. (1991). Reaction mechanism of the reconstituted oxoglutarate carrier from bovine heart mitochondria. Eur J Biochem *198*, 339–347.

Ingerman, E., Perkins, E.M., Marino, M., Mears, J.A., McCaffery, J.M., Hinshaw, J.E., and Nunnari, J. (2005). Dnm1 forms spirals that are structurally tailored to fit mitochondria. J Cell Biol *170*, 1021–1027.

Ishihara, N., Fujita, Y., Oka, T., and Mihara, K. (2006). Regulation of mitochondrial morphology through proteolytic cleavage of OPA1. EMBO J *25*, 2966–2977.

Itoh, K., Nakamura, K., Lijima, M., and Sesaki, H. (2013). Mitochondrial dynamics in neurodegeneration. Trends Cell Biol *23*, 64–71.

Jalil, M.A., Begum, L., Contreras, L., Pardo, B., Iijima, M., Li, M.X., Ramos, M., Marmol, P., Horiuchi, M., Shimotsu, K., et al. (2005). Reduced N-acetylaspartate levels in mice lacking aralar, a brain- and muscle-type mitochondrial aspartate-glutamate carrier. J Biol Chem *280*, 31333–31339.

Johnson, L. V, Walsh, M.L., and Chen, L.B. (1980). Localization of mitochondria in living cells with rhodamine 123. Proc Natl Acad Sci U S A *77*, 990–994.

Jones, B.A., and Fangman, W.L. (1992). Mitochondrial DNA maintenance in yeast requires a protein containing a region related to the GTP-binding domain of dynamin. Genes Dev *6*, 380–389.

Kamga, C.K., Zhang, S.X., and Wang, Y. (2010). Dicarboxylate carrier-mediated glutathione transport is essential for reactive oxygen species homeostasis and normal respiration in rat brain mitochondria. Am J Physiol Cell Physiol *299*, C497–C505.

Karbowski, M., Lee, Y.-J., Gaume, B., Jeong, S.-Y., Frank, S., Nechushtan, A., Santel, A., Fuller, M., Smith, C.L., and Youle, R.J. (2002). Spatial and temporal association of Bax with mitochondrial fission sites, Drp1, and Mfn2 during apoptosis. J Cell Biol *159*, 931–938.

Karbowski, M., Neutzner, A., and Youle, R.J. (2007). The mitochondrial E3 ubiquitin ligase MARCH5 is required for Drp1 dependent mitochondrial division. J Cell Biol *178*, 71–84.

Kasamatsu, H., Robberson, D.L., and Vinograd, J. (1971). A novel closed-circular mitochondrial DNA with properties of a replicating intermediate. Proc Natl Acad Sci U S A *68*, 2252–2257.

Kim, T.-H., Zhao, Y., Ding, W.-X., Shin, J.N., He, X., Seo, Y.-W., Chen, J., Rabinowich, H., Amoscato, A.A., and Yin, X.-M. (2004). Bid-cardiolipin interaction at mitochondrial contact site contributes to mitochondrial cristae reorganization and cytochrome C release. Mol Biol Cell *15*, 3061–3072.

Klingenberg, M. (1979). The ADP, ATP shuttle of the mitochondrion. Trends Biochem Sci *4*, 249–252.

Klingenberg, M., and Buchholz, M. (1973). On the mechanism of bongkrekate effect on the mitochondrial adenine-nucleotide carrier as studied through the binding of ADP. Euro j Biochem *38*, 346–358.

Kobayashi, K., Sinasac, D.S., Iijima, M., Boright, A.P., Begum, L., Lee, J.R., Yasuda, T., Ikeda, S., Hirano, R., Terazono, H., et al. (1999). The gene mutated in adult-onset type II citrullinaemia encodes a putative mitochondrial carrier protein. Nat Genet *22*, 159–163.

Krause, F., Reifschneider, N.H., Goto, S., and Dencher, N.A. (2005). Active oligomeric ATP synthases in mammalian mitochondria. Biochem Biophys Res Commun *329*, 583–590.

Kröger, A., and Klingenberg, M. (1970). Quinones and nicotinamide nucleotides associated with electron transfer. Vitam Horm *28*, 533–574.

Kukat, C., Wurm, C.A., Spahr, H., Falkenberg, M., Larsson, N.G., and Jakobs, S. (2011). Super-resolution microscopy reveals that mammalian mitochondrial nucleoids have a uniform size and frequently contain a single copy of mtDNA. Proc Natl Acad Sci U S A *108*, 13534–13539.

Kushnareva, Y.E., Gerencser, a a, Bossy, B., Ju, W.-K., White, a D., Waggoner, J., Ellisman, M.H., Perkins, G., and Bossy-Wetzel, E. (2013). Loss of OPA1 disturbs cellular calcium homeostasis and sensitizes for excitotoxicity. Cell Death Differ *20*, 353–365.

Lackner, L.L., Horner, J.S., and Nunnari, J. (2009). Mechanistic analysis of a dynamin effector. Science *325*, 874–877.

LaNoue, K.F., and Schoolwerth, A.C. (1979). Metabolite transport in mitochondria. Annu Rev Biochem *48*, 871–922.

LaNoue, K.F., and Williamson, J.R. (1971). Interrelationships between malate-aspartate shuttle and citric acid cycle in rat heart mitochondria. Metabolism *20*, 119–140.

LaNoue, K.F., Meijer, A.J., and Brouwer, A. (1974). Evidence for electrogenic aspartate transport in rat liver mitochondria. Arch Biochem Biophys *161*, 544–550.

Larsson, N.G., Wang, J., Wilhelmsson, H., Oldfors, A., Rustin, P., Lewandoski, M., Barsh, G.S., and Clayton, D.A. (1998). Mitochondrial transcription factor A is necessary for mtDNA maintenance and embryogenesis in mice. Nat Genet *18*, 231–236.

Lash, L.H., Putt, D.A., and Matherly, L.H. (2002). Protection of NRK-52E cells, a rat renal proximal tubular cell line, from chemical-induced apoptosis by overexpression of a mitochondrial glutathione transporter. J Pharmacol Exp Ther *303*, 476–486.

Legros, F., Malka, F., Frachon, P., Lombès, A., and Rojo, M. (2004). Organization and dynamics of human mitochondrial DNA. J Cell Sci *117*, 2653–2662.

Lenaz, G., and Genova, M.L. (2012). Supramolecular organisation of the mitochondrial respiratory chain: a new challenge for the mechanism and control of oxidative phosphorylation. Adv Exp Med Biol *748*, 107–144.

Leung, K.H., and Hinkle, P.C. (1975). Reconstitution of ion transport and respiratory control in vesicles formed from reduced coenzyme Q-cytochrome c reductase and phospholipids. J Biol Chem *250*, 8467–8471.

Liu, J., Rone, M.B., and Papadopoulos, V. (2006). Protein-protein interactions mediate mitochondrial cholesterol transport and steroid biosynthesis. J Biol Chem *281*, 38879–38893.

Mancini, M., Anderson, B.O., Caldwell, E., Sedghinasab, M., Paty, P.B., and Hockenbery, D.M. (1997). Mitochondrial proliferation and paradoxical membrane depolarization during terminal differentiation and apoptosis in a human colon carcinoma cell line. J Cell Biol *138*, 449–69.

Mannella, C. a (2006). Structure and dynamics of the mitochondrial inner membrane cristae. Biochim Biophys Acta *1763*, 542–548.

Mannella, C. a, Lederer, W.J., and Jafri, M.S. (2013). The Connection between Inner Membrane Topology and Mitochondrial Function. J Mol Cell Cardiol *62*, 51–57.

Mannella, C.A., Marko, M., Penczek, P., Barnard, D., and Frank, J. (1994). The internal compartmentation of rat-liver mitochondria: tomographic study using the high-voltage transmission electron microscope. Microsc Res Tech *27*, 278–283.

Mannella, C.A., Pfeiffer, D.R., Bradshaw, P.C., Moraru, I.I., Slepchenko, B., Loew, L.M., Hsieh, C., Buttle, K., and Marko, M. (2001). Topology of the Mitochondrial Inner Membrane: Dynamics and Bioenergetic Implications. IUBMB Life *52*, 93–100.

Mannella CA, Marko M, B.K. (1997). Reconsidering mitochondrial structure: new views of an old organelle. *22*, 37–38.

Mears, J.A., Lackner, L.L., Fang, S., Ingerman, E., Nunnari, J., and Hinshaw, J.E. (2011). Conformational changes in Dnm1 support a contractile mechanism for mitochondrial fission. Nat Struct Mol Biol *18*, 20–26.

Misaka, T., Miyashita, T., and Kubo, Y. (2002). Primary structure of a dynamin-related mouse mitochondrial GTPase and its distribution in brain, subcellular localization, and effect on mitochondrial morphology. J Biol Chem *277*, 15834–15842.

Mitchell, P. (1961). Coupling of phosphorylation to electron and hydrogen transfer by a chemi-osmotic type of mechanism. Nature *191*, 144–148.

Mitra, K., Wunder, C., Roysam, B., Lin, G., and Lippincott-Schwartz, J. (2009). A hyperfused mitochondrial state achieved at G1-S regulates cyclin E buildup and entry into S phase. Proc Natl Acad Sci U S A *106*, 11960–11965.

Nass, M.M. (1966). The circularity of mitochondrial DNA. Proc Natl Acad Sci U S A *56*, 1215–1222.

Nass, M.M., and Nass, S. (1963). Intramitochondrial fibers with DNA characteristics. I. Fixation and electron staining reactions. J Cell Biol *19*, 593–611.

Nunnari, J., Marshall, W.F., Straight, A., Murray, A., Sedat, J.W., and Walter, P. (1997). Mitochondrial transmission during mating in Saccharomyces cerevisiae is determined by mitochondrial fusion and fission and the intramitochondrial segregation of mitochondrial DNA. Mol Biol Cell *8*, 1233–1242.

Oettinghaus, B., Licci, M., Scorrano, L., and Frank, S. (2012). Less than perfect divorces: dysregulated mitochondrial fission and neurodegeneration. Acta Neuropathol *123*, 189–203.

Olichon, A., Emorine, L.J., Descoins, E., Pelloquin, L., Brichese, L., Gas, N., Guillou, E., Delettre, C., Valette, A., Hamel, C.P., et al. (2002). The human dynamin-related protein OPA1 is anchored to the mitochondrial inner membrane facing the inter-membrane space. FEBS Lett *523*, 171–176.

Olichon, A., Baricault, L., Gas, N., Guillou, E., Valette, A., Belenguer, P., and Lenaers, G. (2003). Loss of OPA1 perturbates the mitochondrial inner membrane structure and integrity, leading to cytochrome c release and apoptosis. J Biol Chem *278*, 7743–7746.

Otera, H., Wang, C., Cleland, M.M., Setoguchi, K., Yokota, S., Youle, R.J., and Mihara, K. (2010). Mff is an essential factor for mitochondrial recruitment of Drp1 during mitochondrial fission in mammalian cells. J Cell Biol *191*, 1141–1158.

Otera, H., Ishihara, N., and Mihara, K. (2013). New insights into the function and regulation of mitochondrial fission. Biochim Biophys Acta *1833*, 1256–1268.

Palmer, C.S., Osellame, L.D., Laine, D., Koutsopoulos, O.S., Frazier, A.E., and Ryan, M.T. (2011). MiD49 and MiD51, new components of the mitochondrial fission machinery. EMBO Rep *12*, 565–573.

Palmieri, F. (1994). Mitochondrial carrier proteins. FEBS Lett *346*, 48–54.

Palmieri, F. (2004). The mitochondrial transporter family (SLC25): physiological and pathological implications. Pflügers Arch *447*, 689–709.

Palmieri, F. (2008). Diseases caused by defects of mitochondrial carriers: A review. Biochim Biophys Acta - Bioenerg *1777*, 564–578.

Palmieri, F. (2013). The mitochondrial transporter family SLC25: Identification, properties and physiopathology. Mol Aspects Med *34*, 465–484.

Palmieri, F., Prezioso, G., Quagliariello, E., and Klingenberg, M. (1971). Kinetic study of the dicarboxylate carrier in rat liver mitochondria. Eur J Biochem *22*, 66–74.

Palmieri, F., Quagliariello, E., and Klingenberg, M. (1972). Kinetics and specificity of the oxoglutarate carrier in Rat-liver mitochondria. Eur J Biochem *29*, 408–416.

Palmieri, F., Pierri, C.L., De Grassi, A., Nunes-Nesi, A., and Fernie, A.R. (2011). Evolution, structure and function of mitochondrial carriers: a review with new insights. Plant J *66*, 161–181.

Palmieri, L., Pardo, B., Lasorsa, F.M., del Arco, a, Kobayashi, K., Iijima, M., Runswick, M.J., Walker, J.E., Saheki, T., Satrústegui, J., et al. (2001a). Citrin and aralar1 are Ca(2+)-stimulated aspartate/glutamate transporters in mitochondria. EMBO J *20*, 5060–5069.

Palmieri, L., Agrimi, G., Runswick, M.J., Fearnley, I.M., Palmieri, F., and Walker, J.E. (2001b). Identification in Saccharomyces cerevisiae of two isoforms of a

novel mitochondrial transporter for 2-oxoadipate and 2-oxoglutarate. J Biol Chem *276*, 1916–1922.

Paumard, P., Vaillier, J., Coulary, B., Schaeffer, J., Soubannier, V., Mueller, D.M., Brèthes, D., di Rago, J.-P., and Velours, J. (2002). The ATP synthase is involved in generating mitochondrial cristae morphology. EMBO J *21*, 221–230.

Penefsky, H.S. (1977). Reversible binding of Pi by beef heart mitochondrial adenosine triphosphatase. J Biol Chem *252*, 2891–2899.

Pinton, P., Ferrari, D., Rapizzi, E., Di Virgilio, F., Pozzan, T., and Rizzuto, R. (2001). The Ca2+ concentration of the endoplasmic reticulum is a key determinant of ceramide-induced apoptosis: significance for the molecular mechanism of Bcl-2 action. EMBO J *20*, 2690–2701.

Praefcke, G.J.K., and McMahon, H.T. (2004). The dynamin superfamily: universal membrane tubulation and fission molecules? Nat Rev Mol Cell Biol *5*, 133–147.

Rieske, J.S., Hansen, R.E., and Zaugg, W.S. (1964). STUDIES ON THE ELECTRON TRANSFER SYSTEM. 58. PROPERTIES OF A NEW OXIDATION-REDUCTION COMPONENT OF THE RESPIRATORY CHAIN AS STUDIED BY ELECTRON PARAMAGNETIC RESONANCE SPECTROSCOPY. J Biol Chem *239*, 3017–3022.

Rone, M.B., Fan, J., and Papadopoulos, V. (2009). Cholesterol transport in steroid biosynthesis: role of protein-protein interactions and implications in disease states. Biochim Biophys Acta *1791*, 646–658.

Rone, M.B., Midzak, A.S., Issop, L., Rammouz, G., Jagannathan, S., Fan, J., Ye, X., Blonder, J., Veenstra, T., and Papadopoulos, V. (2012). Identification of a dynamic mitochondrial protein complex driving cholesterol import, trafficking, and metabolism to steroid hormones. Mol Endocrinol *26*, 1868–1882.

Rousseau, D., and Li, S. (2012). ATAD3, a vital membrane bound mitochondrial ATPase involved in tumor progression. J Bioenerg Biomembr *44*, 189–197.

Runswick, M.J., Powell, S.J., Nyren, P., and Walker, J.E. (1987). Sequence of the bovine mitochondrial phosphate carrier protein: structural relationship to ADP/ATP translocase and the brown fat mitochondria uncoupling protein. EMBO J *6*, 1367–1373.

Sagan, L. (1967). On the origin of mitosing cells. J Theor Biol *14*, 255–274.

Saraste, M., and Walker, J.E. (1982). Internal sequence repeats and the path of polypeptide in mitochondrial ADP/ATP translocase. FEBS Lett *144*, 250–254.

Satoh, M., Hamamoto, T., Seo, N., Kagawa, Y., and Endo, H. (2003). Differential sublocalization of the dynamin-related protein OPA1 isoforms in mitochondria. Biochem Biophys Res Commun *300*, 482–493.

Schägger, H., and Pfeiffer, K. (2000). Supercomplexes in the respiratory chains of yeast and mammalian mitochondria. EMBO J *19*, 1777–1783.

Schägger, H., de Coo, R., Bauer, M.F., Hofmann, S., Godinot, C., and Brandt, U. (2004). Significance of respirasomes for the assembly/stability of human respiratory chain complex I. J Biol Chem *279*, 36349–36353.

Scorrano, L., Ashiya, M., Buttle, K., Weiler, S., Oakes, S.A., Mannella, C.A., and Korsmeyer, S.J. (2002). A distinct pathway remodels mitochondrial cristae and mobilizes cytochrome c during apoptosis. Dev Cell *2*, 55–67.

Sesaki, H., and Jensen, R.E. (1999). Division versus fusion: Dnm1p and Fzo1p antagonistically regulate mitochondrial shape. J Cell Biol *147*, 699–706.

Sesaki, H., and Jensen, R.E. (2004). Ugo1p links the Fzo1p and Mgm1p GTPases for mitochondrial fusion. J Biol Chem *279*, 28298–28303.

Sesaki, H., Southard, S.M., Yaffe, M.P., and Jensen, R.E. (2003). Mgm1p, a dynamin-related GTPase, is essential for fusion of the mitochondrial outer membrane. Mol Biol Cell *14*, 2342–2356.

Shin, H.W., Shinotsuka, C., Torii, S., Murakami, K., and Nakayama, K. (1997). Identification and subcellular localization of a novel mammalian dynamin-related protein homologous to yeast Vps1p and Dnm1p. J Biochem *122*, 525–530.

Shin, H.W., Takatsu, H., Mukai, H., Munekata, E., Murakami, K., and Nakayama, K. (1999). Intermolecular and interdomain interactions of a dynamin-related GTP-binding protein, Dnm1p/Vps1p-like protein. J Biol Chem *274*, 2780–2785.

Sigel, E., and Carafoli, E. (1978). The proton pump of cytochrome c oxidase and its stoichiometry. Eur J Biochem *89*, 119–123.

Sinclair, J.H., and Stevens, B.J. (1966). Circular DNA filaments from mouse mitochondria. Proc Natl Acad Sci U S A *56*, 508–515.

Smeitink, J.A.M., Jonckheere, A.I., and Rodenburg, R.J.T. (2012). Mitochondrial ATP synthase: architecture, function and pathology. J Inherit Metab Dis *35*, 211–225.

Smirnova, E., Shurland, D.L., Ryazantsev, S.N., and van der Bliek, A.M. (1998). A human dynamin-related protein controls the distribution of mitochondria. J Cell Biol *143*, 351–358.

Smirnova, E., Griparic, L., Shurland, D.L., and van der Bliek, A.M. (2001). Dynamin-related protein Drp1 is required for mitochondrial division in mammalian cells. Mol Biol Cell *12*, 2245–2256.

Sondheimer, N., Fang, J.-K., Polyak, E., Falk, M.J., and Avadhani, N.G. (2010). Leucine-rich pentatricopeptide-repeat containing protein regulates mitochondrial transcription. Biochemistry *49*, 7467–7473.

Song, Z., Chen, H., Fiket, M., Alexander, C., and Chan, D.C. (2007a). OPA1 processing controls mitochondrial fusion and is regulated by mRNA splicing, membrane potential, and Yme1L. J Cell Biol *178*, 749–755.

Song, Z., Chen, H., Fiket, M., Alexander, C., and Chan, D.C. (2007b). OPA1 processing controls mitochondrial fusion and is regulated by mRNA splicing, membrane potential, and Yme1L. J Cell Biol *178*, 749–755.

Song, Z., Ghochani, M., McCaffery, J.M., Frey, T.G., and Chan, D.C. (2009). Mitofusins and OPA1 mediate sequential steps in mitochondrial membrane fusion. Mol Biol Cell *20*, 3525–3532.

Spelbrink, J.N., Li, F.Y., Tiranti, V., Nikali, K., Yuan, Q.P., Tariq, M., Wanrooij, S., Garrido, N., Comi, G., Morandi, L., et al. (2001). Human mitochondrial DNA deletions associated with mutations in the gene encoding Twinkle, a phage T7 gene 4-like protein localized in mitochondria. Nat Genet *28*, 223–231.

Strauss, M., Hofhaus, G., Schröder, R.R., and Kühlbrandt, W. (2008). Dimer ribbons of ATP synthase shape the inner mitochondrial membrane. EMBO J *27*, 1154–1160.

Sun, M.G., Williams, J., Munoz-Pinedo, C., Perkins, G.A., Brown, J.M., Ellisman, M.H., Green, D.R., and Frey, T.G. (2007). Correlated three-dimensional light and electron microscopy reveals transformation of mitochondria during apoptosis. Nat Cell Biol *9*, 1057–1065.

Szarkowska, L. (1966). The restoration of DPNH oxidase activity by coenzyme Q (ubiquinone). Arch Biochem Biophys *113*, 519–525.

Taguchi, N., Ishihara, N., Jofuku, A., Oka, T., and Mihara, K. (2007). Mitotic phosphorylation of dynamin-related GTPase Drp1 participates in mitochondrial fission. J Biol Chem *282*, 11521–11529.

Tal, M.C., Sasai, M., Lee, H.K., Yordy, B., Shadel, G.S., and Iwasaki, A. (2009). Absence of autophagy results in reactive oxygen species-dependent amplification of RLR signaling. Proc Natl Acad Sci U S A *106*, 2770–2775.

Tuppy, H., Schatz, G., and Haslbrunner, E. (1964). Deoxyribonucleic acid associated with yeast mitochondria. Biochem Biophys Res Commun *15*, 127–132.

W.Th. Daems, E.W. (1966). Shape and Attachment of the Cristae Mitochondriales in Mouse Hepatic Cell Mitochondria Laboratory for Electron Microscopy , University of Leiden , The Netherlands. *140*, 123–140.

Wakabayashi, J., Zhang, Z., Wakabayashi, N., Tamura, Y., Fukaya, M., Kensler, T.W., Iijima, M., and Sesaki, H. (2009). The dynamin-related GTPase Drp1 is required for embryonic and brain development in mice. J Cell Biol *186*, 805–816.

Walker, J.E. (2012). The ATP synthase: The understood, the uncertain and the unknown. Biochim Biophys Acta - Bioenerg *1817*, S1.

Walker, J.E., Saraste, M., Runswick, M.J., and Gay, N.J. (1982). Distantly related sequences in the alpha- and beta-subunits of ATP synthase, myosin, kinases and other ATP-requiring enzymes and a common nucleotide binding fold. EMBO J *1*, 945–951.

Wallace, D.C. (2005). A mitochondrial paradigm of metabolic and degenerative diseases, aging, and cancer: a dawn for evolutionary medicine. Annu Rev Genet *39*, 359–407.

Wang, Y., and Bogenhagen, D.F. (2006). Human mitochondrial DNA nucleoids are linked to protein folding machinery and metabolic enzymes at the mitochondrial inner membrane. J Biol Chem *281*, 25791–25802.

Wasiak, S., Zunino, R., and McBride, H.M. (2007). Bax/Bak promote sumoylation of DRP1 and its stable association with mitochondria during apoptotic cell death. J Cell Biol *177*, 439–450.

Wasilewski, M., Semenzato, M., Rafelski, S.M., Robbins, J., Bakardjiev, A.I., and Scorrano, L. (2012). Optic Atrophy 1-Dependent Mitochondrial Remodeling Controls Steroidogenesis in Trophoblasts. Curr Biol *22*, 1228–1234.

Wikstrom, M.K.F. (1977). Proton pump coupled to cytochrome c oxidase in mitochondria. Nature *266*, 271–273.

Wikström, M. (1984). Two protons are pumped from the mitochondrial matrix per electron transferred between NADH and ubiquinone. FEBS Lett *169*, 300–304.

Wilkins, H.M., Kirchhof, D., Manning, E., Joseph, J.W., and Linseman, D. a (2013). Mitochondrial glutathione transport is a key determinant of neuronal susceptibility to oxidative and nitrosative stress. J Biol Chem *288*, 5091–5101.

Wittig, I., Braun, H.-P., and Schägger, H. (2006). Blue native PAGE. Nat Protoc *1*, 418–428.

Wittig, I., Velours, J., Stuart, R., and Schägger, H. (2008). Characterization of domain interfaces in monomeric and dimeric ATP synthase. Mol Cell Proteomics *7*, 995–1004.

Wurm, C.A., and Jakobs, S. (2006). Differential protein distributions define two sub-compartments of the mitochondrial inner membrane in yeast. FEBS Lett *580*, 5628–5634.

Yamaguchi, R., Lartigue, L., Perkins, G., Scott, R.T., Dixit, A., Kushnareva, Y., Kuwana, T., Ellisman, M.H., and Newmeyer, D.D. (2008). Opa1-mediated cristae opening is Bax/Bak and BH3 dependent, required for apoptosis, and independent of Bak oligomerization. Mol Cell *31*, 557–569.

Yasuda, T., Yamaguchi, N., Kobayashi, K., Nishi, I., Horinouchi, H., Jalil, M.A., Li, M.X., Ushikai, M., Iijima, M., Kondo, I., et al. (2000). Identification of two novel mutations in the SLC25A13 gene and detection of seven mutations in 102 patients with adult-onset type II citrullinemia. Hum Genet *107*, 537–545.

Yoon, Y., Krueger, E.W., Oswald, B.J., and McNiven, M.A. (2003). The mitochondrial protein hFis1 regulates mitochondrial fission in mammalian cells through an interaction with the dynamin-like protein DLP1. Mol Cell Biol *23*, 5409–5420.

Zanna, C., Ghelli, A., Porcelli, A.M., Karbowski, M., Youle, R.J., Schimpf, S., Wissinger, B., Pinti, M., Cossarizza, A., Vidoni, S., et al. (2008). OPA1 mutations associated with dominant optic atrophy impair oxidative phosphorylation and mitochondrial fusion. Brain *131*, 352–367.

Zhao, J., Liu, T., Jin, S., Wang, X., Qu, M., Uhlen, P., Tomilin, N., Shupliakov, O., Lendahl, U., and Nister, M. (2011). Human MIEF1 recruits Drp1 to mitochondrial outer membranes and promotes mitochondrial fusion rather than fission. EMBO J *30*, 2762–2778.

Zhong, Q., Putt, D.A., Xu, F., and Lash, L.H. (2008). Hepatic mitochondrial transport of glutathione: studies in isolated rat liver mitochondria and H4IIE rat hepatoma cells. Arch Biochem Biophys *474*, 119–127.

Zick, M., Rabl, R., and Reichert, A.S. (2009). Cristae formation-linking ultrastructure and function of mitochondria. Biochim Biophys Acta *1793*, 5–19.

Ziegler, D.M., and Doeg, K.A. (1962). Studies on the electron transport system XLIII. The isolation of a succinic-coenzyme Q reductase from beef heart mitochondria. Arch Biochem Biophys *97*, 41–50.

Zuchner, S., Mersiyanova, I. V, Muglia, M., Bissar-Tadmouri, N., Rochelle, J., Dadali, E.L., Zappia, M., Nelis, E., Patitucci, A., Senderek, J., et al. (2004). Mutations in the mitochondrial GTPase mitofusin 2 cause Charcot-Marie-Tooth neuropathy type 2A. Nat Genet *36*, 449–451.